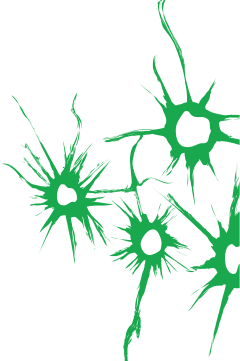


On-chip separation of spermatozoa using dielectrophoresis

Master thesis

REPORT NUMBER: 07/BIOS/2011



8 July 2011
Enschede, NL

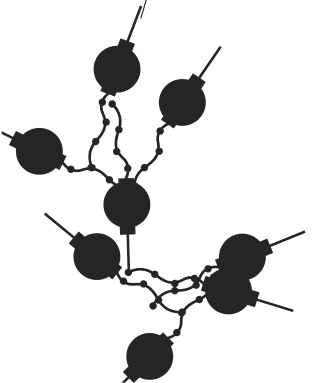
Author:
C.E. van Eijkeren
S0027634

Graduation committee:
L.I. Segerink, MSc
Dr.ir. A.J. Sprenkels
Prof.dr. J.G.E. Gardeniers
Prof.dr.ir. A. van den Berg

Supervisors:
L.I. Segerink, MSc
Dr.ir. A.J. Sprenkels

University of Twente

Faculty / Chair:
EWI / BIOS, Lab on a Chip group



UNIVERSITY OF TWENTE.



Preface - In Dutch

Met dit afstudeer verslag, waarin ik mijn onderzoek naar een leuk en aansprekend onderwerp zal presenteren, sluit ik mijn studie elektrotechniek af. Voor dit onderzoek heb ik veel hulp van anderen gekregen zonder wie het uiteindelijke resultaat niet behaald zou zijn. Allereerst wil ik Loes en Ad bedanken voor het begeleiden van mijn afstudeer project, en voor het vertrouwen dat al het te verzetten werk binnen de gestelde tijd af te ronden zou zijn. Ook zeer dankbaar ben ik ze de motivatie die ik putte uit de voortgangs gesprekken. Ook wil ik Lennart bedanken voor het binnen een record tijd fabriceren van mijn chips. Om zelf een idee te krijgen van alle fabricage processen mocht ik in de cleanroom meekijken, een super leuke ervaring. Ook wil ik alle mensen die aan de BIOS vakgroep verbonden zijn bedanken. De goede sfeer op de studenten werkplekken en binnen BIOS, die ik al tijdens mijn bachelor opdracht meemaakte, was ook nu weer aanwezig.

Ook wil ik mijn ouders bedanken voor hun steun aan en het vertrouwen in mij gedurende mijn studie periode. Natuurlijk moet ik ook hier mijn lieve vriendin bedanken voor haar steun niet alleen tijdens mijn afstudeer periode, maar ook tijdens de laatste jaren van mijn studie.

Abstract

The aim of the fertility project in the BIOS group of the University of Twente is to develop a portable point of care semen quality analyzer. This should enable couples who are staying unwanted childless to perform semen quality tests themselves in a convenient environment. The quality of semen depends on four important factors, these are the concentration, motility, viability and morphology. This master thesis is focused on the separation of spermatozoa based on their motility and viability.

The research described in this thesis was focused on the possibility to separate motile and non-motile spermatozoa and to separate viable and non-viable spermatozoa on-chip with a technique called dielectrophoresis. Based on theory, simulations were performed, resulting in six different lab-on-a-chips are designed that have been manufactured. Measurements with boar-semen were performed to verify the simulations and to measure the sorting functioning of these chips.

It was not possible to test the separation operation of the chip, due to experimental problems and the limited time available. However, some of the simulation results were confirmed by the experiments. More research is necessary to investigate the separation of spermatozoa.

Table of Contents

Preface - In Dutch	i
Abstract.....	ii
1 Introduction.....	6
1.1 Background	6
1.2 Project description.....	6
1.3 Report overview.....	6
2 Theory.....	7
2.1 Semen	7
2.2 Spermatozoa	7
2.3 Analysis.....	8
2.4 Existing products and methods	8
2.4.1 Products	8
2.4.2 Separation methods	9
2.5 Dielectrophoresis.....	11
2.5.1 DEP force on a sphere (Pohl).....	12
2.5.2 DEP force on a ellipsoid (Pethig)	13
2.5.3 DEP force, a broader definition	13
2.5.4 Other forces	15
2.5.5 Side effects	16
2.5.6 Usage of DEP.....	17
2.6 Single Shell.....	18
2.7 Electrochemical cell.....	20
3 Simulations	23
3.1 Single shell permittivity	24
3.2 Electrochemical cell.....	26
3.3 Circuit simulation	27
3.4 DEP	28
3.4.1 Geometry	28
3.4.2 Physics	29
3.4.3 Post-processing and Results.....	30
3.5 Side effects.....	35
3.5.1 Electroporation	35
3.5.2 Heating.....	36

3.6	Total forces.....	37
3.7	Simulation summary and conclusions	38
4	Design & fabrication of the chips	39
4.1	Design aspects.....	39
4.2	Different versions	39
4.2.1	45° and 60° sorting electrodes	40
4.2.2	Laminar flow chip	41
4.3	Fabrication process.....	43
4.4	Results.....	47
5	Experiments.....	49
5.1	Impedance spectrum measurements	49
5.1.1	Conductivity measurements.....	49
5.1.2	Impedance measurement protocol.....	49
5.2	Spermatozoa experiments	49
5.2.1	Measurement setup.....	49
5.2.2	Sorting electrodes	50
5.2.3	Focusing electrodes.....	50
6	Results and discussion	51
6.1	Conductivity measurements	51
6.2	Impedance measurements.....	51
6.3	Spermatozoa experiments	54
6.3.1	Sorting electrodes	54
6.3.2	Focusing electrodes.....	55
6.3.3	Encountered experimental problems.....	58
7	Conclusions and recommendations.....	59
7.1	Conclusions	59
7.2	Recommendations.....	59
	Literature	61
	Appendix A Maple code	A-1
A.1	Maple – singleshell_3formulas.mw	A-1
A.2	Maple – CellConstant.wms	A-1
A.3	Maple – ElectrochemicalCellImpedance.mw.....	A-2
A.4	Maple – SingleShell_Ohta.wm	A-2
	Appendix B LTspice IV model.....	B-3
	Appendix C Matlab scripts.....	C-4

C.1	Matlab - ImpedanceMeasurements.m.....	C-4
Appendix D	Chip results, numbering and wafer layout.....	D-5

1 Introduction

1.1 Background

When a couple is unwanted childless, one of the first steps in treatment is to analyze the semen quality. Besides properties of the seminal fluid, four aspects of the spermatozoa are rated: the concentration, the motility, the viability and the morphology. The gold standard to assess these properties involves the use of a microscope in a laboratory [1]. It is expensive and involves labor intensive work and this method can be experienced as shameful by some men. Therefore it is proposed to develop a test which can be performed by the man himself at his own home.

Currently a glass based microfluidic chip has been developed which can determine the concentration of spermatozoa [2]. To be able to make a more reliable assessment of the semen quality the other properties need to be assessed as well. The motility and viability properties of the spermatozoa are important for the semen quality. Therefore the assessments of these properties need to be implemented together with the concentration assessment on-chip.

In literature dielectrophoresis (DEP) is used to separate cells in microfluidic devices, therefore DEP seems an interesting technique to separate spermatozoa.

1.2 Project description

The aim of this project is to develop a lab-on-a-chip to separate spermatozoa using DEP. The separation is based on the vitality and, or motility of the spermatozoa. More information about DEP will be presented in chapter 2.5.

In this master thesis project it is tried to answer the following research question:

Is it possible to separate spermatozoa on chip using DEP?

To answer this question the following sub questions need to be answered:

- *What are the electrical parameters of spermatozoa and the medium?*
- *What is the optimal geometry of the chip to separate spermatozoa?*
- *What are the optimal parameters to separate spermatozoa?*
- *Can live and dead spermatozoa be separated?*
- *Can motile and non-motile spermatozoa be separated?*

The study load for the master thesis in the curriculum of the master Electrical Engineering at the University of Twente is 45 EC. This is equivalent to 28 weeks full time work. The research is carried out at the BIOS chair of the EWI faculty at the University of Twente.

1.3 Report overview

In chapter 2 of this report the necessary theory related to this project is presented. In chapter 3 simulations based on the theory are shown. The simulation results are used for the design of a lab-on-a-chip (chapter 4) and for the parameter settings used in the experiments (chapter 5) to evaluate the performance of the design. The results of these experiments are presented and discussed in chapter 6. Conclusions and recommendations based on the results are given in chapter 7.

2 Theory

2.1 Semen

Human semen is a mixture of various components. It contains sperm cells, but also sugars, proteins, ions and other cells [1, 3]. When a man ejaculates the semen, it is first coagulated and after a few minutes the semen liquefies and immobilized spermatozoa begin to move. This liquefaction process occurs due to prostatic proteases [1].

2.2 Spermatozoa

A spermatozoon consists of a head, a mid piece and a tail. A picture of a spermatozoon can be seen in Figure 1. The head is 5 μm by 3 μm and the tail, which propels the cell, is 50 μm long [3]. It is reported that spermatozoa tend to swim against the direction of flow depending on the flow gradient [3, 4].

Not all spermatozoa are alive (vital), and not all the living spermatozoa are motile. So there are three types of spermatozoa. The dead spermatozoa have different electrical properties compared with the living ones, due to cell membrane defects [1]. The cell membranes of the dead cells are permeable to ions. The membranes of living cells are not permeable to ions, so they are not conductive [5]. The motile and non-motile spermatozoa have the same electrical properties, but they have different “mechanical” properties. The motile spermatozoa are able to swim, so they have a velocity and a swimming force.

During the experiments the spermatozoa were suspended in a medium. Normally this is seminal fluid, but for research purposes Solusem boar semen diluent from AIM Worldwide is used as a medium.

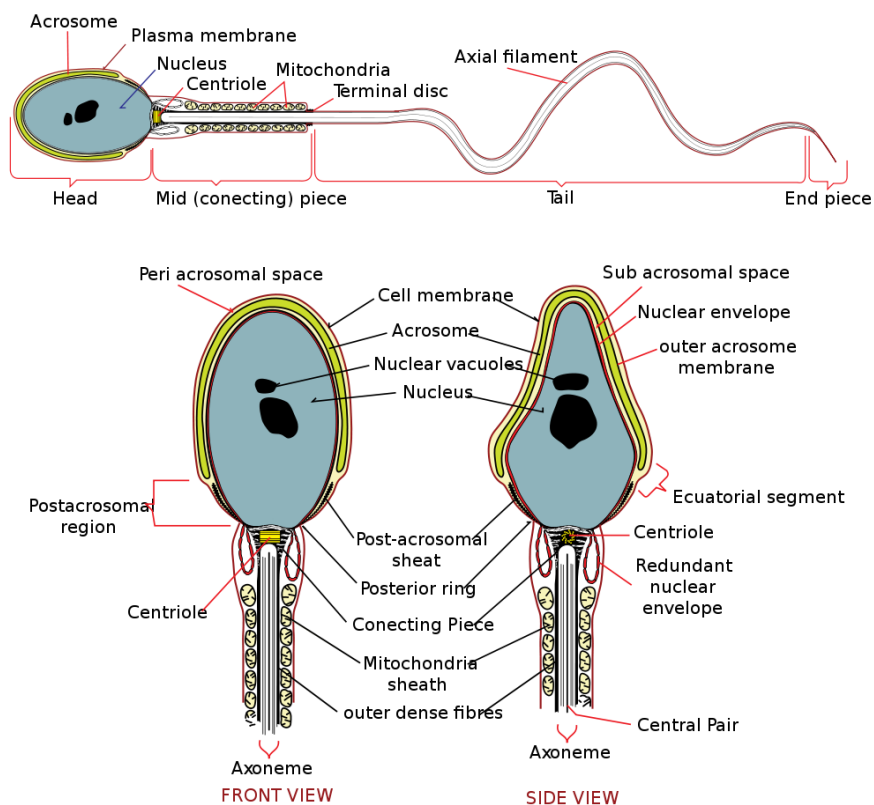


Figure 1 Spermatozoon [6].

2.3 Analysis

To determine the quality of semen there are a number of properties which can be assessed [1], these are the:

- Number of spermatozoa, can be expressed as a concentration or the total number.
- Total fluid volume, can be determined by weighting the sample, or by direct measurement.
- Vitality, the percentage of living cells. Cells with an intact cell membrane are vital. Living non-motile cells are counted as vital cells.
- Motility, only vital cells are used to determine the motility. There are three grades of motility:
 1. Progressive motility, cells are moving actively linearly or in large circles.
 2. Non-progressive motility, motile cells which are not moving progressively. These are hardly moving cells, or not moving cells with a propelling tail.
 3. Immotility, no movement at all.
- Morphology: the appearance of the cells.

2.4 Existing products and methods

Currently there are some products and methods to assess the semen quality, or to separate motile and non-motile spermatozoa.

2.4.1 Products

At this moment the ContraVac SpermCheck is one of the male fertility tests commercially available which does not require the use of a microscope (see Figure 2). This is a qualitative test of the number of spermatozoa. Other parameters such as motility and morphology are not tested.

The test measures the concentration of the protein SP-10. This protein is testis specific and is present in all males. SP-10 is present in the anterior segment of the acrosome of the sperm head and therefore the concentration of SP-10 can be related to the sperm count. A detergent is added to a semen sample to solubilize the acrosomal membranes of the spermatozoa and the protein is released. The sample is then applied to the nitrocellulose test strip where it rehydrates colloidal gold monoclonal antibodies that binds to SP-10. Due to capillary forces the solution migrates to a region where a second monoclonal antibody is dried onto the strip. These antibodies will bind to the gold-antibody-SP-10 complexes, resulting in a reddish color if the concentration is above a certain threshold [7, 8].

This test only gives a qualitative indication of the number of spermatozoa present. It does not take the motility in account and will give therefore limited insight in the sperm quality.

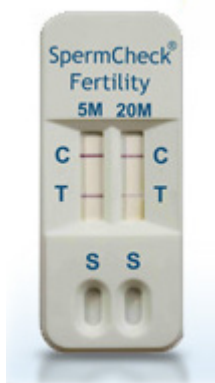


Figure 2 The SpermCheck Fertility test from ContraVac [9].

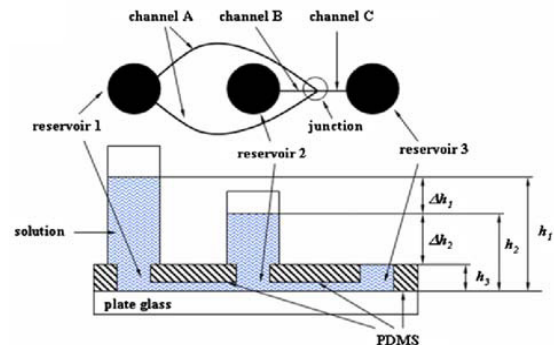


Figure 3 Motile sperm sorting device made by Seo et al. (2007) [4].

2.4.2 Separation methods

In literature several methods to separate motile and non-motile spermatozoa are presented. Three of those methods, which are making use of lab-on-a-chip technology, are discussed here.

Swimming against the flow

Seo et al. (2007) used the tendency of spermatozoa to swim against the flow to separate motile and non-motile spermatozoa. They designed a chip and introduces flow in the chip using hydrostatic pressure, see Figure 3. There are two inlets and one outlet in which the motile spermatozoa will be present. Reservoir 2 is the sample inlet and reservoir 1 is filled with media. Due to the height, h_1 , a higher hydrostatic pressure is present under reservoir 1 compared with reservoir 2. Therefore fluid from reservoir 1 will flow through channel A and B to reservoirs 2 and 3. The motile spermatozoa in reservoir 2 will swim against the flow in channel B, and after the junction the spermatozoa are flushed through channel C into reservoir 3. In this way the motility of bull sperm with a motility rate of about 20% in reservoir 2 is increased to a motility rate of 80% in reservoir 3 after 20 minutes. Different chips with the same layout show different behavior because the height differences vary [4].

Unfortunately nothing is reported about the absolute number of spermatozoa present in the in- and outlet, so the yield (the ratio of motile spermatozoa in the motile outlet to the total number of motile spermatozoa) remains unknown.

Crossing streamlines in a laminar flow

Cho et al. (2003) used the properties of laminar flows inside the channels on the chip. Particles inside a laminar flow tend to stay inside one streamline, because there is only diffusion and the diffusion coefficient of these particles is small, such that it takes long to diffuse in the other streamlines. However, motile spermatozoa inside a laminar flow can swim, and move from streamline to streamline. Motile spermatozoa will therefore be present in locations in the channel where non-motile spermatozoa and other cells cannot be present. This principle can be seen in Figure 4.

This principle is used in the design of the chip shown in Figure 5. There are two inlets, one for the sperm sample, and one for media. These two flows come together in one large

channel and the cells stays 20 seconds in this channel. The cells inside the sperm sample are focused to one side of the channel. The motile spermatozoa are able to swim to other places. The large channel is then split in two outlet channels. The focused sperm sample stream, which consists now of non-motile sperm, a leftover of motile sperm and other cells, is going to the non-motile outlet. The other part of the channel in which motile sperm is present is directed to the motile outlet. In Figure 6 the results of this chip are presented. In the outlet nearly 100% of the spermatozoa are motile, while the inlet motility rate is about 20%. The yield is about 40% [10].

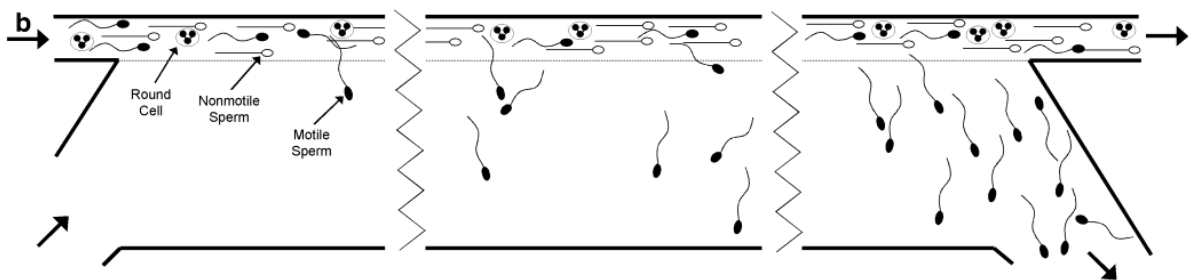


Figure 4 Drawing showing the working principle of the chip made by Cho et al. (2003) [10].

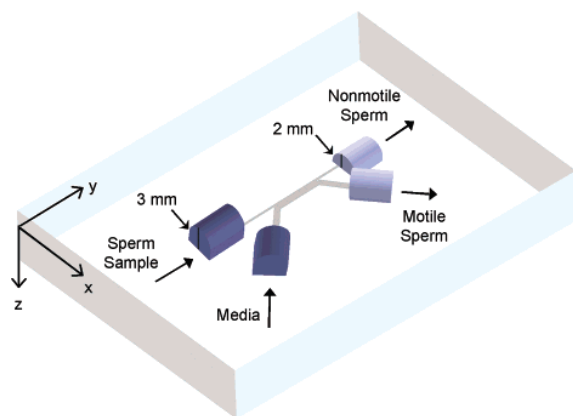


Figure 5 Motile sperm sorting device made by Cho et al. (2003) [10].

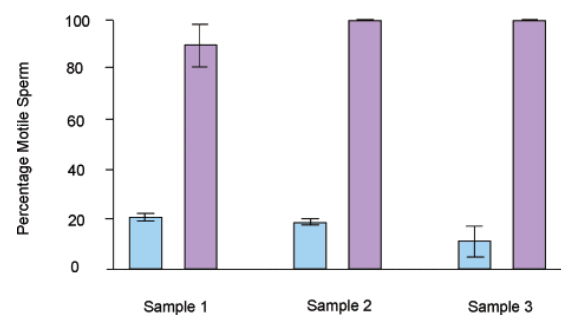


Figure 6 Motility rate of unsorted (blue) and sorted (purple) spermatozoa [10].

Optoelectronic

Ohta et al. (2010) have developed a chip which makes use of a photosensitive layer. The impedance of this layer can be changed due to exposure to light. Due to the impedance change, the electric field will also change. Light patterns create regions with low and high electric fields and the resulting gradient of the electric field can give rise to DEP forces. These forces are dependent on electrical and non-electrical properties of particles inside the electric field. Therefore DEP can be used to sort particles. The theory around DEP will be explained in more detail in chapter 2.5. Ohta made use of the differences in electrical properties in living and dead spermatozoa. These differences resulted in different forces on living and dead spermatozoa, and therefore different velocities of these cells, see Figure 7 [5].

Unfortunately the design of the chip is unknown and only the difference in velocity of the spermatozoa is mentioned. Nothing is said about the actual separation of spermatozoa. This study shows that DEP can be used to differentiate between living and dead spermatozoa.

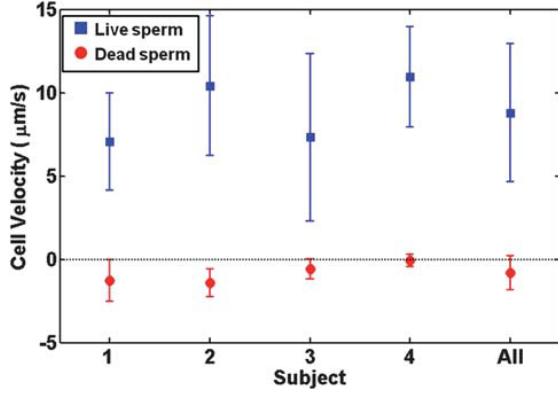


Figure 7 Different velocities of living and dead spermatozoa due to optoelectronic induced DEP forces [5].

2.5 Dielectrophoresis

Dielectrophoresis (DEP) is a phenomenon defined as “the motion of matter caused by polarization effects in a non-uniform electric field” [11]. DEP must not be confused with electrophoresis. The main difference between the two is that DEP is concerned with the motion of *uncharged* particles in *non-uniform* electric fields.

When a charged particle with charge q is placed in an electric field \mathbf{E} , it is attracted to the electrode with the opposite charge with a force \mathbf{F}_{ep} which is described by the following equation [11]:

$$\mathbf{F}_{ep} = q \cdot \mathbf{E} \quad (1)$$

An uncharged particle in a uniform electric field will be polarized, but is not attracted to one of the electrodes, see Figure 8. An uncharged particle placed in a non-uniform electric field will also polarize, but this particle is attracted to the side where the electric field is the strongest or the weakest, depending on the properties of the particle and the material in which the electric field is present. This will be explained in more detail later in this text. The case of a particle attracted to a stronger field can be seen in Figure 9, where the electric field on the left side of the particle is stronger than the electric field on the right side of this particle ($E_l > E_r$). The induced negative and positive charges are the same, and therefore $qE_l > qE_r$. This will cause a net force towards the negative electrode on the left which is called the DEP force. When the polarity of the electrodes in Figure 9 is reversed the positive charged particle will now move to the right side. But the neutral particle on the other hand will still move to the left side, because it will still move to the place with the strongest field! In alternating fields the mean force in time on a charged particle is zero, but this is not the case for the neutral particle. The field on the left side will always be stronger than the field on the right side, so the particle will move to the position with the strongest electrical field.

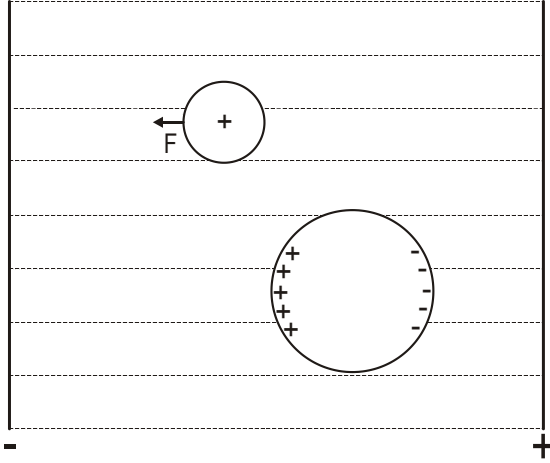


Figure 8 A neutral polarized, and a charged particle inside a uniform electric field [11].

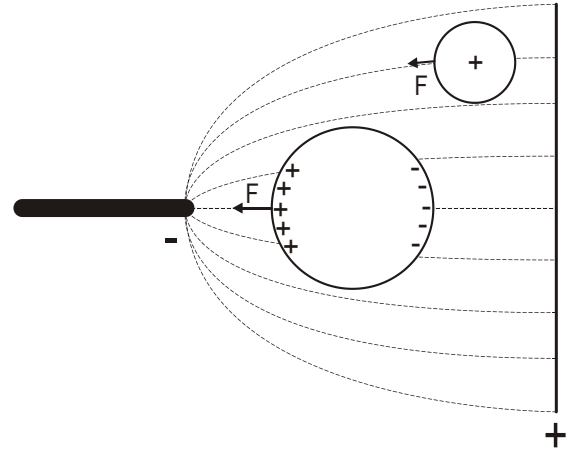


Figure 9 A neutral polarized, and a charged particle inside a non-uniform electric field [11].

Pethig deduces two equations to calculate the DEP force on *small* spherical or ellipsoid particles. Because the particles are small, the divergent electric field will not cause a change in polarization throughout the volume of the particle. Pethig based his deduction on work done by Pohl [11]. Pohl was one of the first who described DEP. His description is based on the in-phase dipole force [12]. Since then the term DEP broadened, and it includes all higher order forces and traveling wave forces as well. The deduction given by Pethig (based on Pohl) is given in the following text. Thereafter the more extended definition of DEP is given.

2.5.1 DEP force on a sphere (Pohl)

In a static field the force (F_{dep}) on a particle is given by:

$$F_{DEP} = (\mathbf{m} \cdot \nabla) \mathbf{E}$$

$$\mathbf{m} = \alpha V \mathbf{E} \quad (2)$$

$$F_{DEP} = \alpha V (\mathbf{E} \cdot \nabla) \mathbf{E} = \frac{\alpha V}{2} |\mathbf{E}|^2$$

in which \mathbf{m} is the dipole moment vector, α is the polarizability and V is the volume of the particle. The electric field inside this particle (\mathbf{E}_{in}) can be expressed by:

$$\mathbf{E}_{in} = \left(\frac{3\epsilon_{med}}{\epsilon_p + 2\epsilon_{med}} \right) \mathbf{E} \quad (3)$$

in which ϵ_p is the permittivity of the particle and ϵ_{med} is the permittivity of the medium. The induced polarization (\mathbf{P}) is given by:

$$\mathbf{P} = (\epsilon_p - \epsilon_{med}) \mathbf{E}_{in} \quad (4)$$

From this it follows that the direction of the polarization is dependent on the difference between the permittivities of the particle and the medium. The dipole moment is given by:

$$\mathbf{m} = V \mathbf{P} = \alpha V \mathbf{E} \quad (5)$$

When equation (3) is substituted in equation (4) and when subsequently equation (4) is substituted in equation (5), then the polarizability α per volume is given by:

$$\alpha = \frac{\mathbf{P}}{\mathbf{E}} = (\varepsilon_p - \varepsilon_{med}) \frac{\mathbf{E}_{in}}{\mathbf{E}} = \frac{3\varepsilon_{med}(\varepsilon_p - \varepsilon_{med})}{\varepsilon_p + 2\varepsilon_{med}} \quad (6)$$

When equation (6) is substituted in equation (2) the dielectrophoretic force acting on a small sphere ($V = 4\pi r^3/3$, with r the radius of the particle) is given by the following equation:

$$\mathbf{F}_{DEP} = 2\pi r^3 \varepsilon_{med} \left(\frac{\varepsilon_p - \varepsilon_{med}}{\varepsilon_p + 2\varepsilon_{med}} \right) \nabla |\mathbf{E}|^2 \quad (7)$$

From this equation it becomes clear that the dielectrophoretic force depends on three parameters.

1. The volume of the particle.
2. The intensity and gradient of the electric field.
3. The permittivity of the medium and the particle.

The DEP force will be negative when the permittivity of the medium is higher than the permittivity of the particle ($\varepsilon_{med} > \varepsilon_p$), this is called nDEP. A positive DEP force occurs when $\varepsilon_{med} < \varepsilon_p$ and is called pDEP.

2.5.2 DEP force on an ellipsoid (Pethig)

Equation (3) is valid when the particle is spherical. When the particle is an ellipsoid (with radii a, b, c) and the external electric field is parallel to a the internal electric field ($\mathbf{E}_{in,a}$) is given by [11]:

$$\mathbf{E}_{in,a} = \left(\frac{\varepsilon_{med}}{\varepsilon_{med} + L_a(\varepsilon_p - \varepsilon_{med})} \right) \mathbf{E} \quad (8)$$

in which L_a is the depolarization factor along a . The depolarization factor for an ellipsoid is given by the following equation [13]:

$$L_a = \frac{abc}{2} A_a \quad (9)$$

$$A_a = \int_0^\infty \frac{1}{(s+a^2)\sqrt{(s+a^2)(s+b^2)(s+c^2)}} ds$$

When equation (8) is substituted in (6), the DEP force for an ellipsoid ($\mathbf{F}_{DEP,e}$) can be calculated with the following equation [11]:

$$\mathbf{F}_{DEP,e} = \frac{2\pi abc}{3} \frac{\varepsilon_{med}(\varepsilon_p - \varepsilon_{med})}{\varepsilon_{med} + L_a(\varepsilon_p - \varepsilon_{med})} \nabla |\mathbf{E}|^2 \quad (10)$$

When the ellipsoid is actually a sphere ($a=b=c$), the depolarization factor L_a from equation (9) is equal to $1/3$. When this is substituted in equation (10), equation (10) becomes equal to equation (7), which is the equation describing the DEP force on a sphere.

2.5.3 DEP force, a broader definition

A more complete definition of the DEP force is based on the following equation [12]:

$$\mathbf{F}_{elec} = q\mathbf{E} + (\mathbf{m}\nabla)\mathbf{E} + \frac{1}{6}\nabla(\vec{Q}:\nabla\mathbf{E}) + \dots \quad (11)$$

\mathbf{F}_{elec} is the force a particles experiences in an electric field, \mathbf{m} is the dipole moment. The first term is the force charged particles experience inside an electric field. The other terms (including a quadrupole (\vec{Q}) and higher order terms) are due to induced dielectric polarization components. The DEP force consists of all these (complex) terms. Pohl described the DEP force of the real part of the second term of equation (11) [12]:

$$\mathbf{F}_{DEP} = (\mathbf{m}\nabla)\mathbf{E} = 2\pi r^3 \varepsilon_{med} Re\{f_{CM}(\omega)\} \nabla |\mathbf{E}|^2 \quad (12)$$

$$f_{CM}(\omega) = \frac{\varepsilon_p^*(\omega) - \varepsilon_{med}^*(\omega)}{\varepsilon_p^*(\omega) + 2\varepsilon_{med}^*(\omega)} \quad (13)$$

$$\varepsilon_j^*(\omega) = \varepsilon_j - \frac{j\sigma_j}{\omega} \quad (j = med, p) \quad (14)$$

Equation (13) is the so called ‘‘Clausius-Mossotti factor’’ (f_{cm}). This is a complex number and is determined by the complex permittivities $\varepsilon_j(\omega)$ (indicated with an *) of the particle and the medium. Equation (14) gives the definition of the complex permittivity in which ε_j is the dielectric constant, σ_j the conductivity and ω the frequency of the electric field [12]. When the Clausius-Mossotti factor is negative ($\varepsilon_{med} > \varepsilon_p$) the DEP force is negative (nDEP). When the Clausius-Mossotti factor is positive ($\varepsilon_{med} < \varepsilon_p$) the DEP force is positive (pDEP).

The time average DEP force ($\langle \mathbf{F}_{DEP} \rangle$) can be calculated using the root mean square (rms) value of the electric field intensity, see the following equation [12].

$$\langle \mathbf{F}_{DEP} \rangle = 2\pi r^3 \varepsilon_{med} Re\{f_{CM}(\omega)\} \nabla |\mathbf{E}_{rms}|^2 \quad (15)$$

The imaginary part of the second term of equation (11) will also contribute to the DEP force when a phase gradient is present, this is called a traveling wave dielectrophoretic force (\mathbf{F}_{TWD}). A phase gradient can only be present in a setup with more than two electrodes. The following equation gives the relation between the phase gradient and this force [14]:

$$\mathbf{F}_{TWD} = 2\pi \varepsilon_{med} r^3 Im\{f_{CM}\} (E_x^2 \nabla \varphi_x + E_y^2 \nabla \varphi_y + E_z^2 \nabla \varphi_z) \quad (16)$$

According to Hughes et al. (2002) the phase gradient can be rewritten as [15]:

$$\nabla \varphi = \frac{2\pi}{\lambda} \quad (17)$$

Then \mathbf{F}_{TWD} becomes [15]:

$$\mathbf{F}_{TWD} = \frac{4\pi^2 r^3 \varepsilon_{med} Im\{f_{CM}(\omega)\} \mathbf{E}^2}{\lambda} \quad (18)$$

In this study the time average DEP force from equation (15) will be used. In these equations it is assumed that the particle is a homogenous sphere. In reality the spermatozoa are not spheres and are not homogenous. To overcome this problem the ‘‘single shell’’ approximation for the permittivity of the particle can be used. This approximation is explained in chapter 2.6 in more detail.

The electric field involved in the DEP force results from a potential drop over the electrical resistance between the two electrodes. A model in which this resistance is calculated is explained in chapter 2.7.

2.5.4 Other forces

Besides the DEP force the spermatozoa experience other forces as well. The most important are the drag force due to laminar fluidic flow and, when the cells are motile, a swimming force. The net force (F_{result}) acting on the cells resulting from these three forces is shown in Figure 10 and Figure 11. In the first picture the forces on a motile spermatozoon are shown. In the second picture the forces on a non-motile spermatozoon are shown.

The DEP force is also dependent on the electrical properties of the cell. Therefore the DEP force will be different for dead and living spermatozoa.

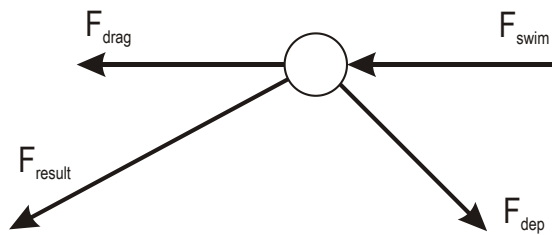


Figure 10 Forces on motile spermatozoa.

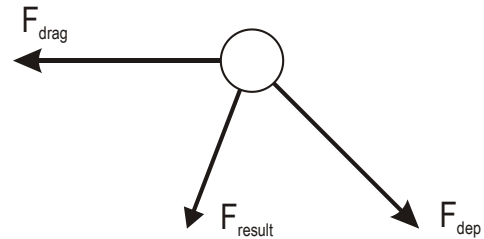


Figure 11 Forces on non-motile spermatozoa.

Drag force

Particles inside a fluidic flow will experience a drag force. In a situation with laminar flow this drag force can be calculated with the following equation [16]:

$$F_{drag} = 6\pi\eta r v \quad (19)$$

In this equation η is the viscosity of the fluid, v the velocity difference between the fluid and the particle and r the radius of the particle.

Swimming force

The swimming force and velocity of spermatozoa of four different primates (including human) has been determined by Nascimento et al. (2008). The result of this research is showed in the box plot in Figure 12. The first box plot shows the swim velocity of spermatozoa of four different primates. The second box plot shows the swimming force of these primates. The results of the human spermatozoa are shown in the third column. It can be seen in the inset that the median of the swimming force of human spermatozoa is 4 pN [17].

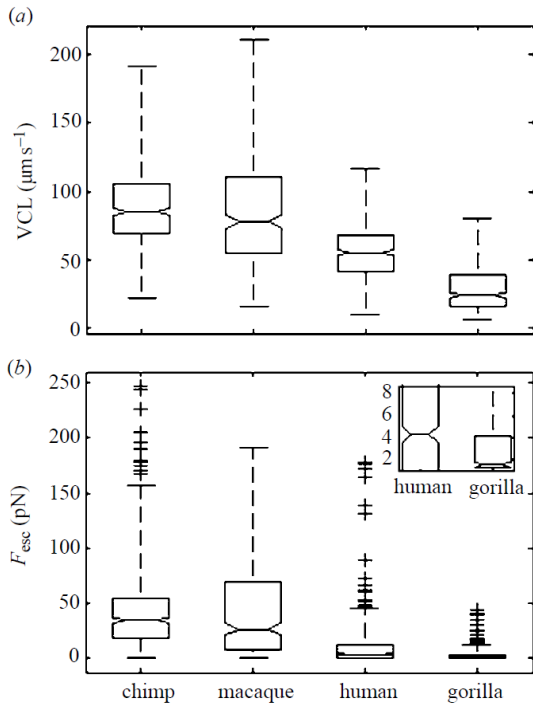


Figure 12 Swim velocity and swimming force [17].

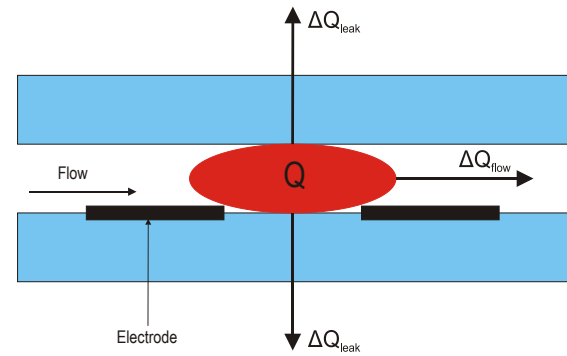


Figure 13 Heat generation.

2.5.5 Side effects

Some side effects of the DEP force can pose a danger on living cells. Heat production due to electrical energy loss in fluid and the high electric fields present can damage cells.

Heat

Due to the resistivity of the fluid between the two electrodes, which are used to generate the electrical field, electrical energy is lost. This energy is transformed into heat energy and the temperature of the fluid will increase. The total amount of thermal energy released W is dependent on the resistance between the electrodes R_{el} and the voltage V_{Rel} across the electrodes ($W=V_{Rel}^2/R_{el}$). The generated heat will leak through the glass walls and is transferred with the fluid due to the flow of this fluid. Figure 13 gives an overview of the situation. In this picture the channel can be seen as the white space between two plates (blue layers). The generation of heat is shown as the red area. The heat flows are the three arrows. As can be seen in this picture heat will leak through the glass plates (ΔQ_{leak}) and is carried away due to the fluid flow (ΔQ_{flow}).

The heat flow through the plates (thermal conduction) can be described by the following formula [18]:

$$\frac{\Delta Q_{leak}}{\Delta t} = kA \frac{\Delta T}{x} \quad (20)$$

In this equation ΔQ_{leak} is the conducted heat, Δt is the time in which the heat is conducted, k is the thermal conductivity of the material, A is the area of the conducting surface, ΔT is the temperature increase due to the generated heat (temperature difference between the channel and the surrounding) and x is the thickness of the heat conducting material. If Δt is 1 second, then the left side (and the right side) of the equation is expressed in Watt.

With this equation it is possible to calculate the amount of heat energy which is transferred through the glass of the chip when the temperature of the fluid inside the channel increases a certain amount. Only the heat energy transferred through the bottom and top layer of the channel are taken into account (2 times ΔQ_{leak}). The energy transferred through the sides of the channel is neglected. It is known how much electrical energy is turned into heat. Therefore it is also known how much energy needs to be dissipated due to the fluid flow to maintain a constant temperature ($Q_{fluid} = Q_{electrical, dissipated} - 2 \cdot Q_{leak}$, in which $Q_{electrical, dissipated}$ is the dissipated electrical energy). This is where the specific heat capacity of the fluid comes into play.

The specific heat capacitance c of a material tells how much the temperature increases per volume due to supplied heat energy. This is described by the following equation [19]:

$$Q_{fluid} = cV\Delta T \quad (21)$$

In this equation Q_{fluid} is the amount of heat energy added to the material, V is the volume and ΔT the temperature increase. Because it is known how much heat energy per second must be dissipated due to the fluidic flow to maintain a certain constant temperature, it can be calculated what the total volume (V) of the fluid per second is to maintain this.

Electroporation

The electric field used for the DEP force will cause charging of the cell membrane. When the membrane potential difference is about 500 mV to 1 V membrane breakdown occurs [20] and the membrane will become permeable for ions, this is called electroporation [20]. The membrane can be irreversibly damaged, but this is not necessary. To calculate the membrane potential (V_m) of a cell inside an electric field the following formula can be used [20]:

$$V_m = \frac{r \cdot E \cdot 1.5 \cdot \cos(\alpha)}{\sqrt{1 + (2\pi f\tau)^2}} \quad (22)$$

$$\tau = rC_m(\rho_i + 0.5\rho_m)$$

In this equation r is the radius of the cell, E the electric field intensity, $\cos(\alpha)$ the angle at which the electric field enters the cell, f the frequency of the electric field. C_m , ρ_i and ρ_m are the specific membrane capacitance and the specific resistances of the cell interior and membrane respectively.

To prevent electroporation of the spermatozoa the potential across the electrodes and its frequency must be chosen such that the membrane potential will not exceed 500 mV.

2.5.6 Usage of DEP

DEP can be used for different purposes. In this paragraph a few of these purposes which are described in literature are reviewed.

Sorting

Sorting of living and dead cells is a common application of DEP. The cell membrane of dead cells is defective and therefore permeable to ions, this results in a higher conductivity of the cell interior than of living cells. Therefore the Clausius-Mossotti factor between dead and living cells is different. This can be used to separate these cells. An example is the separation of viable and non-viable yeast cells [21].

Traveling wave force (TWF)

TWF can be used as a pumping mechanism. When particles experience this force they will accelerate. TWF can also be used to give different kind particles a different specific velocity. Because TWF is also dependent on the Claussius-Mossotti factor, see equation (16), there is a positive and a negative variant.

Field-flow fractionation (FFF)

With field flow fractionation the flow profile of the fluid is used to separate different particles. A negative DEP force is used to position particles at different position in the flow based on the DEP response. Because the flow rate at the walls of the channel is lower than in the center of the channel, particles will move slower near the channel walls. So different kinds particles will have a different specific velocity [12, 14, 15].

Focusing

DEP can be used to focus particles inside a channel. Randomly spread particles can be focused to a specific position in the channel due to a negative DEP force [22], see Figure 14

Trapping

Trapping of cells can be done with DEP. This is often done with a four electrode setup as can be seen in Figure 15. Fuhr et al. (1998) reports that they are able to trap spermatozoa. The negative DEP force from the electrodes prevents that the cell can escape from the center. A remarkable side effect of this setup is the temporarily stop of motion from the spermatozoa after they were trapped [23]. Probably this is due to electroporation due to the high electric fields involved. Heida (2002) uses DEP to trap neuron cells in a similar setup [20].

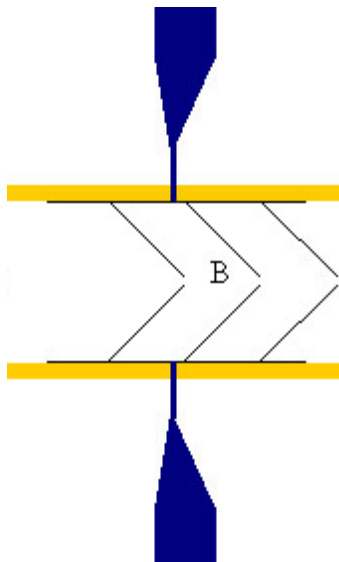


Figure 14 DEP focusing, particles are focused in the center of the channel [22].

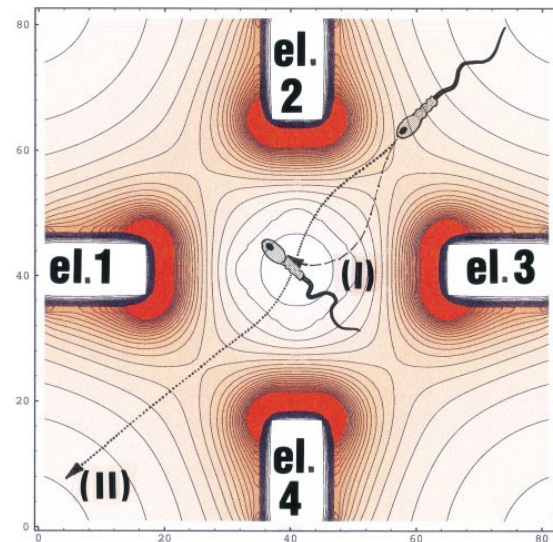


Figure 15 Quadrupole electrode setup for sperm trapping [23].

2.6 Single Shell

The electrical properties of a spermatozoon are needed to calculate the DEP force. A spermatozoon is not a homogenous particle. Without the tail the spermatozoon can be seen as a conducting sphere (the cytoplasm) with permittivity ϵ_i and with an insulating shell with permittivity ϵ_m (the cell membrane), see Figure 16. The radius of the shell is r and the thickness of the shell is d . C_m is the membrane capacitance per unit area.

The equivalent permittivity of a cell can be approximated with the single shell model [5, 24, 25]. Unfortunately there are different equations used for this model. The equation used by Burgarella et al. (2007) is equation (23) [25] which is equal to equation (24) which is used by Asami et al. (2002) [24]. Ohta uses a simplification, because the membrane thickness is very small compared to the total radius of the cell ($d \ll r$) [5]. It is unclear how the rest of this equation is deduced from the other equations. To check the simplification all three equations are used to calculate the effective permittivity of human B-lymphocytes. The parameters used are the same as Burgarella uses for his calculations [25]. These are given in Table 1. Maplesoft Maple 13 (2009) is used for the calculations. In appendix A.1 the used Maple-sheet can be found. The outcome is shown in Table 2. The absolute value of the outcome of the simplification used by Ohta differs only 0.23% from the absolute value of the other two equations. Therefore it can be assumed that the simplification from Ohta is. To calculate the DEP force, the simplification shown in equation (25) is used to calculate permittivity of a spermatozoon.

Burgarella:
[25]

$$\varepsilon_p^* = \varepsilon_m^* \left(\frac{\left(\frac{r}{r-d}\right)^3 + 2 \left(\frac{\varepsilon_i^* - \varepsilon_m^*}{\varepsilon_i^* + 2\varepsilon_m^*}\right)}{\left(\frac{r}{r-d}\right)^3 - \left(\frac{\varepsilon_i^* - \varepsilon_m^*}{\varepsilon_i^* + 2\varepsilon_m^*}\right)} \right) \quad (23)$$

Asami:
[24]

$$\varepsilon_p^* = \varepsilon_m^* \left(\frac{2\varepsilon_m^* + \varepsilon_i^* - 2v(\varepsilon_m^* - \varepsilon_i^*)}{2\varepsilon_m^* + \varepsilon_i^* + v(\varepsilon_m^* - \varepsilon_i^*)} \right) \quad (24)$$

$$v = \left(1 - \frac{d}{r}\right)^3$$

Ohta:
[5]

$$\varepsilon_p^* = \frac{rC_m\varepsilon_i^*}{\varepsilon_i^* + rC_m} \quad (25)$$

$$C_m = \frac{\varepsilon_m - j\sigma_m}{d}$$

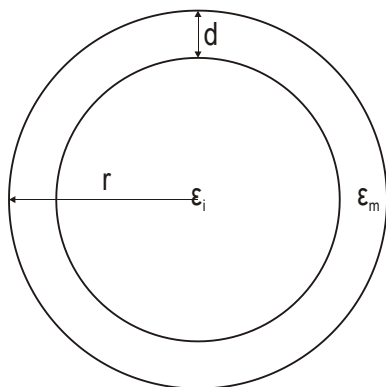


Figure 16 Single Shell model

Table 1 Properties of B-lymphocytes [25].

Property	Value
Radius (r)	8 μm
Membrane thickness (d)	8 nm
Permittivity membrane (ϵ_m)	$3 \cdot 8.85 \cdot 10^{-12}$ F/m
Conductivity membrane (σ_m)	3 $\mu\text{S/m}$
Permittivity interior (ϵ_i)	$50 \cdot 8.85 \cdot 10^{-12}$ F/m
Conductivity interior (σ_i)	0.45 S/m

Table 2 Outcome of equations (23), (24) and (25).

Who	Particle permittivity (ϵ_p^*)
Burgarella	$6.1492 \cdot 10^{-9} - j1.0792 \cdot 10^{-8}$
Asami	$6.1492 \cdot 10^{-9} - j1.0792 \cdot 10^{-8}$
Ohta	$6.1734 \cdot 10^{-9} - j1.0813 \cdot 10^{-8}$

2.7 Electrochemical cell

The potential difference between the electrodes in contact with the electrolyte is not only dependent on the applied potential difference at the connections to the outside world, but also on some other resistances and capacitances in series and parallel to the electrolyte resistance. The resistance of the electrodes, the capacitance between these electrodes and the double layer capacitance also play a role. The potential difference resulting in a DEP force is the potential difference over the “resistance” of the electrolyte (R_{el}) [26]. This resistance is also important for the calculation of the dissipated energy inside the solution. Because of this dissipation the temperature of the solution will rise, which can influence the fluidic flow or can damage the cells [15].

An electrical model of the electrochemical cell can be seen in Figure 17. A formula for the total impedance of this model can be found in equation (26). The absolute value of this complex number is plotted in Figure 18. The first plateau corresponds with the value of R_{el} , and the second plateau corresponds with R_{lead} .

As explained earlier the electrical field responsible for the DEP force is due to the potential drop over R_{el} . To get most of the potential difference applied to the electrodes over R_{el} the frequency must be chosen such that it is in the range of the first plateau.

$$Z_{cell} = (R_{lead1} + R_{lead2}) + \left(\frac{X}{j\omega X C_{cell} + 1} \right) \quad (26)$$

$$X = \frac{1}{j\omega C_{d11}} + \frac{1}{j\omega C_{d12}} + R_{el}$$

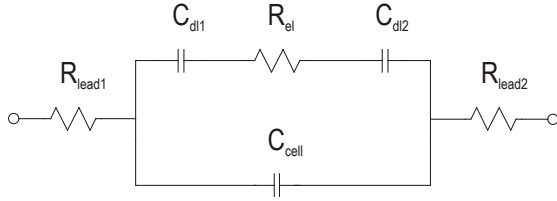


Figure 17 Electrical circuit model of an electrochemical cell.

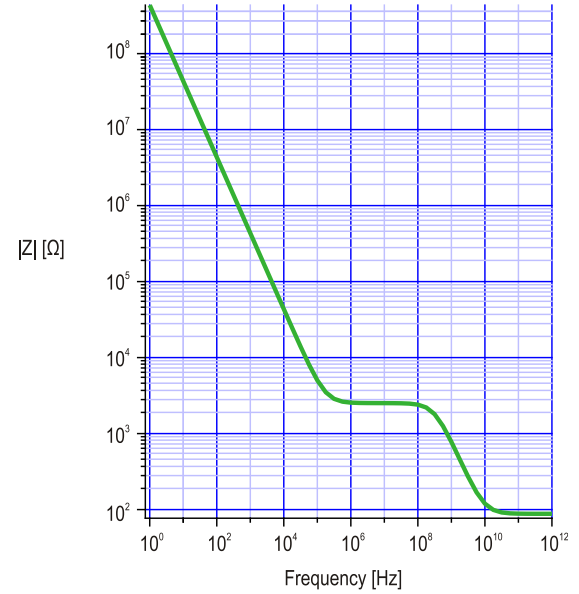


Figure 18 Typical impedance curve of an electrochemical cell

The values of R_{el} and C_{cell} can be calculated by using the conductivity and the permittivity of the fluid and the cell constant κ . The cell constant is dependent on the geometry of the electrodes. The cell constant for *two* electrodes can be calculated with the following equations [27]:

$$\kappa = \frac{2}{L} \frac{K(k)}{K(\sqrt{1-k^2})}$$

$$K(k) = \int_0^1 \frac{1}{\sqrt{(1-t^2)(1-k^2t^2)}} dt \quad (27)$$

$$k = \frac{s}{s+2w}$$

In these equations L is the length of the electrodes, w the width and s the distance between the two electrodes.

The resistance R_{el} can be calculated with the cell constant and the conductivity of the medium (σ_{med}) with the following equation [27]:

$$R_{el} = \frac{\kappa}{\sigma_{med}} \quad (28)$$

The capacitance C_{cell} can be calculated with the following equation in which ϵ_{med} is the absolute permittivity of the medium [27]:

$$C_{cell} = \frac{\epsilon_{med}}{\kappa} \quad (29)$$

The two double layer capacitances C_{dl} (one for each electrode) consists of two capacitances in series. The first is the Stern layer capacitance, which is not dependent on the electrolyte concentrations. The second is the diffusion layer capacitance, which is dependent on the electrolyte concentrations. However, for solutions with a high ionic strength the double

layer capacitance per area can be approximated by the Stern layer capacitance which capacitance is between 10 to 20 $\mu\text{F}/\text{cm}^2$ [28]:

$$C_{dl,square} \approx C_{stern,square} = 10 - 20 \mu\text{F}/\text{cm}^2 \quad (30)$$

The double layer capacitance C_{dl} can be calculated with the following equation [28]:

$$C_{dl} = 0.5 \cdot w \cdot L \cdot N \cdot C_{dl,square} \quad (31)$$

in which w is the width of the electrodes, L the length of the electrodes and N the number of electrodes.

All the information to calculate R_{el} is now known, therefore all the information to calculate the electric field for the DEP force is known.

3 Simulations

Before a design is made, it is desirable to get some insight in the DEP force and its dependence on the geometry of the electrodes. Furthermore some estimates about the needed voltage and frequency are needed for the experiments.

It is very difficult to calculate the created electrical field in space by two planar electrodes. The electrical field strength in space is necessary to calculate the DEP force, see equation (15). Therefore the electrical field is simulated with a finite element model. This model is made and simulated with Comsol AB. Comsol Multiphysics 3.5a (2008).

For the simulations a geometry is needed, because the simulation results depends on the dimensions of the electrodes and the fluidic channel. As a starting point the geometry of an already existing chip is used, with slight modifications. This existing chip was used for some first measurements of a DEP force acting on beads [29]. The width and the distance between the electrodes are taken a factor $\sqrt{2}$ smaller. Another modification is the addition of focusing electrodes. The focusing electrodes will focus the spermatozoa in a certain region in the fluidic channel. The width of and distance between these focusing electrodes are the same as the used sorting electrodes. The angle of the electrodes with the channel walls is 45° . This geometry can be seen in Figure 19. In a second geometry the angle of the electrodes is changed to 60° .

In paragraph 3.1 the permittivity of a spermatozoon and the Claussius-Mossotti factor are estimated. The electric field responsible for the DEP force is dependent on the voltage across R_{el} . To calculate this voltage all the impedances in the electrochemical cell model must be calculated. This is done in paragraph 3.2. The Claussius-Mossotti factor and the electrochemical cell impedance leads to an optimal frequency of the applied voltage responsible for the DEP force. The simulations of the electric field and the DEP force are discussed in paragraph 3.4.

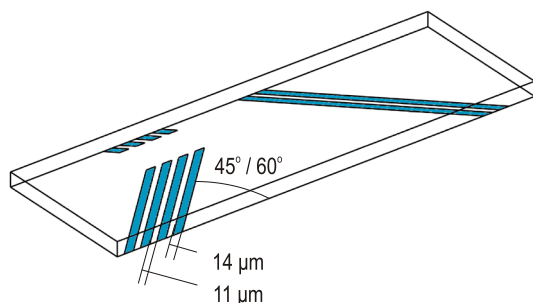


Figure 19 3D geometry used for the simulations. The electrodes are blue regions. The electrodes on the left side are used to focus the spermatozoa. The longer electrodes on right side are used for sorting. These last electrodes are used in the calculations of the electrochemical cell.

3.1 Single shell permittivity

The permittivity of a spermatozoon is needed to calculate the Claussius-Mossotti factor and is thus of importance for the DEP force. The single-shell model is used to calculate this permittivity. Therefore a spermatozoon is simplified to a conducting sphere with a thin non-conducting shell. To estimate the permittivity of a spermatozoon Ohta et al. (2010) uses the input parameters given in Table 3 [5]. The Claussius-Mossotti factor with three types of medium are calculated, one for a medium with a conductivity of 0.01 S/m, one for a medium with a conductivity of 0.7 S/m, and another with a conductivity of 1.4 S/m. Equation (32) (equal to equation (25)) is used to calculate the permittivity of a spermatozoon. Equation (33) (equal to equation (14)) is used to plot the Claussius-Mossotti factor. The plots are made with Maplesoft Maple 13 (2009), see appendix A.4.

$$\varepsilon_p^* = \frac{rC_m\varepsilon_i^*}{\varepsilon_i^* + rC_m} \quad (32)$$

$$C_m = \frac{\varepsilon_m - j\sigma_m}{d}$$

$$f_{CM}(\omega) = \frac{\varepsilon_p^*(\omega) - \varepsilon_{med}^*(\omega)}{\varepsilon_p^*(\omega) + 2\varepsilon_{med}^*(\omega)} \quad (33)$$

In Figure 20 the real part of the Claussius-Mossotti factor is plotted for living (green) and dead (red) spermatozoa inside a medium with a conductivity of 0.7 S/m. At frequencies above 10 MHz the living cells experience a positive DEP force while the dead cell experience no DEP force at all (the Claussius-Mossotti factor is equal to 0).

In Figure 21 the conductivity of the medium is increased to 1.4 S/m. In this case a difference in the negative DEP force experienced by living and dead spermatozoa in the 5 MHz to 200 MHz band can be seen. In this band the living spermatozoa experience a more negative force.

In Figure 23 the conductivity of the medium is decreased to 0.01 S/m. In this case a positive DEP force is experienced by living cells above 5 kHz, while the dead spermatozoa experience a negative or no DEP force.

Later in this chapter the plotted Claussius-Mossotti factors are used to calculate the DEP force on spermatozoa.

Table 3 Single shell input parameters.

Parameters		Value (living)	Value (dead)
Radius of the cell (r)	[5]	3.29 μm	3.29 μm
Cell membrane capacitance (C_m)	[5]	0.0126 F/m ²	0.0126 F/m ²
Permittivity of the cell interior ($\varepsilon_{i,r}$)	[5]	154·8.85·10 ⁻¹² F/m	Same as medium
Conductivity of the cell interior (σ_i)	[5]	0.73 S/m	Same as medium
Permittivity of the medium 1 ($\varepsilon_{med,r}$)		78·8.85·10 ⁻¹² F/m	78·8.85·10 ⁻¹² F/m
Conductivity of the medium 1 (σ_{med})		0.7 S/m	0.7 S/m
Permittivity of the medium 2 ($\varepsilon_{med,r}$)		78·8.85·10 ⁻¹² F/m	78·8.85·10 ⁻¹² F/m
Conductivity of the medium 2 (σ_{med})		1.4 S/m	1.4 S/m
Permittivity of the medium 3 ($\varepsilon_{med,r}$)		78·8.85·10 ⁻¹² F/m	78·8.85·10 ⁻¹² F/m
Conductivity of the medium 3 (σ_{med})		0.01 S/m	0.01 S/m

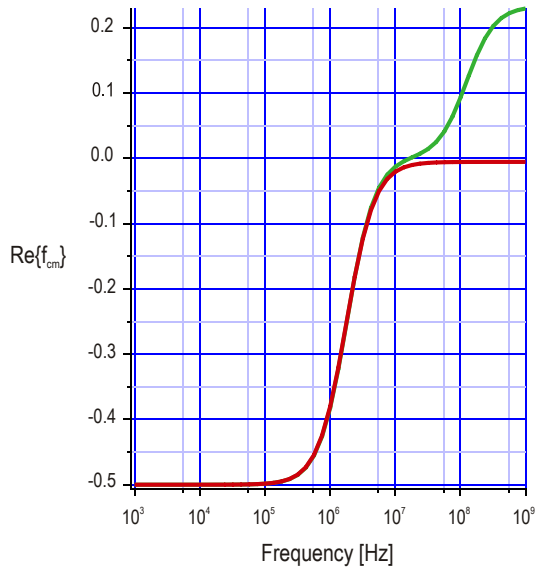


Figure 20 Output: real part of the Claussius-Mossotti factor for living (green) and dead (red) spermatozoa in a medium with a conductivity of 0.7 S/m.

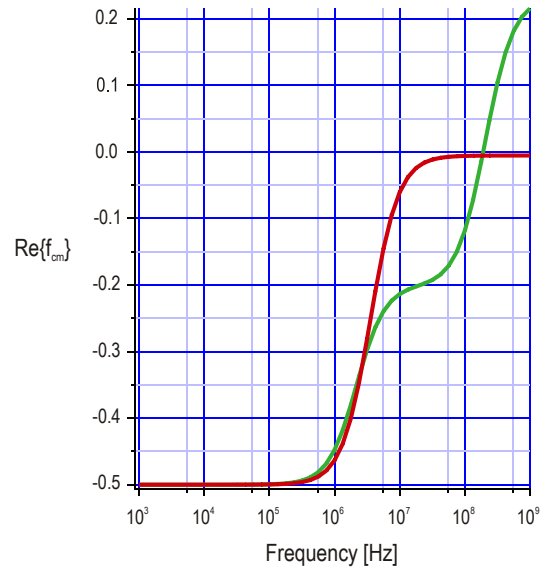


Figure 21 Output: real part of the Claussius-Mossotti factor for living (green) and dead (red) spermatozoa in a medium with a conductivity of 1.4 S/m.

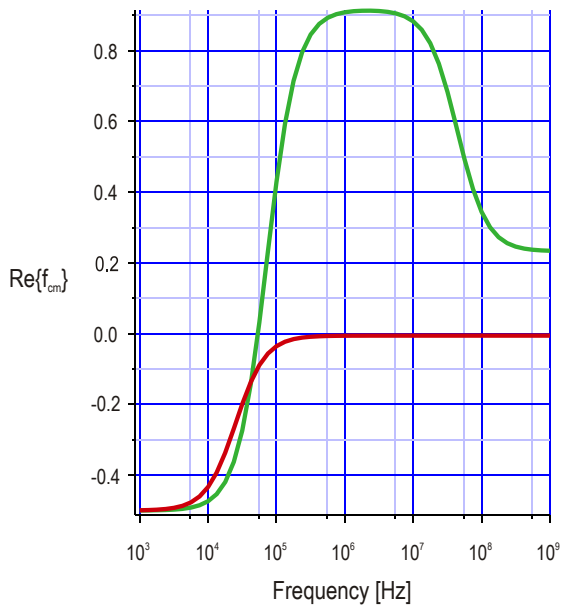


Figure 22 Output: real part of the Claussius-Mossotti factor for living (green) and dead (red) spermatozoa in a medium with a conductivity of 0.01 S/m.

3.2 Electrochemical cell

The voltage across the resistance R_{el} in the electrochemical cell model is needed to calculate the DEP force. Therefore all impedances involved in this model are needed. These impedances are calculated for the model with 45° and 60° electrodes.

The cell constant κ must be known to calculate R_{el} and C_{cell} . The double layer capacitance depends on the area of the electrodes and the stern layer capacitance per unit area. It is estimated that this value is about 15 $\mu\text{F}/\text{cm}^2$ (which is between 10 and 20 $\mu\text{F}/\text{cm}^2$, see chapter 2.7). The lead resistance is estimated to be 44 Ω . This value is based on the dimensions of the platinum electrodes of the existing chip [29]. All the input parameters can be found in Table 4.

A Maplesoft Maple 13 (2009) worksheet (see appendix A.2) is used to calculate the cell constant and all the impedances. The results of these calculations can be found in Table 5. The absolute value of the electrochemical cell impedance is plotted in Figure 23 and Figure 24 for the 60° and 45° electrodes respectively. These plots are made with Maple, the Maple input can be found in appendix A.3. In this plot it can be seen that the plateau, resulting from R_{el} , starts at 1 MHz and ends at 100 MHz. To get most of the source voltage over R_{el} , the input voltage frequency must be between 1 and 100 MHz.

Together with the Claussius-Mossotti plot in Figure 20, the optimal input frequency can be determined. When a distinction between motile and non-motile spermatozoa must be made based on the presence of a swimming force which is counteracting the DEP force, the difference in DEP force between vital and non-vital spermatozoa is not important. However all the cells must experience a negative DEP force, therefore the input frequency must be somewhere between 1 and 10 MHz. The Claussius-Mossotti factor is in this case between -0.5 and 0. This frequency range is also in the range of the first impedance plateau.

Table 4 Input parameters electrochemical cell.

Parameter	60° electrodes	45° electrodes
Conductivity medium (σ_{med}) [S/m]	0.7 S/m	0.7 S/m
Permittivity medium (ϵ_{med})	78·8.85·10 ⁻¹² F/m	78·8.85·10 ⁻¹² F/m
Stern layer capacitance ($C_{stern,square}$)	15 $\mu\text{F}/\text{cm}^2$	15 $\mu\text{F}/\text{cm}^2$
Lead resistance (R_{lead})	44 Ω	44 Ω
Electrode width (w)	14.1 μm	14.1 μm
Electrode length (L)	346 μm	424 μm
Distance between electrodes (s)	10.6 μm	10.6 μm

Table 5 Output of the electrochemical cell model.

Parameter	60° electrodes	45° electrodes
Cell constant (κ)	3408 m ⁻¹	2781 m ⁻¹
Resistance (R_{el})	4868 Ω	3972 Ω
Double layer capacitance (C_{dl})	0.7318 nF	0.8968 nF
Parasitic electrode capacitance (C_{cell})	0.2026 pF	0.2482 pF

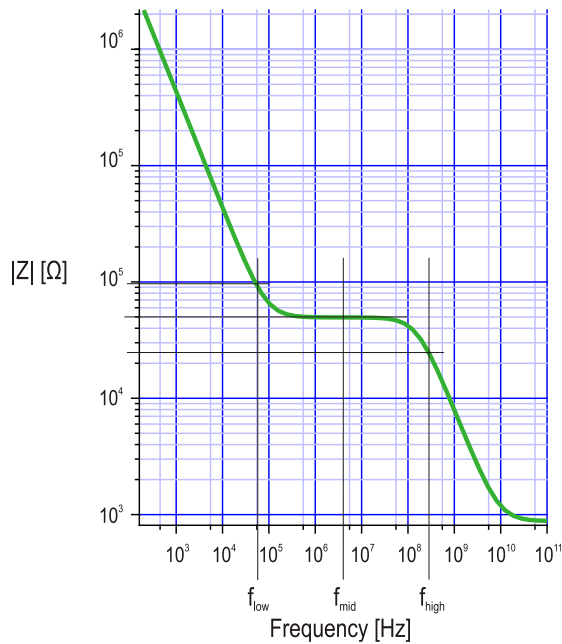


Figure 23 Impedance of the electrochemical cell with 60° electrodes in a medium with a conductance of 0.7 S/m.

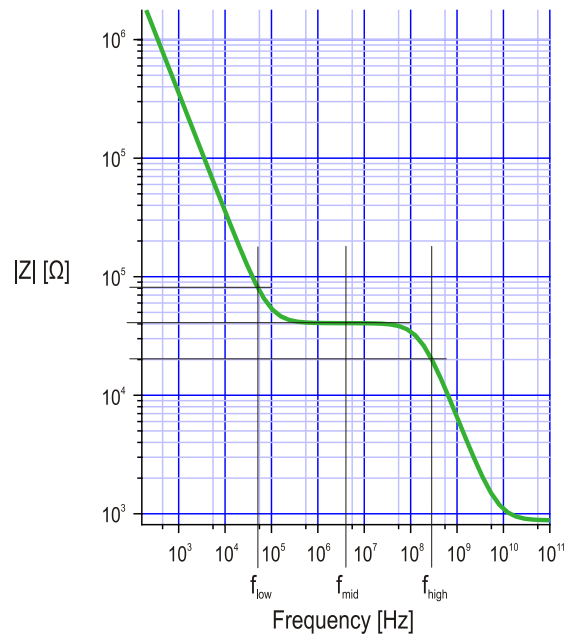


Figure 24 Impedance of the electrochemical cell with 45° electrodes in a medium with a conductance of 0.7 S/m.

3.3 Circuit simulation

With all the impedances known, the voltage across the resistor R_{el} can be calculated. Linear Technology Corporation LTspice IV (2011) is used for this simulation (see Appendix B for the LTspice IV model).

The amplitude of the source is 5 V and the input frequency is 5 MHz. The input parameters used are the values calculated with the electrochemical cell model shown in Table 5. The voltage over R_{el} is responsible for the DEP force. The average DEP force can be determined with the rms voltage. The maximum and rms voltage can be found in Table 6. To limit the number of subsequent simulations the voltage generating the DEP force is chosen to be 3.40 V_{rms} .

Table 6 LTspice output, voltage over R_{el} .

<i>Parameter</i>	<i>60° electrodes</i>	<i>45° electrodes</i>
Maximum voltage	4.83 V	4.81 V
Rms voltage	3.41 V	3.40 V

3.4 DEP

To simulate the DEP force a finite element simulation is performed. Comsol 3.5a is used for this. A specific geometry is needed for these simulations. The used geometry is discussed in paragraph 3.4.1. The equations solved by Comsol must be specified, therefore boundary conditions and physics are applied to the geometry, which is described in paragraph 3.4.2. Comsol calculates the electrical field inside the channel and this field is used to calculate the DEP force. These results can be found in paragraph 3.4.3.

3.4.1 Geometry

Only the electrical field inside the medium in the channel is of interest. Therefore the channel is modeled as a block (3D). On the bottom of this block the electrodes are placed. These are flat (2D) and divide the bottom into different boundaries. Two kinds of electrodes are present. There are the focusing electrodes used to focus the cells into a specific position inside the channel. The other kind are the sorting electrodes, used to differentiate between the motile and non-motile cells. The dimensions of these electrodes are the same (angle with the channel wall, width of and distance between the electrodes). Simulations are performed on a geometry with 60° electrodes and on a geometry with 45° electrodes. These geometries with all the dimensions are shown in Figure 25 and Figure 26 respectively.

To be able to calculate the electrical field, the structure is divided into small elements, which is called “meshing”. The structure is automatically meshed with the “initialize mesh” and “refine mesh” functions in Comsol until about 150,000 elements were present.

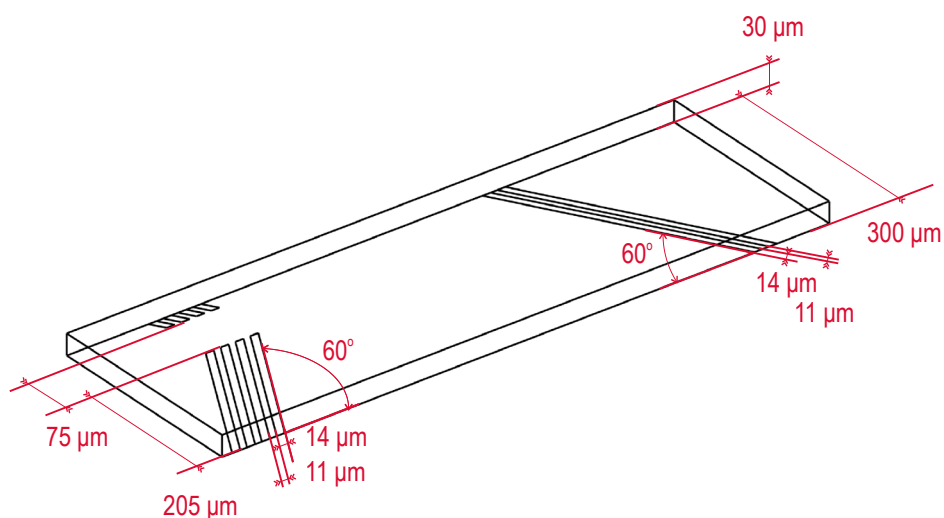


Figure 25 Dimensions of the modeled channel with 60° electrodes.

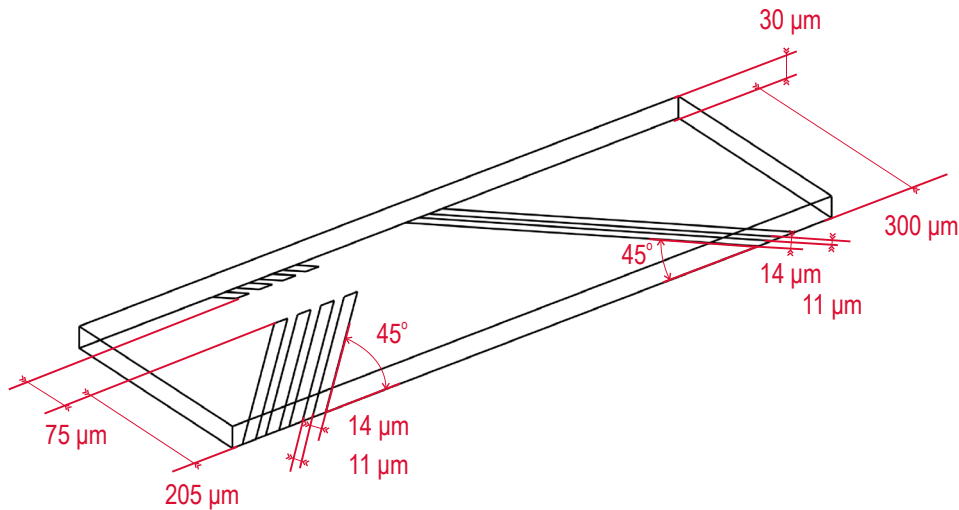


Figure 26 Dimensions of the modeled channel with 45° electrodes.

3.4.2 Physics

Comsol needs to know what to calculate in which part of the geometry. A part of the geometry is called a “subdomain”. In this case there is only one subdomain. This subdomain is the block consisting of the inside of the channel. The following parameters are set:

- Constitutive relation: $\mathbf{D} = \epsilon_0 \epsilon_r \mathbf{E}$; Field inside a non-polarized material
- External current density (\mathbf{J}^e): $(0, 0, 0)$; No external current
- Electric conductivity (σ): 0.7 S/m ; Conductivity of the medium
- Relative permittivity (ϵ_r): 78 ; Relative permittivity of the medium

The boundary conditions for the equations to be solved must be set. In this case there are four kinds of boundaries.

1. The walls of the channel which are made of glass.
2. The cross-section of the channel which is made of the medium inside the channel.
3. The electrodes with an electrical potential.
4. The electrodes which are connected to ground.

The walls and the cross-section of the channel are defined as “electrical insulating”, because no currents will flow through these boundaries. The boundary condition of one electrode of an electrode pair is defined as “electrical potential”, the potential of the sorting electrodes can be set separately from the potential of the focusing electrodes. The other electrode of an electrode pair is defined as “ground”. These boundary conditions are depicted in Figure 27.

The potential at the focusing and sorting electrodes are set at the same value in these simulations. The value used is the rms voltage resulting from the circuit simulations in chapter 3.3, see Table 6. Because negative DEP is desired, the value of the Claussius-Mossotti (CM) factor must be negative. At 2 MHz the CM factor is -0.22 which is in between the maximum (0) and minimum value (-0.5). All the input parameters used in the Comsol simulation are listed in Table 7.

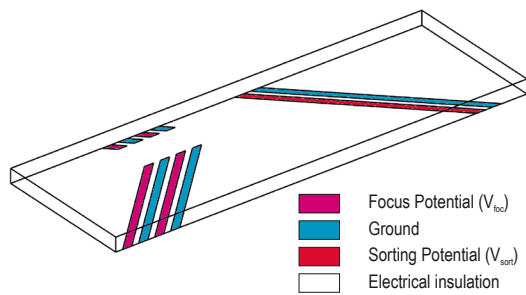


Figure 27 Applied boundary conditions.

Table 7 Comsol input parameters, the variable names between brackets are pre-defined names in Comsol.

Parameter	Variable name in Comsol	Value
Relative permittivity of the medium	remed (ϵ_r)	78
Conductivity of the medium	smed (σ)	0.7 S/m
Permittivity of the medium	emed	$78 \cdot 8.85 \cdot 10^{-12}$ F/m
Potential focusing electrode	Vinfoc	3.4 V
Potential sorting electrode	Vindef	3.4 V
Radius of the particle	r	$3.29 \mu\text{m}$
Real part of the Claussius-Mossotti factor	ReCM	-0.22

3.4.3 Post-processing and Results

Comsol will calculate the electric field in space. This field distribution is necessary to calculate the DEP force because it depends on the gradient of the squared electric field in space. After the simulations this information is available. In the post-processing the following equation is used in Comsol to calculate the DEP force:

$$2 \cdot 3.14 \cdot r^3 \cdot emed \cdot ReCM \cdot d(Ex_{emqvw}^2, x)$$

The following defined constants are used, r , $emed$ and $ReCM$, see Table 7 for their values. Ex_{emqvw} is the electric field in the x direction calculated by Comsol. The electric fields in the y and z direction are Ey_{emqvw} and Ez_{emqvw} respectively. To calculate the DEP force the derivative of the field in space is needed. Comsol can give the derivative by using the “d” operator and specifying in which direction the derivative must be taken. In the Comsol equation above it is in the x direction.

There is a negative DEP (nDEP) because the Claussius-Mossotti factor is negative. In the next section the nDEP force at different places in the channel is discussed. The direction of the force is relative to the axis in the plot. Therefore it is possible that a nDEP force has a positive value, because it points in positive direction.

To visualize the nDEP force arrow plots are made. In Figure 28 the blue lines are the electrodes (seen from above). The black lines are the channel walls. The nDEP force is visualized by red arrows. It can be seen that the arrows are perpendicular to the electrodes and the largest nDEP force is encountered near the space between the electrodes where the gradient of the electric field is very large. In Figure 29 the nDEP force is depicted looking from the side over the electrodes. In this case it can be seen that there is also a nDEP force in the z direction, forcing the cells to the top of the channel.

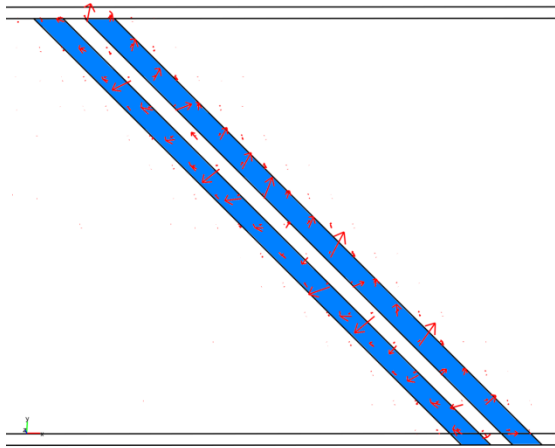


Figure 28 DEP force at the sorting electrodes, seen from above (xy plane).

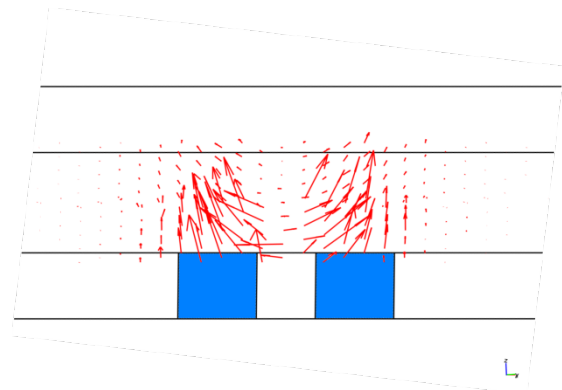


Figure 29 DEP force at the sorting electrodes, seen from the side (xz plane).

In Figure 30 to Figure 32 the nDEP forces seen from above are depicted. These slices give the nDEP forces at a height of $15\ \mu\text{m}$ in the channel. The color is a measure for the force. On the left side of these pictures the focusing electrodes can be seen. On the right side the sorting electrodes. Figure 30 shows the nDEP force in the x direction. Between the focusing electrodes there is no nDEP force, so cells can flow between these electrodes. The maximum force is about $-4\ \text{pN}$. In Figure 31 the nDEP force in the y direction is shown. At the focusing electrodes the nDEP force is positive in the y direction at the lower electrodes and negative at the opposite electrodes, therefore the cells will be forced to the gap between the focusing electrodes. At the sorting electrodes all cells are pushed in a negative y direction.

In Figure 32 the nDEP force in the z direction is shown. In the gap between the focusing electrodes there is no nDEP force in the z direction. All cells passing the sorting electrodes will encounter a nDEP force in the positive z direction and are therefore pushed to the upper side of the channel.

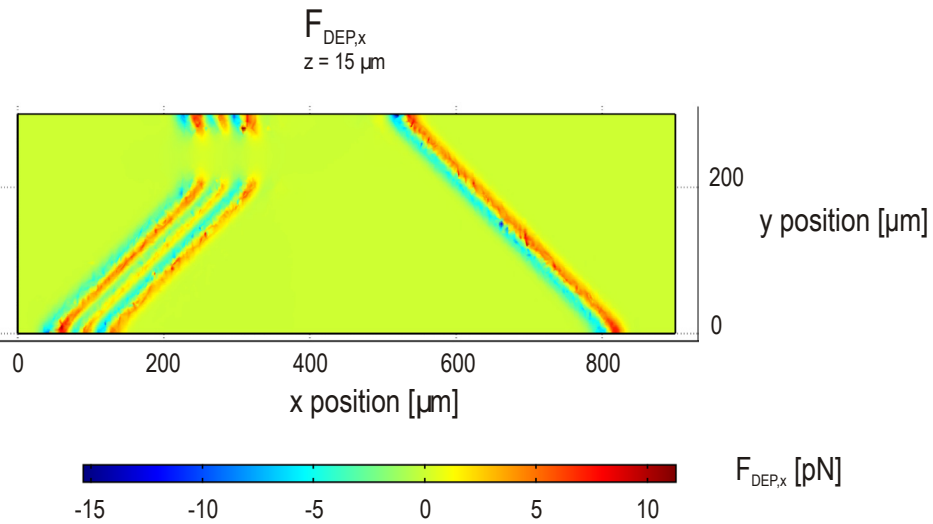


Figure 30 DEP force in the x direction.

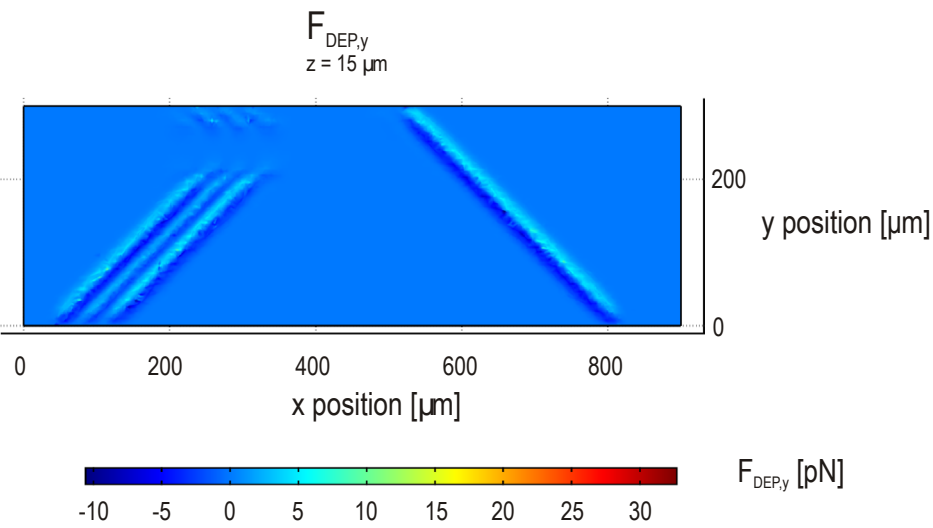


Figure 31 DEP force in the y direction

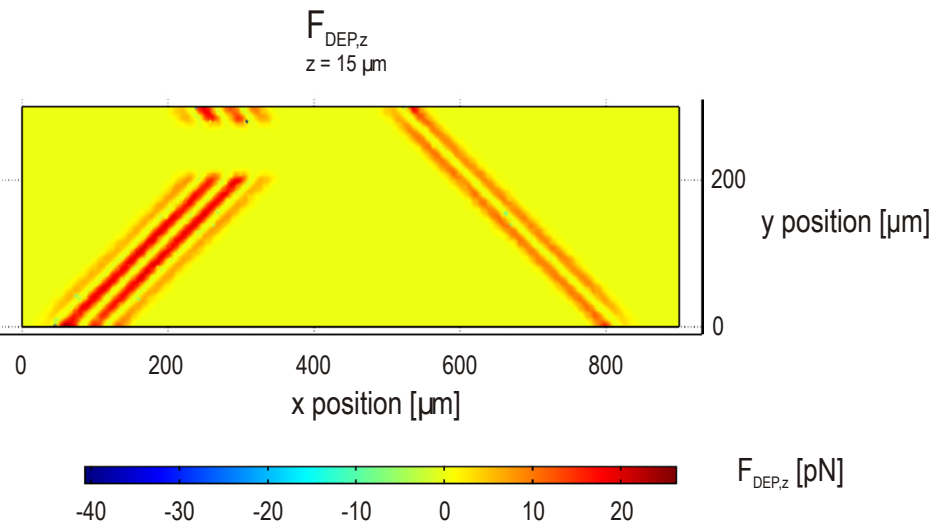


Figure 32 DEP force in the z direction.

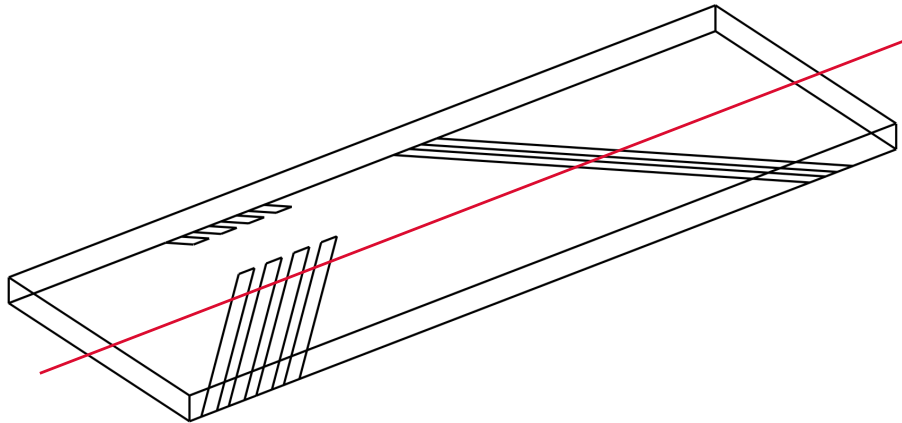


Figure 33 The DEP force is measured along the red line.

To determine the nDEP force more accurately, the nDEP force in the x direction is plotted along a line through the geometry. This can be seen in Figure 33, the red line is the line at which the nDEP force in the x direction is calculated. This line is placed in the center of the channel at three different heights. The chosen heights are 5 μm (bottom), 15 μm (center) and 25 μm (top). The geometries with electrodes under an angle of 45° and 60° are used. In this way the difference in the nDEP force between these geometries can be seen.

The plots are presented in Figure 34 to Figure 39. In the left column the results with 45° electrodes are shown. In the first row the results at a height of 5 μm are shown. The green line in the graphs is nDEP force in the x direction. The first 4 peaks are due to the focusing electrodes, the last two peaks are due to the sorting electrodes. The lines are not very smooth. This is probably due to the coarse mesh used in these 3D simulations.

It can be seen that the nDEP force in the x direction decreases at places higher in the channel. Just above the electrodes the nDEP force in the x direction is -40 pN, in the center of the channel this is decreased to -4 pN and just below the top of the channel it is decreased to -1 pN. Because a nDEP force positive in the z direction is present, the cell will be pushed to regions with lower DEP forces. As expected the DEP force in the x direction with 60° electrodes are a factor 1.2 ($\sin(60)/\cos(45)$) stronger, this is best seen at a height of 25 μm .

It is not known at which height in the channel the cells will encounter the DEP force, but due to the positive DEP force in the z direction it is likely that the cells are somewhere in the top region of the channel. Therefore it is estimated that the encountered DEP force in the x direction is somewhere in between -1 and -4 pN.

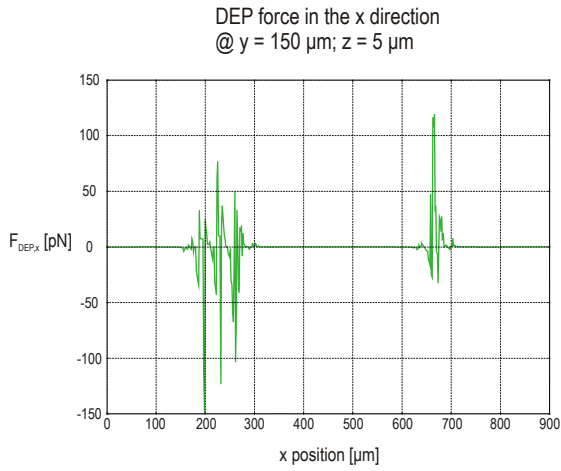


Figure 34 DEP force in the x direction with 45° electrodes, measured along the x axis in the middle of the channel ($y = 150 \mu\text{m}$) and at a height of $z = 5 \mu\text{m}$.

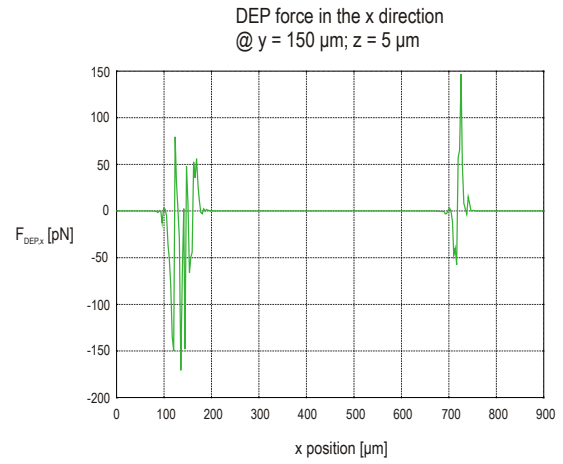


Figure 35 DEP force in the x direction with 60° electrodes, measured along the x axis in the middle of the channel ($y = 150 \mu\text{m}$) and at a height of $z = 5 \mu\text{m}$.

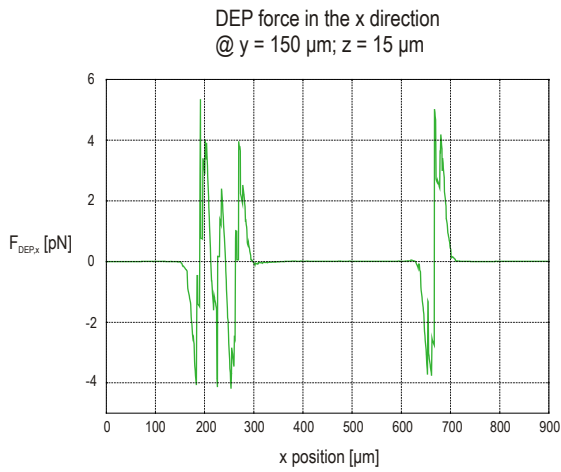


Figure 36 DEP force in the x direction with 45° electrodes, measured along the x axis in the middle of the channel ($y = 150 \mu\text{m}$) and at a height of $z = 15 \mu\text{m}$.

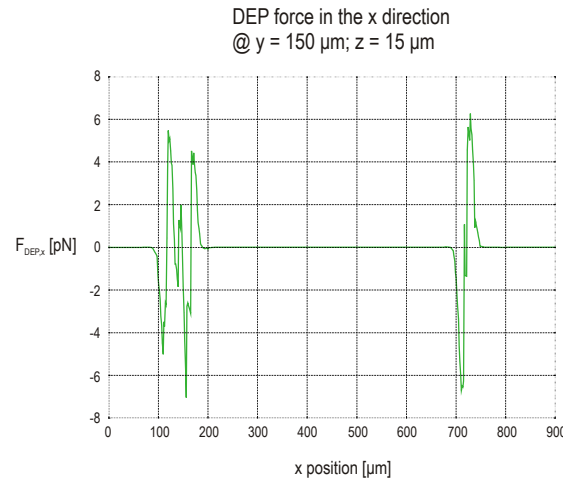


Figure 37 DEP force in the x direction with 60° electrodes, measured along the x axis in the middle of the channel ($y = 150 \mu\text{m}$) and at a height of $z = 15 \mu\text{m}$.

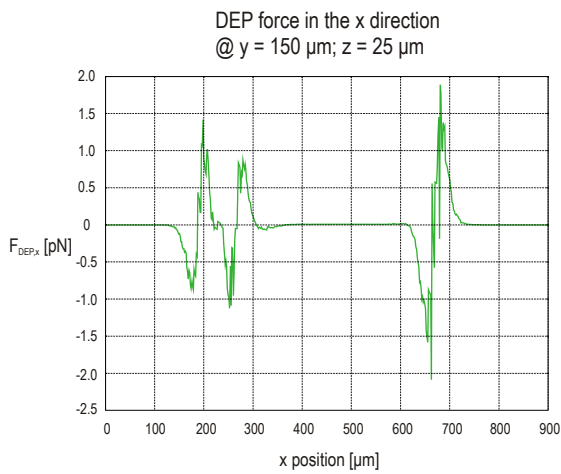


Figure 38 DEP force in the x direction with 45° electrodes, measured along the x axis in the middle of the channel ($y = 150 \mu\text{m}$) and at a height of $z = 25 \mu\text{m}$.

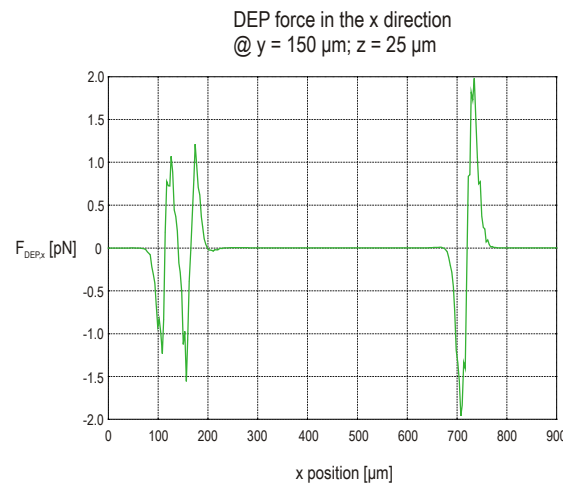


Figure 39 DEP force in the x direction with 60° electrodes, measured along the x axis in the middle of the channel ($y = 150 \mu\text{m}$) and at a height of $z = 25 \mu\text{m}$.

3.5 Side effects

Due to the strong electric field electroporation can occur and the fluid inside the channel will heat up. These side effects are discussed in the following sections.

3.5.1 Electroporation

As discussed in chapter 2.5.5 electroporation can be a potential problem. To be able to calculate the membrane voltage the electric field must be known. The normalized electric field (this is the total field strength independent on direction) can be calculated with Comsol. In Figure 40 the field strength is plotted over the line depicted in Figure 33 at a height of 5 μm . The maximum electric field strength is about 170 kV/m. Equation (34) (equal to equation (22)) is used to calculate the membrane potential, all parameters used are shown in Table 8. The membrane potential in this situation will be 0.57 V. Membrane breakdown occurs between 0.5 and 1.0 volt, so this membrane potential is just inside the zone at which breakdown can occur. However these strong electric fields are just close above the electrodes and as stated before it is unlikely that the cells will be inside this region. Therefore the membrane potential of the cell at a height of 15 μm is calculated as well. The electric field in this situation is plotted in Figure 41. The maximum electric field strength is about 60 kV/m. In this situation the membrane potential will be 0.20 V. This membrane potential should not cause electroporation.

$$V_m = \frac{r \cdot E \cdot 1.5 \cdot \cos(\alpha)}{\sqrt{1 + (2\pi f \tau)^2}} \quad (34)$$

$$\tau = r C_m (\rho_i + 0.5 \rho_m)$$

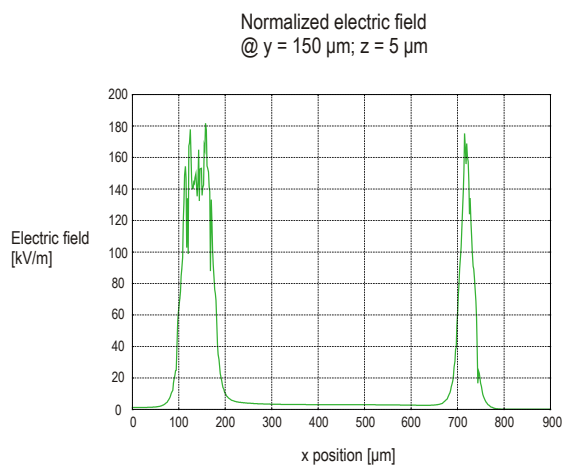


Figure 40 The normalized electric field inside the center of the channel at a height of 5 μm .

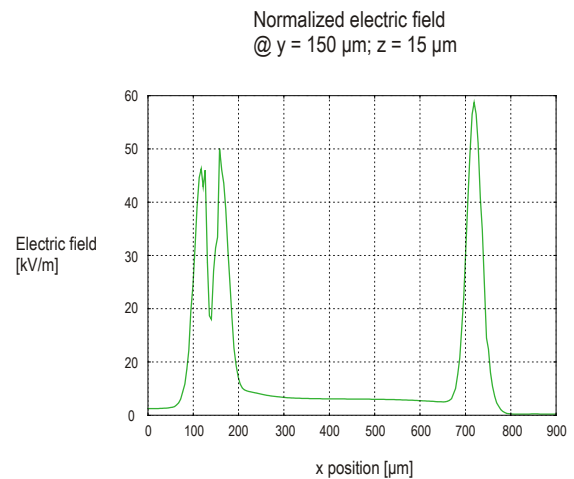


Figure 41 The normalized electric field inside the center of the channel at a height of 15 μm .

Table 8 Electroporation parameters.

Parameter	Value
Radius of the cell (r)	3.29 μm
Maximum electric field (E)	170 kV/m (60 kV/m)
Angle between electric field and cell (α)	0°
Frequency (f)	2 MHz
Membrane capacitance (C_m)	0.0126 F/m ²
Resistivity of the cell interior (ρ_i)	1.33 Ωm ($1/\sigma_i$)
Resistivity of the cell exterior (ρ_e)	1.43 Ωm ($1/\sigma_{\text{med}}$)

3.5.2 Heating

Due to the potential difference between the electrodes an electrical current will flow. The resistivity of the fluid will cause a conversion of electrical energy into heat energy. This heat energy will cause a rise of the temperature of the fluid. High temperatures can damage the cells. The theory about this phenomenon can be found in chapter 2.5.5. A minimum fluidic flow rate will be calculated to ensure that the temperature increase of the medium is not more than 5 degrees Celsius. First the amount of heat energy produced is calculated using equation (35). Then the amount of heat leaking through the glass to the outside world is calculated using equation (36) (equal to equation (20)). And subsequently the temperature increase of the fluid is going to be calculated using equation (37) (equal to equation (21)). The values used for the different parameters can be found in Table 9.

$$W = \frac{V^2}{R} \quad (35)$$

$$\frac{\Delta Q_{leak}}{\Delta t} = kA \frac{\Delta T}{x} \quad (36)$$

$$Q_{fluid} = cV\Delta T \quad (37)$$

The dissipated electrical power is 2.4 mW. Some of this power is dissipated through the glass and will not contribute to the heating of the medium inside the channel. It is assumed that the medium is originally at room temperature and that it is safe to increase the temperature by 5 °C. The total glass area where energy is transferred between the medium and the surrounding is assumed to be the area above and beneath the electrodes (including the space between the electrodes). When all the values of the parameters are substituted into equation (36) the resulting leaked power is 364 μW. This gives us a remaining power of 2.0 mW which contributes to the heating of the medium inside the channel.

The volume of water of which the temperature is increased by 5 °C due to the added energy can be calculated with equation (37). Because the energy added *per second* is used, this will result in a volume *per second* of which the temperature is increased by 5 °C. This volume per second is equal to $96 \cdot 10^{-12} \text{ m}^3/\text{s}$ (96 nL/s or 5.8 μL/min).

This value can be lowered in two ways when necessary. The temperature increase allowed can be made higher, or the voltage over the electrodes can be lowered. When the voltage is lowered, the DEP force will decrease as well. This can be compensated with an increase of the Clausius-Mossotti factor which can be obtained by decreasing the frequency.

Table 9 Parameters used to calculate the fluidic heating.

Parameter	Value
Voltage	3.4 V
Resistance	4.868 kΩ
Δt	1 s
Thermal conductivity of glass (k)	0.93 W·m ⁻¹ ·K ⁻¹ [30]
Area of the conducting surface (A)	27·10 ⁻⁹ m ²
Thickness of the glass (x)	500 μm
Temperature increase (ΔT)	5 °C
Specific heat capacitance of water (c)	4.18 J·cm ⁻³ ·K ⁻¹ [30]

3.6 Total forces

In case of separation of non-motile cells from motile cells the non-motile cells may not pass the electrodes. Therefore the DEP force must counteract the drag force, but must not counteract the swimming force. All the forces acting on a cell are depicted in Figure 10 and Figure 11. The DEP force simulations indicated a DEP force of about 4 pN, so the drag force must be a little less. The following equation (equal to equation (19)) is used to calculate the velocity difference between the particle and fluid for a drag force of 4 pN:

$$F_{drag} = 6\pi\eta r v \quad (38)$$

All values of the parameters used are given in Table 10. A drag force of 4 pN will act on the spermatozoa when a velocity difference of 65 $\mu\text{m/s}$ is present between the spermatozoa and the medium. With the dimensions of the channel used for the simulation this velocity can be translated into a flow rate of the medium. The width and height of the channel are 300 μm x 30 μm , so the flow rate is $585 \cdot 10^{-12} \text{ m}^3/\text{s}$, which is equal to 0.035 $\mu\text{L}/\text{min}$. This is the maximum flowrate at which non-motile cells cannot pass the electrodes, because the DEP force is equal to the drag force. However, motile cells can pass the electrodes, because the swim force and the drag force are greater than the DEP force.

Table 10 Parameters used to calculate the forces acting on a cell.

<i>Parameter</i>	<i>Value</i>
Viscosity of water (η)	$1.00 \cdot 10^{-3} \text{ Pa}\cdot\text{s}$ [30]
Radius of the cell (r)	3.29 μm
DEP force	4 pN
Swimming force	4 pN

3.7 Simulation summary and conclusions

The preceding sections gave a lot of information, which is summarized here. The most important boundaries are listed in Table 11.

The frequency range of the applied potential is determined by the Clausius-Mossotti factor and the impedance plateau of the electrodes. The low frequency limit is determined by the impedance of the electrodes and is 100 kHz. The high frequency limit is determined by the Clausius-Mossotti factor and is 5 MHz.

The limits of the applied potential are more difficult to determine. Heating of the medium inside the channel, electroporation and the DEP force resulting from the electrical field are all dependent on this potential. The calculated DEP force is equal to -4 pN. The used electrode potential is on the edge of causing electroporation, higher potentials must be avoided. This DEP force is just strong enough to stop spermatozoa inside a medium with a flow rate of 0.035 $\mu\text{L}/\text{min}$. But when the temperature is allowed to increase 5 $^{\circ}\text{C}$ the flow rate must be 5.8 $\mu\text{L}/\text{min}$. To lower the released electrical energy the potential must be lowered, but then the DEP force will be smaller as well. For the weaker DEP force can be compensated by increasing the Clausius-Mossotti factor, which can be done by decreasing the frequency. The model used to calculate the increased temperature is not very sophisticated. The temperature of the medium will be higher than room temperature to increase the motility of the spermatozoa. Most of the electrical energy is dissipated near the electrodes. It is not dissipated uniformly in the channel. The electrodes can work as a kind of heat sink. Heat energy is transported away from the channel. Therefore the heating of the medium is not expected to be a crucial factor.

The small electrodes create a small region where a DEP force is present. So motile spermatozoa only needs to pass a small area. The chance that they will succeed in passing this barrier is therefore high. When the temperature problem is neglected the used geometry in the simulation shows a good behavior and it is expected that it will work in reality. Therefore this geometry is used in the design of the test chip.

It is not possible to separate dead and living spermatozoa with a medium with a conductivity of 0.7 S/m. To be able to separate dead and living spermatozoa with the geometry used in the simulations, a medium with higher conductivity is needed.

Table 11 Boundary conditions

<i>Parameter</i>	<i>Value</i>
Minimum frequency	100 kHz
Maximum frequency	10 MHz
Maximum potential (rms)	3.4 V
Maximum flow rate by a DEP force of 4pN	0.035 $\mu\text{L}/\text{min}$

4 Design & fabrication of the chips

In this chapter the design aspects and the resulting designs are treated. In the last section of the fabrication process and the resulting chips are described.

4.1 Design aspects

In this project it will be tried to sort spermatozoa using a DEP force. This DEP force must be strong enough to counteract the drag force. The DEP force is frequency dependent, but only a limit frequency window can be used due to the impedance characteristics of the electrochemical cell and the Clausius-Mossotti factor. The geometry used in the performed simulations showed that it is possible to create a DEP force with the same magnitude as the drag force. Therefore the channel and electrode geometries used in the different designs are the same as the geometries used in the simulations.

The chips can be made of different materials. Glass and PDMS are used often for microfluidic devices. In the fertility chip project there is already experience with spermatozoa experiments with glass chips [2], therefore glass is chosen as the basic material.

The chip needs electrical as well as fluidic connections. In the BIOS group a standard fluidic chip layout template is present. In this standard the dimensions of the chip and the locations of the connections are predefined. This standard layout is used to simplify experiments. Standard chip holders with fluidic and electrical connections are already available. There is also a bracket available which can be used with some of the microscope setups. In this standard layout 6 fluidic connections are available as well as 10 electrical connections. The dimensions of this layout are 20 x 15 x 1 mm (length, width, height). The designed chips need to be incorporated into this template.

Two glass wafers are used. One wafer is used for the fluidic channels and in- and outlets. The other wafer is used for the electrodes. The mask set consists of three masks. One mask describes the fluidic channels. The second mask is used for the fluidic in- and outlets. The third mask is used to define the electrodes.

During the fabrication process the fluidic channels are etched into the glass. This etching process is isotropic, this means that the etch rate is equal in all directions. When the channels are for example etched 30 μm deep, the width of the channel is increased by 60 μm compared to the design in the mask. This increase in width has to be taken into account during the design process.

4.2 Different versions

In total six different designs are being made, these are grouped into three groups. These groups are treated in the next paragraphs. In two groups the non-motile cells will be deflected into a side channel. In the third group laminar fluidic flows are used to separate the cells. In Table 12 the groups and the different chips are shown.

Table 12 the six chip designs grouped into three groups

45°electrodes	60° electrodes	Laminar flow
“far focusing” Focusing on the opposite side of the channel at the side channel	“far focusing” Focusing on the opposite side of the channel at the side channel	Focusing electrodes 60° Sorting electrodes 45°
“mid focusing” Focusing in the center of the channel	“mid focusing” Focusing in the center of the channel	Focusing electrodes 60° Sorting electrodes 60°

4.2.1 45° and 60° sorting electrodes

In these design spermatozoa will be sorted based on their motility by a DEP force. These spermatozoa do not swim and will be pushed into a side channel due to the DEP force.

This chip consists of a main channel which is 300 μm wide and 30 μm high. The DEP force at the electrodes will not only push the spermatozoa to the side of the channel, but also to the top of the channel. When the channel height is too low it is expected that the spermatozoa will hit the channel ceiling and will stick there due to the DEP force. When the channel ceiling is too high the DEP force at the top of the channel will be very low, because it is far away from the electrodes. When the DEP force is too low all spermatozoa may pass the electrodes and there is no sorting function anymore.

The inlet is the hole closest to the electrode connections, see Figure 42. In the main channel two kinds of electrodes are present. The electrodes are the eight green stripes in the top of Figure 44. The focusing electrodes consist of four electrode pairs, two pairs on each side of the channel. The electrodes are 14 μm wide and 150 nm thick and are placed under an angle of 45° with respect to the channel walls. The distance between the electrode fingers is 11 μm . This is exactly the same geometry as used in the simulations. After passing the focus electrodes, the focused cells will flow to the sorting electrodes, which consist of one electrode pair. These electrodes have again the same geometry as used in the simulations. The sorting electrodes end in a side channel. The side channel is 100 μm wide and 30 μm high. All the electrodes and a small piece of the side channel can be seen at the bottom in Figure 44. The cells which cannot flow over the sorting electrodes are pushed inside this channel and will flow to the fluidic outlet located at the bottom left on the chip, see Figure 42.

There are two different versions of this chip. One in which the spermatozoa are focused near the channel wall opposite to the side channel, see Figure 44. This chip is referred as the “45 degree, far focusing chip”. In the other design the spermatozoa are focused in the center of the channel, see Figure 45. This chip is referred as “45 degree, mid focusing chip”. The spermatozoa in the far focusing chip have a chance to pass the sorting electrodes over the whole length of these electrodes. This gives the motile spermatozoa the biggest chance to swim over these electrodes and this could enhance the sorting efficiency. In the chip with the mid focusing chip the spermatozoa are in the center of the channel where the flow velocity of the medium is the highest. Because the spermatozoa reach the sorting electrodes with a higher velocity, less time is available for the spermatozoa to reach the top of the ceiling of the channel due to the upward DEP force. Therefore it is more likely that the spermatozoa will *not* be in a region with weak DEP forces against the flow direction which are present near the ceiling of the channel and may unintended pass the electrodes. During the time DEP force is acting on the spermatozoa the drag force will decrease because the spermatozoa are not in the center of the main channel. The reduced drag force compensates a bit for the decreased DEP force at the top of the channel.

The 60 degree chip has basically the same layout as the 45 degree chip. The differences are the angle between the sorting electrodes and the channel wall and the angle between the side channel and the main channel. All other dimensions are the same.

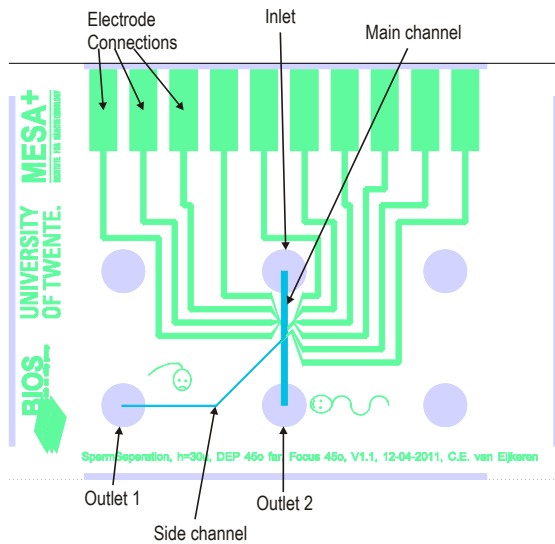


Figure 42 Overview of the chip with 45° sorting electrodes. Green colored areas are platinum electrodes. Dark blue areas are fluidic channels and the light blue circles are the fluidic in- and outlets.

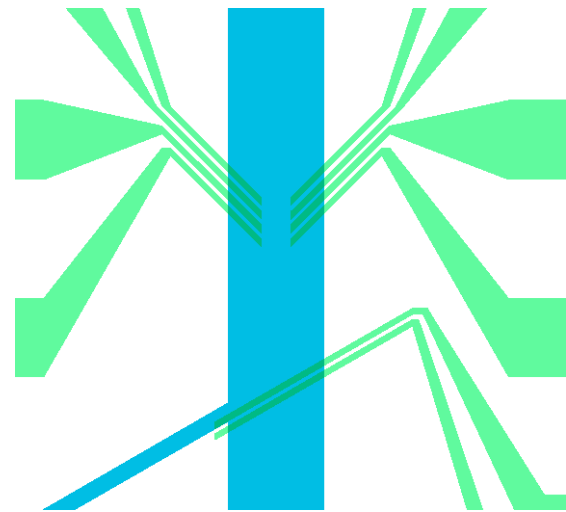


Figure 43 Overview of the electrodes of the 60° mid chip. The focusing electrodes are under an angle of 45° and the sorting electrodes under an angle of 60°.

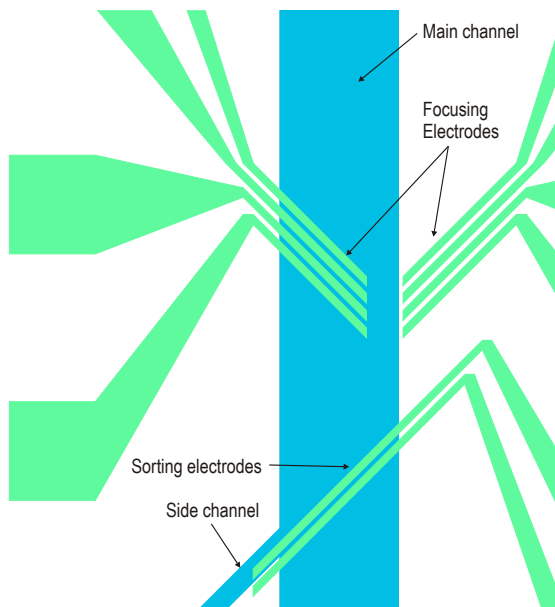


Figure 44 Overview of the electrodes of the “45° far” chips. The focusing electrodes focus the cells on the right side of the channel. The channel will be wider in the real chips due to the isotropic etching process.

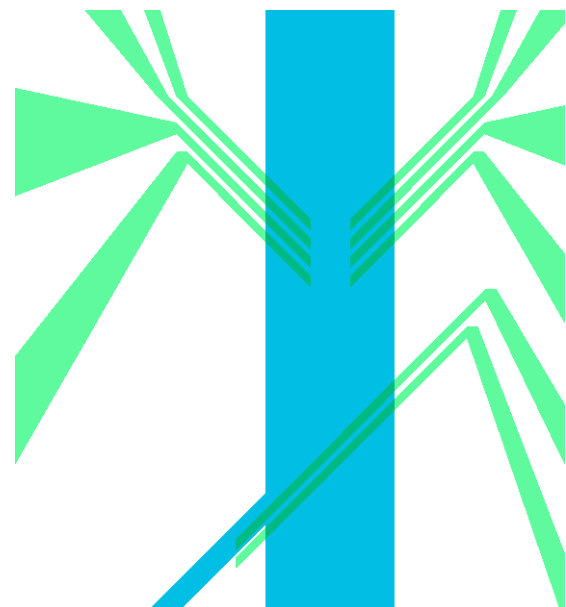


Figure 45 Overview of the electrodes of the “45° mid” chip. The focusing electrodes focus the cells in the center of the channel.

4.2.2 Laminar flow chip

In this chip (Figure 46) the spermatozoa are not separated actively. The motile spermatozoa will swim to regions which the non-motile spermatozoa cannot reach.

In small microfluidic channels a laminar fluid flow is present. There will be no mixture of particles inside the channel. Small particles can only migrate to other streamlines by diffusion. Larger particles diffuse only very slow. In this case motile spermatozoa will swim and are therefore able to move to other streamlines. The non-motile spermatozoa are trapped in a streamline. This principle is used by Cho et al. (2003) which is discussed before in chapter 2.4.2.

Motile and non-motile spermatozoa are focused into a streamline at the beginning of a fluidic channel. At the end the channel is separated into two channels. Motile spermatozoa are present in one channel. In the other channel motile and non-motile spermatozoa will be present. Cho et al. (2003) used fluidic focusing to focus the spermatozoa. With this technique two inlets are necessary. The pressure at both inlets must be regulated precisely. In the design presented here DEP focusing is used and only one fluidic inlet is necessary. In this way the complex regulation of the pressures in two inlets is omitted.

The motile spermatozoa must have enough time to swim to other streamlines. In Figure 12 it can be seen that human spermatozoa will swim at a velocity greater than $30 \mu\text{m/s}$. The channel is $500 \mu\text{m}$ wide, so they need about 15 seconds to swim to the other side of the channel. The distance between the focusing electrodes and the channel separation at the end is 5 mm. The maximum flow speed of the spermatozoa is $333 \mu\text{m/s}$ which is obtained by dividing the distance between the electrodes and the channel separation by the time needed to reach the other side of the channel ($5 \text{ mm} / 15 \text{ s}$). The channel dimensions are $500 \mu\text{m} \times 30 \mu\text{m}$ (width x height) this leads to a maximum flow rate of $0.3 \mu\text{L/min}$.

The dimensions of the focusing electrodes are the same as in the chips discussed previously. There is an extra electrode pair at the end of the channel, just before the channel split. There is no particular function of this electrode pair. It can be used for testing purposes.

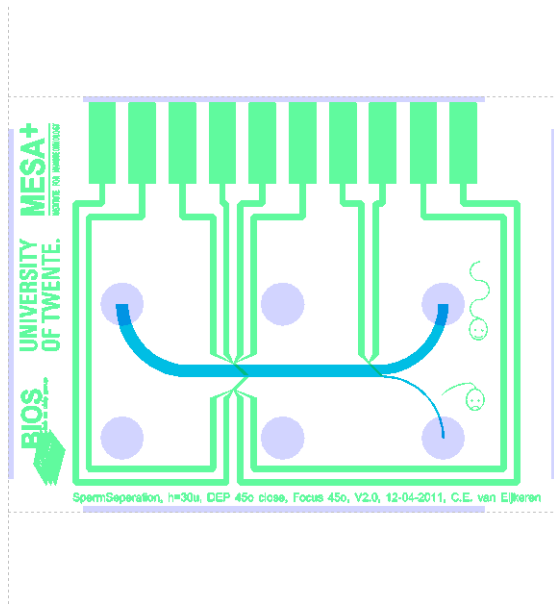


Figure 46 Overview of the laminar flow chip. The inlet is the top left fluidic inlet. The outlet with the motile spermatozoa is the top right outlet. The outlet with the non-motile spermatozoa is the bottom left outlet.

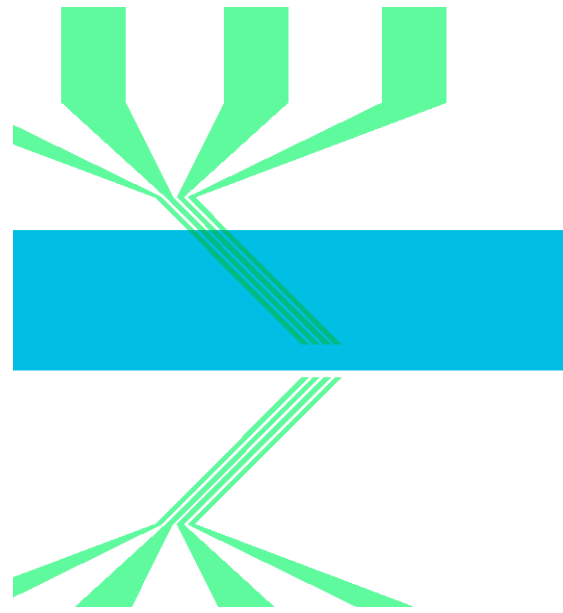


Figure 47 Shown are the focusing electrodes that focus the spermatozoa to the bottom of the main channel

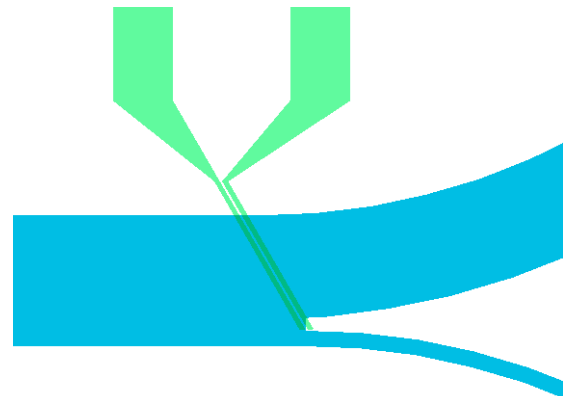
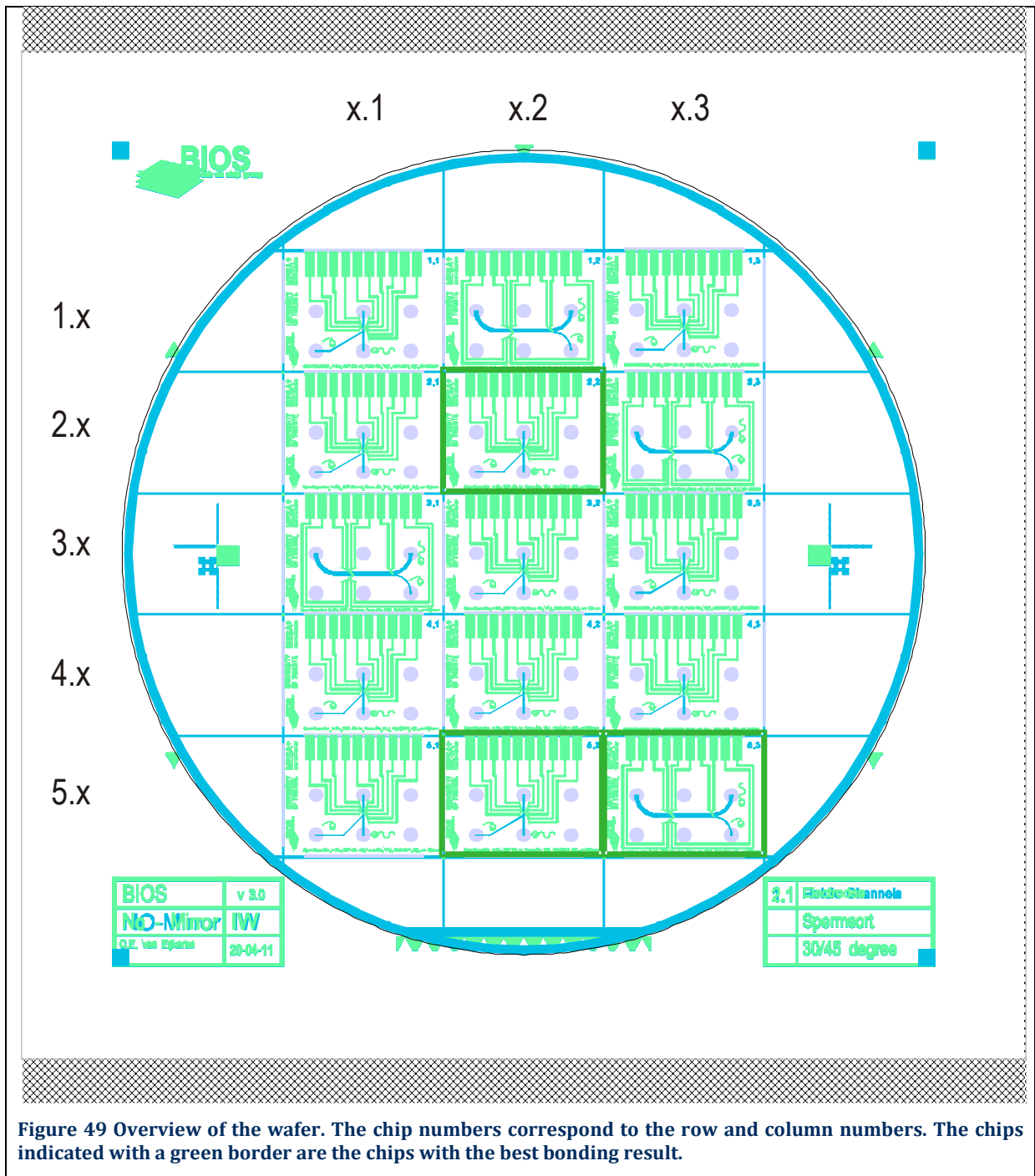


Figure 48 This is the extra electrode pair before the channel split, which may be used for testing purposes.

4.3 Fabrication process

All the different designs are combined into one layout, this layout is shown in Figure 49. In this layout the numbers of all the chips are also shown. Because all the different chip designs are combined into one design only one mask set is used to produce all the chips, which will reduce costs. One chip is made from two borofloat glass wafers. One wafer is used for the fluidic channels, the other for the electrodes. After processing the two wafers are bonded together. All the processing steps necessary are described in the text below together with schematic drawings. These drawings are a cross section of the wafer and the thickness of the different layers in these drawings do not correspond to the thickness of the layers in reality.



Wafer 1

The fluidic channels are etched in the glass wafer with 30% hydrofluoric acid (HF). A layer of gold is used as an etching mask to protect the areas which should not be etched away. A thin layer of chrome is used to improve the adhesion of the gold layer to the glass. These metal layers are sputtered onto the glass. Photoresist is used for the photolithography, see Figure 50a. After developing, Figure 50b, the gold and chrome layers are etched away and the glass area where the channel should be created is exposed, Figure 50c. The HF etching of glass is isotropic, therefore under etching occurs, Figure 50d. After the HF etching the photo resist is stripped away and the remaining gold and chrome layers are etched away, resulting finally a channel inside the glass, Figure 50e.

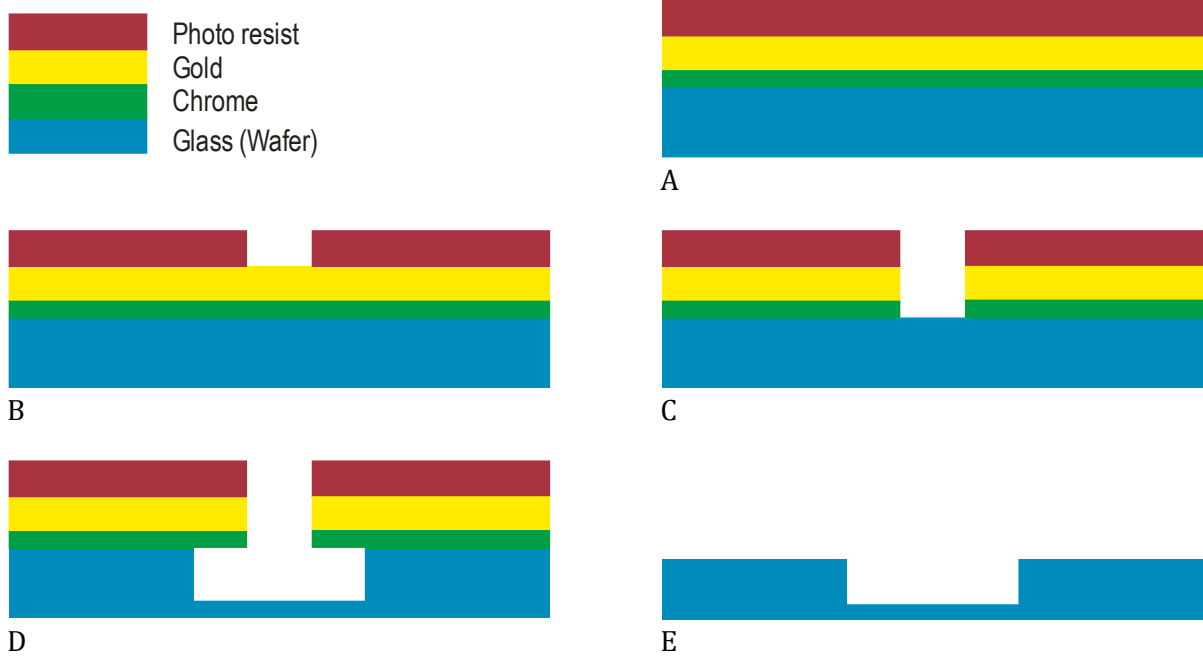


Figure 50 Fabrication of the channels. A) First a chrome, gold layer is sputtered with on top photo resist layer spinned on top. B) Developed photo resist. C) Gold and chrome etch. D) HF glass etch. E) Strip photo resist and gold and chrome etch.

Wafer 2

The electrodes are made of platinum (125 nm thick). To insure a good adhesion of the platinum onto the glass, a thin layer (25 nm thick) of tantalum is used between the glass and the platinum. These layers are sputtered onto the wafer. The electrodes are not directly on top of the glass, because this would cause an uneven surface, which interferes with the bonding of the two glass wafers. A small trench is etched into the glass in which the electrodes are formed. First a layer of photo resist is spinned onto the glass, Figure 51a, and is developed, Figure 51b. Then a shallow trench is etched into the glass with buffered HF solution, Figure 51c. Tantalum and platinum layers are sputtered on top of the whole structure, Figure 51d. The photo resist is stripped and the layers of tantalum and platinum on top of the resist are washed away. This process is called lift off. The end product is glass with a shallow trench filled with a thin layer of tantalum and a layer of platinum, which are the electrodes.

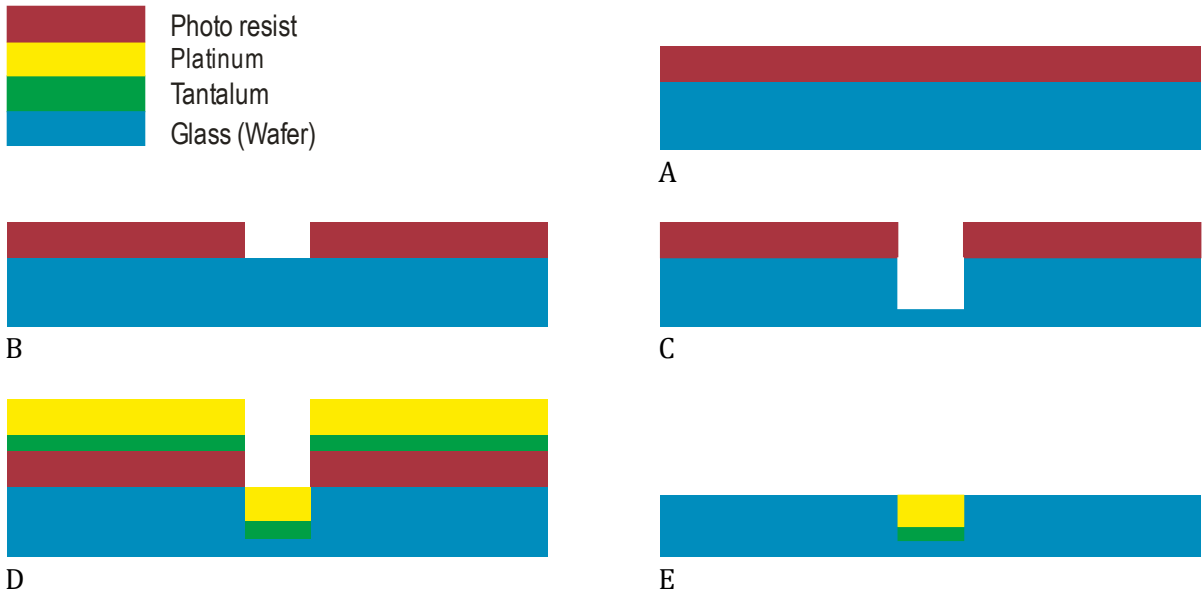


Figure 51 Fabrication of the electrodes. A) Spinned photo resist layer. B) Developed photo resist. C) BHF glass etch. D) sputtered tantalum and platinum layers. E) Lift-off photoresist.

Wafer 1

Holes acting as fluidic in- and outlets are needed. These holes are created by powder blasting the glass, whereby the other areas of the glass are protected with a foil, see Figure 52a. This foil is photo sensitive and photo lithography is used to pattern it. The developed foil will expose glass where a hole should be created, Figure 52b. Powder blasting will create a hole into the glass, Figure 52c. A wafer with fluidic channels and in- and outlets is the results when the remaining foil is removed.

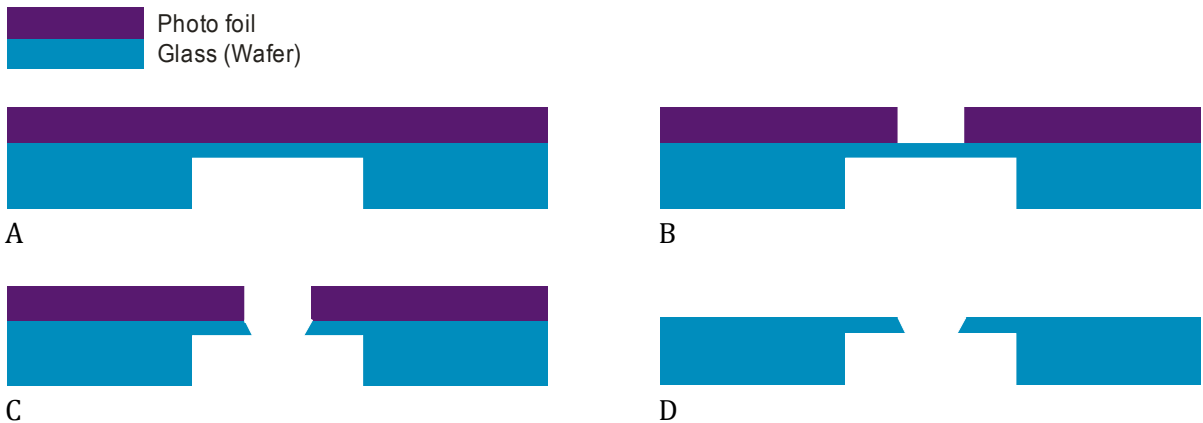


Figure 52 Fabrication of the in- and outlets. A) Photosensitive foil attached to wafer. B) Developed photosensitive foil. C) Powder blasted hole. D) Remaining foil removed.

The two wafers, one with the fluidic channels and in- and outlets and the other with the electrodes are bonded together. Because the wafers are really flat they will stick to each other. After annealing at 600 °C for 8 hours a strong bonding is guaranteed, see Figure 53. Next the bonded wafers are diced (sawn) and the chips are ready.



Figure 53 Wafer bonding. The two wafers on top of each other. This is the final structure.

4.4 Results

During processing in the clean room problems with the bonding of the two borofloat wafers were encountered. The machine used for the alignment and bonding of the two wafers did not produce the desired quality. The bonding was not good. Therefore the two wafers were aligned and placed on top of each other by hand, leading to a somewhat better result.

Wafers cannot bond when there is a small space between the wafers, which is visible by the occurrence of Newton rings. In Figure 54 these Newton rings can be seen. These are the colored circles on the left side the Mesa+ logo. There are also a couple of rings on the top side of the chip, starting at the BIOS logo and extending over the fluidic inlets. When the bonding is not good the fluidic channels are not sealed creating leakage between the two glass plates.

There is also another abnormality present in the produced chips, which could be a cause of the bonding problems. The sputtered platinum was not completely removed in some areas. These areas are the enclosed spaces in the lettering on the chip. It can be clearly seen that the B of the BIOS logo is still filled with platinum. A shallow trench is etched in the regions where platinum is supposed to be. At the regions where the unwanted platinum is present the glass was not etched. Therefore the glass is not flat anymore, because "hills" of platinum are present on top of the glass. This problem is worsened by the fact that underneath the platinum a photoresist layer is still present.

Because of the manual alignment problems can be expected with the location of the electrodes with respect to the fluidic channels. The position of the electrodes is examined with a microscope. An example of a misaligned electrode can be seen in Figure 55. The electrodes in this picture are the focusing electrodes of a laminar flow chip. It can be clearly seen that the lower electrodes are not inside the channel. Pictures of the electrodes of all produced chips can be found in Table 16 in Appendix D.

Finally one wafer pair was bonded and after dicing this resulted into three chips which were sufficiently bonded. More results of the quality of the bonding and the alignment per chip can also be found in Table 16 in Appendix D.

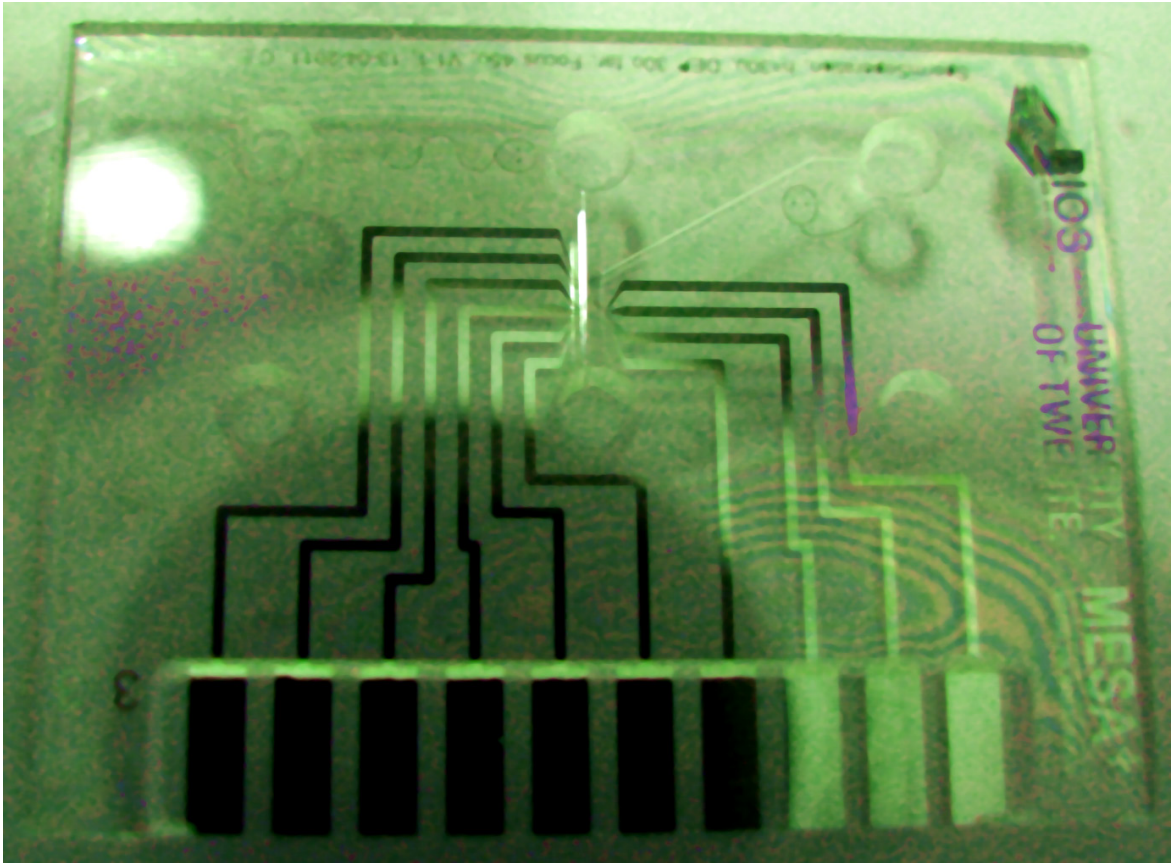


Figure 54 Visible Newton rings.

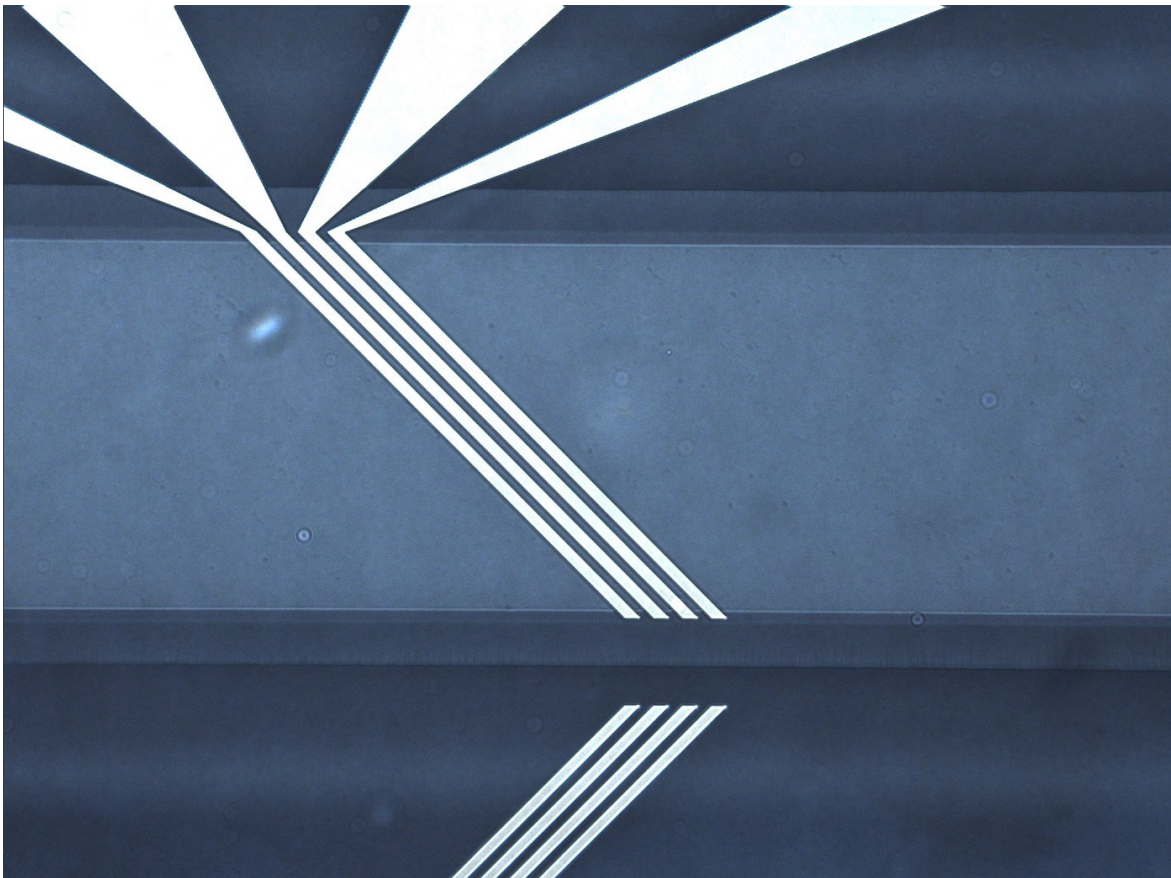


Figure 55 Aligning problems with the focus electrodes

5 Experiments

The performed experiments are described in this chapter. First the experiments for medium and chip characterization are discussed. Then the experiments to separate the spermatozoa are described.

5.1 Impedance spectrum measurements

Impedance measurements of the electrochemical cell are carried out to verify the predicted impedance. The most important information to be obtained is the frequency range of the first plateau. The applied frequency during the DEP experiments must be in this range to ensure that most of the applied electrode voltage is across the electrolyte resistance R_{el} .

Three chips are used for the impedance measurements, one chip with 45° sorting electrodes, one with 60° sorting electrodes and one chip based on the laminar flow chip with 45° focusing electrodes. Before the impedance spectrum is measured the conductivity of the medium used in these experiments, is measured.

5.1.1 Conductivity measurements

The conductivity of the medium is an important factor in the experiments. The impedance of the electrochemical cell and the Clausius-Mossotti factor are both dependent on this parameter.

The medium used during the impedance measurements is Solusem boar semen diluent from AIM Worldwide. The medium is made with 5.3 g of Solusem powder dissolved in 100 mL DI water. This solution is filtered to remove any small particles.

Medium measurement protocol

The conductivity of the medium is measured with a Mettler Toledo SevenMulti dual pH/conductivity meter. Before the measurements the measurement probe is cleaned with DI water. The conductivity is measured at room temperature.

5.1.2 Impedance measurement protocol

Before the impedance is measured the chips are filled with medium and it is checked with a microscope that no air bubbles are present directly above the electrodes. The impedance is measured with a Hewlett-Packard HP4194A impedance, phase analyzer. A frequency sweep from 100 Hz to 40 MHz is used to determine the impedance at different frequencies. There are 400 measurement points on a logarithmic scale. These impedance measurements are performed 25 times. The mean of these measurements is calculated and plotted with Matlab 2009a, the Matlab script can be found in appendix C.1.

After the experiments it is checked again that no air bubbles have formed above the electrodes.

5.2 Spermatozoa experiments

The functioning of the sorting and focusing electrodes is determined with experiments with boar spermatozoa. The behavior of the spermatozoa under different conditions is of interest.

5.2.1 Measurement setup

First of all semen samples are necessary to conduct any experiments with spermatozoa. The semen used is boar semen obtained from Coöperatie Varkens KI Twenthe. The medium

used in these semen samples is the same as used for the conductivity and impedance measurements. Therefore it is assumed that the conductivity of the semen samples is the same as the conductivity of the medium without spermatozoa.

A steady flow rate is needed to maintain a steady drag force. A Harvard Apparatus PHD 2000 syringe pump and Hamilton 100 μL syringe are used for pumping.

As a voltage source for the DEP sorting electrodes an Agilent technologies 33250A function generator is used. For the focusing electrodes a Stanford Research Systems DS340 functions generator is used as a source. To monitor the voltage at the electrodes an Agilent technologies DSO3062A oscilloscope is used.

To see what is going on inside the chip a Leica DMI 5000M microscope with Leica DFC 310 FX camera is used.

The motility of the spermatozoa is dependent on the temperature. Therefore a boar semen sample of 1 mL is warmed in a tub of water at 37 °C for 5 minutes. This is done to activate the spermatozoa and to degas the sample.

5.2.2 Sorting electrodes

The DEP force created at the sorting electrodes must be strong enough to counteract the drag force, but should be weak enough to let motile spermatozoa pass.

One of the factors determining the DEP force is the Claussius-Mossotti factor. The in the simulations calculated Claussius-Mossotti curve is verified in these experiments. It is predicted that the Claussius-Mossotti factor becomes 0 at a frequency of 10 MHz. It is difficult to quantitatively measure this factor. Therefore it is checked by eye if the spermatozoa experience a DEP force. It should be possible to see if the flow of spermatozoa is stopped at the electrodes.

The flow rate is an important factor in these experiments because the drag force depends on the flow rate. A flow rate of 0.03 $\mu\text{L}/\text{min}$ is used which creates a drag force of 3.5 pN.

The voltage applied to the electrodes is 15 V_{pp} . This is higher than the electrode voltage used in the simulations. This is done to check if the Claussius-Mossotti factor is really close to 0. When this factor is small, the drag force will be stronger than the DEP force and the spermatozoa are able to pass the electrodes. This can lead to the false conclusion that the Claussius-Mossotti factor is 0. Therefore the DEP force is increased again by increasing the electric field intensity. The increase in field intensity compensates for the decrease in the Claussius-Mossotti factor. So if the spermatozoa are able to pass the electrodes even with the increased potential, it can be assumed that the DEP force is close to 0.

5.2.3 Focusing electrodes

The function of the focusing electrodes is checked during these experiments. These electrodes should focus the spermatozoa inside the channel. The spermatozoa should initially be pushed towards the opening between the electrodes. When the spermatozoa passed the focusing electrodes a nice stream of spermatozoa should be seen. The width of this stream should be equal to the width of the gap between the electrodes.

The first experiments are performed with an electrode voltage of 15 V_{pp} , to be sure that a strong DEP force is created.

6 Results and discussion

The obtained experimental results are presented and discussed in this chapter. First the characterization of the medium and the electrodes of the chip are shown. Thereafter the experiments with spermatozoa will be discussed.

6.1 Conductivity measurements

The medium used during the impedance measurements of the electrodes has a measured conductivity of 0.70 S/m at a temperature of 23.4 °C. This conductivity has the same value as used in the simulations.

6.2 Impedance measurements

The impedance characteristics from three chips are measured. From two chips (45° and 60° electrodes) the impedance of the sorting electrodes has been measured. From the third chip (laminar flow chip) the impedance of the long sorting electrodes has been measured. The results are plotted in Figure 58, Figure 59 and Figure 60 respectively. The frequency range of the plateau is visualized in these plots. All three chips have the frequency plateau in the same frequency range. However, the absolute impedance of the plateau is different between the chips. The frequency range and the impedance of the plateau are summarized in Table 13.

The measured low cutoff frequency is of the same magnitude as the expected frequency based on the simulations. The estimated double layer capacitance of 15 $\mu\text{F}/\text{cm}^2$ seems to be a good estimate of this capacitance. The measured high cutoff frequency is more than 10 times lower than the estimated high cutoff frequency. The parasitic capacitance between the electrodes is higher than predicted. This comes not as a surprise, because only the capacitance between the electrodes inside the channel is taken into account in the estimated capacitance. The capacitance between the platinum leads on the chip and the capacitance of the wires connecting the chip to the measurement apparatus are not taken into account in the estimate. The lower than expected high cutoff frequency does not have any practical implications, because the Clausius-Mossotti factor becomes 0 at 10 MHz. The highest frequency which could be used is therefore still not limited by the high cutoff frequency of the electrodes.

The measurement impedance of the plateau is lower than expected. This can be explained by the fact that the area of the electrodes in contact with the medium is larger than expected. The electrodes extend into the side channel, see Figure 56 and Figure 57 in which the channel wall are visualized by black lines. So the length of the electrodes is larger than assumed in the simulations. Due to the increased electrode area the resistance is lowered. The 45° electrodes are 25% larger and the 60° electrodes are 20% larger in the chips used for the measurements than in the simulations. When the theoretical impedance of the electrolyte is recalculated with this increased length it will be 3.2 k Ω and 4.1 k Ω respectively. These values are close to the measured values. Due to the decreased impedance the current increases and therefore the dissipated power inside the channel will be higher.

Table 13 Results of the impedance measurements of three different chips.

Parameter	45° sort (chip 1.3)	60° sort (chip 1.1)	Laminar flow (chip 3.1)
Frequency range	65 kHz – 25 MHz	65 kHz – 20 MHz	70 kHz – 25 MHz
Impedance plateau	3.2 k Ω	3.9 k Ω	2.7 k Ω
Expected freq. range	75 kHz – 380 MHz	51 kHz – 280 MHz	
Expected impedance	4.1 k Ω	4.9 k Ω	
Recalculated imp.	3.2 k Ω	4.1 k Ω	

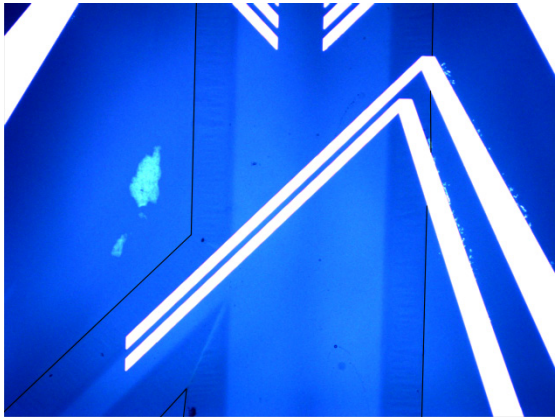


Figure 56 45° sorting electrodes extending into the side channel (chip 1.3).

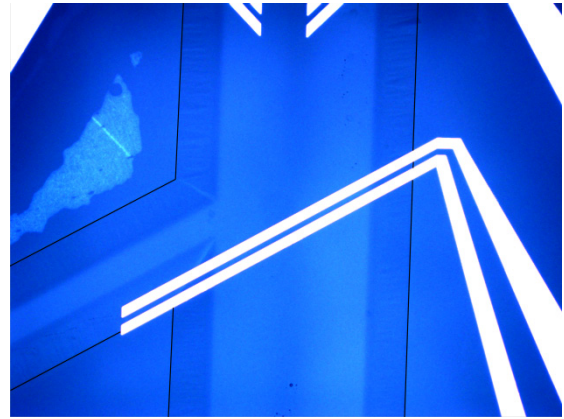


Figure 57 60° sorting electrodes extending into the side channel (chip 1.1).

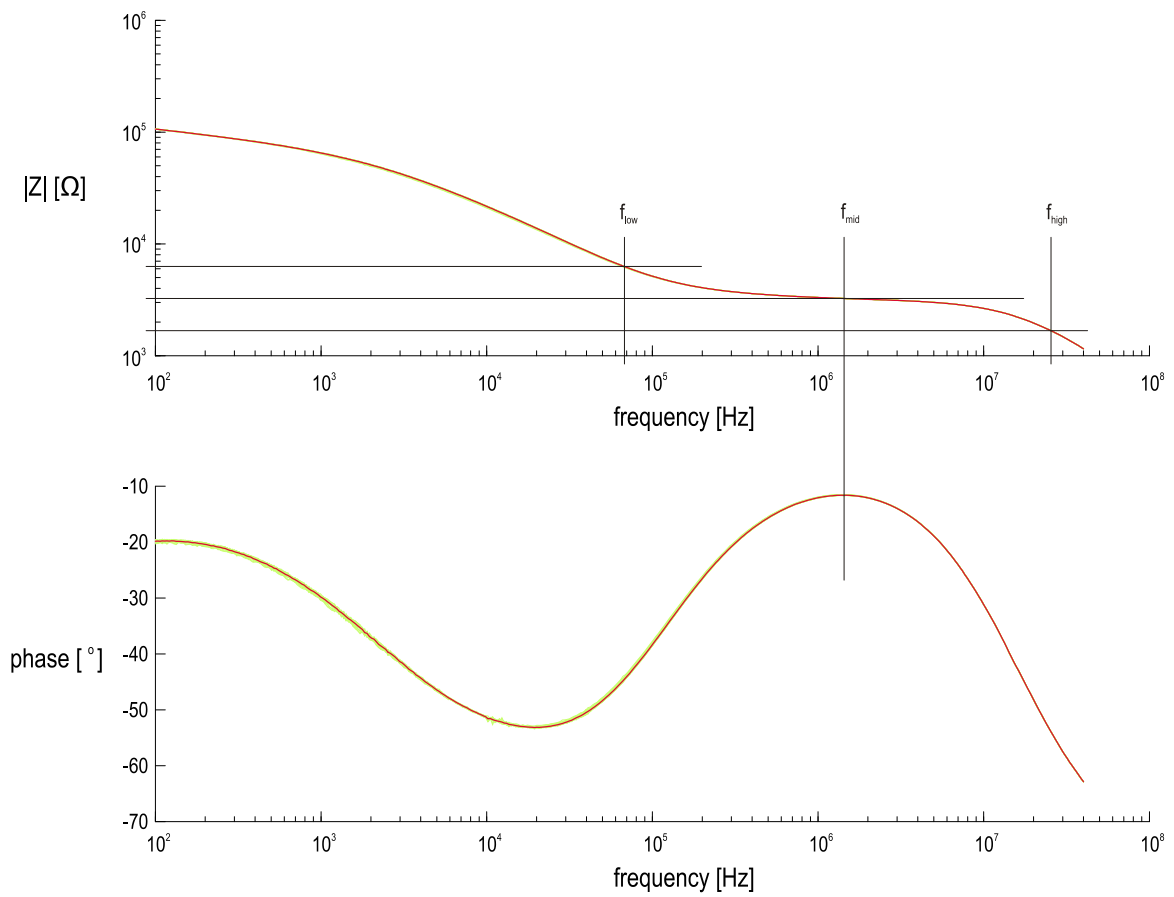


Figure 58 Impedance measurement 45° sorting electrodes (chip 1.3).

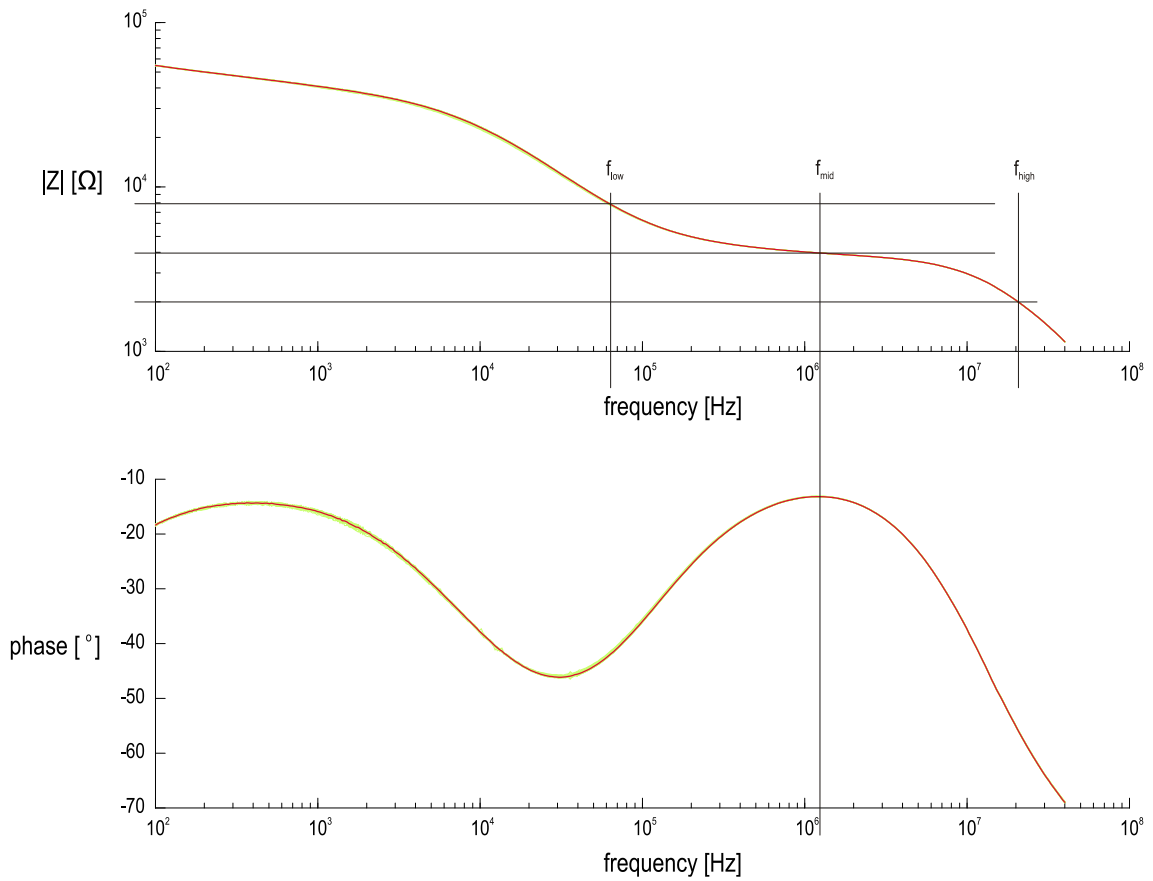


Figure 59 Impedance measurement 60° sorting electrodes (chip 1.1).

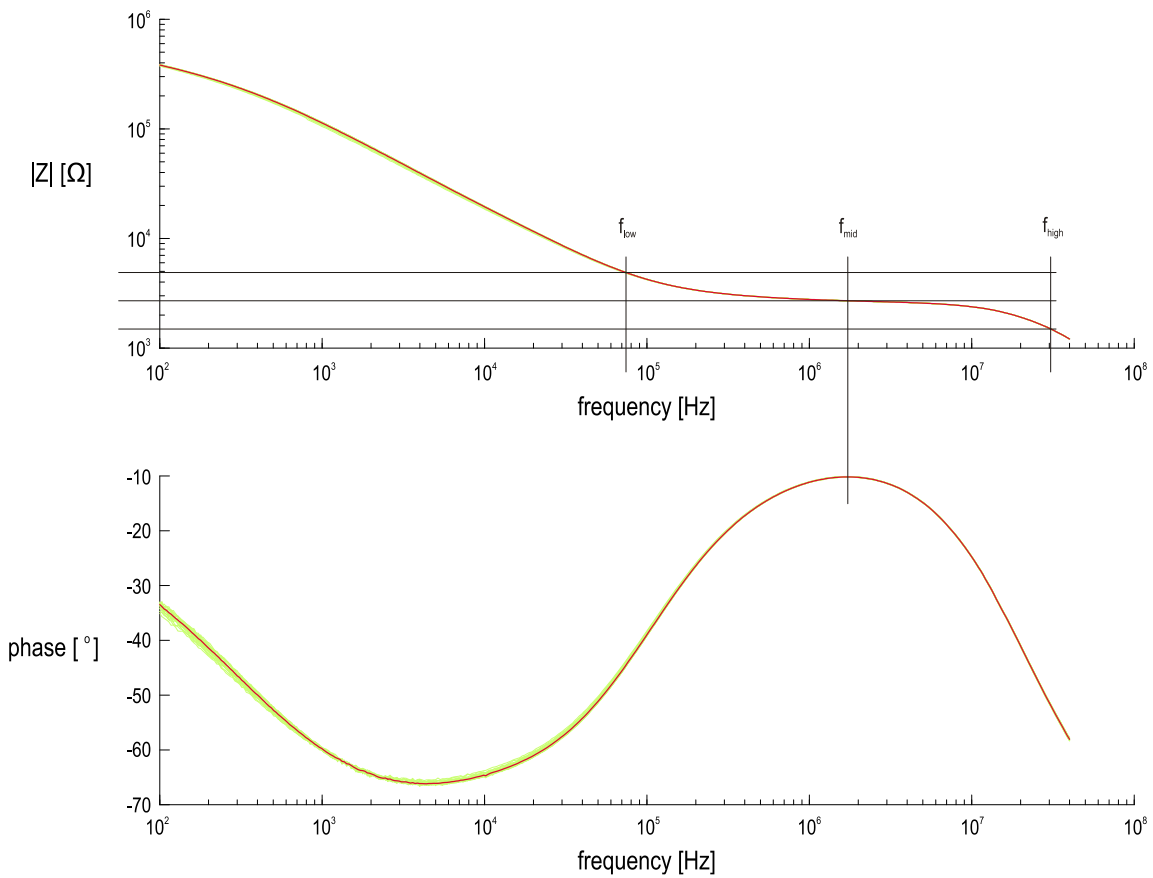


Figure 60 Impedance measurement 60° long focusing electrodes (laminar flow chip (3.1)).

6.3 Spermatozoa experiments

Experiments with spermatozoa are carried out to examine the influence of the created DEP force at the sorting and focusing electrodes.

6.3.1 Sorting electrodes

First the predicted Clausius-Mossotti factor (see Figure 20) is verified. Then the sorting function of the electrode pair is tested with the predicted optimum voltage and frequency.

Clausius-Mossotti curve verification

The first experiments are performed to verify the predicted Clausius-Mossotti plot which can be seen Figure 20. Chip 2.2 is used. This is a chip with 45° sorting electrodes. A flow rate of 0.03 $\mu\text{L}/\text{min}$ is applied. A voltage of 15 V_{pp} is applied to the sorting electrodes during the following experiments. The rms voltage is measured afterwards with chip 3.1 (45° sorting electrodes) and shown in Table 14. All experiments are filmed. The file names of the films are shown in Table 14.

At low frequencies the DEP force should be the strongest. Therefore measurements are started at a low frequency. At 1 MHz it is observed that the spermatozoa are pushed away from the electrodes. To ensure that this is due to a DEP force the experiment is repeated with no voltage applied to the electrodes. It is observed that the spermatozoa are able to pass the electrodes.

At 5 MHz a weak DEP force should be present, because the Clausius-Mossotti factor is small. It is observed that spermatozoa cannot pass the electrode pair at a frequency of 5 MHz. However it can be seen that a spermatozoon passes the first electrode, but cannot pass the gap between the electrodes. This is not observed at 1 MHz. A cause for this can be that the DEP force is weaker at 5 MHz.

At 10 MHz the Clausius-Mossotti factor is expected to be zero. Therefore no DEP force should be present and spermatozoa must be able to pass the electrode pair. This expected behavior is observed during the experiments when a potential of 15 V_{pp} with a frequency of 10 MHz is applied to the electrodes.

All results are summarized in Table 14. It is difficult to quantify the Clausius-Mossotti factor, but these experiments give an indication of this factor. The obtained results did not show any remarkable differences with the predicted results. Unfortunately the Clausius-Mossotti factor is only checked at three different frequencies and only one measurement is performed. This is due to experimental problems as discussed in paragraph 6.3.3.

Sorting function

The sorting function is checked at a frequency of 2 MHz with an applied voltage of 10 V_{pp} at a flow rate of 0.03 $\mu\text{L}/\text{min}$. At this frequency voltage and flow rate the DEP force and drag force should cancel out each other and motile spermatozoa should be able to pass the electrodes. Chip 3.2 with 45° sorting electrodes is used for this experiment. All experimental results are summarized in Table 14.

In the first minute of the experiment there is no noticeable flow. It is unknown why this happens. After 80 seconds there is some flow present. It can be seen that no spermatozoa cross the electrodes. Non-motile spermatozoa did not pass the electrodes. This is as expected. It can be seen that there are not many motile spermatozoa present during this experiment. Therefore it is unknown if there is a sorting function.

As a reference the experiment is repeated without an applied voltage. It can be seen that spermatozoa do pass the electrodes. Unfortunately the experiment had to be aborted because of bubble formation after 15 seconds.

There is no other experimental data collected due to experimental problems which are discussed in paragraph 6.3.3.

Table 14 Sorting electrode results.

<i>Chip</i>	<i>Electrode configuration</i>	<i>Voltage [V_{pp}]</i>	<i>Voltage [V_{rms}]</i>	<i>Frequency [MHz]</i>	<i>behavior</i>	<i>Movie file</i>
2.2	45° sorting	15	5.22	1	Stopping at the electrodes	110622-01_2.2_45sort_01MHz-15Vpp_Stopping-OK.avi
2.2	45° sorting	0	-	-	Flowing over the electrodes	110622-00_2.2_45sort_01MHz-00Vpp_Going-OK.avi
2.2	45° sorting	15	5.52	5	Just stopping at the electrodes	110622-16_2.2_45sort_05MHz-15Vpp_JustStopping-OK.avi
2.2	45° sorting	0	-	-	Flowing over the electrodes	110622-15_2.2_45sort_05MHz-00Vpp_Going-OK.avi
2.2	45° sorting	15	6.11	10	Flowing over the electrodes	110622-13_2.2_45sort_10MHz-15Vpp_Going-OK.avi
2.2	45° sorting	0	-	-	Flowing over the electrodes	110622-12_2.2_45sort_10MHz-00Vpp_Going-OK.avi
3.2	45° sorting	10	3.61	2	Stopping at the electrodes	110624-00_3.2_45sort_02MHz-10Vpp_Stopping-OK.avi
3.2	45° sorting	0	-	-	Flowing over the electrodes	110624-00_3.2_45sort_02MHz-10Vpp_Stopping-OK.avi

6.3.2 Focusing electrodes

The focusing electrodes should focus the cells to one side of the channel. Chip 5.3 is used for these experiments. Due to misalignment during the manufacturing process of the chip one side of the focusing electrodes is not in contact with the medium see Figure 61. This should not have influence on the function of the other part of the focusing electrodes. The width of the channel is 500 μm which is wider than the chips used in the previous experiments. Therefore the flow rate must be higher. The flow rate during this experiment is set at 0.05 μL/min. A voltage of 15 V_{pp} with a frequency of 1 MHz is applied to the electrodes. This resulted in a measured rms voltage of 4.99 V_{rms}. The experiment is recorded and stored in the file mentioned in Table 15.

The first 8 seconds of the experiment no voltage is applied to the electrodes. From 8 to 60 seconds the above voltage is applied to the electrodes. It can be observed that spermatozoa cannot pass the electrodes. They are pushed downwards and will flow between the channel wall at the bottom and the electrode ends. However they are attracted by the second electrode end from the left. The spermatozoa are pulled onto the electrode fingers and seem to be trapped between the second and third electrode finger. This is shown in Figure 62. The lower left circle marks two spermatozoa which follow the arrow and are pulled onto the electrodes. After a while a lot of trapped spermatozoa can be seen between the electrodes. After 60 seconds no voltage is applied anymore to the electrodes and it can be seen that spermatozoa will flow over the electrodes. So the DEP force at the focusing electrodes push the spermatozoa downwards at the left side of the electrodes, but will also pull the spermatozoa from the electrode onto the electrodes.

This is not the behavior which was expected. There must be a nDEP force which is pulling the spermatozoa between the electrodes. In Figure 63 the simulated DEP force in the y direction is showed again. In this picture it can be seen that near the electrodes a positive nDEP force into the y direction is present. It was not expected that spermatozoa flowed so close to the electrodes. Due to these measurements no more experiments were conducted with the laminar flow chip.

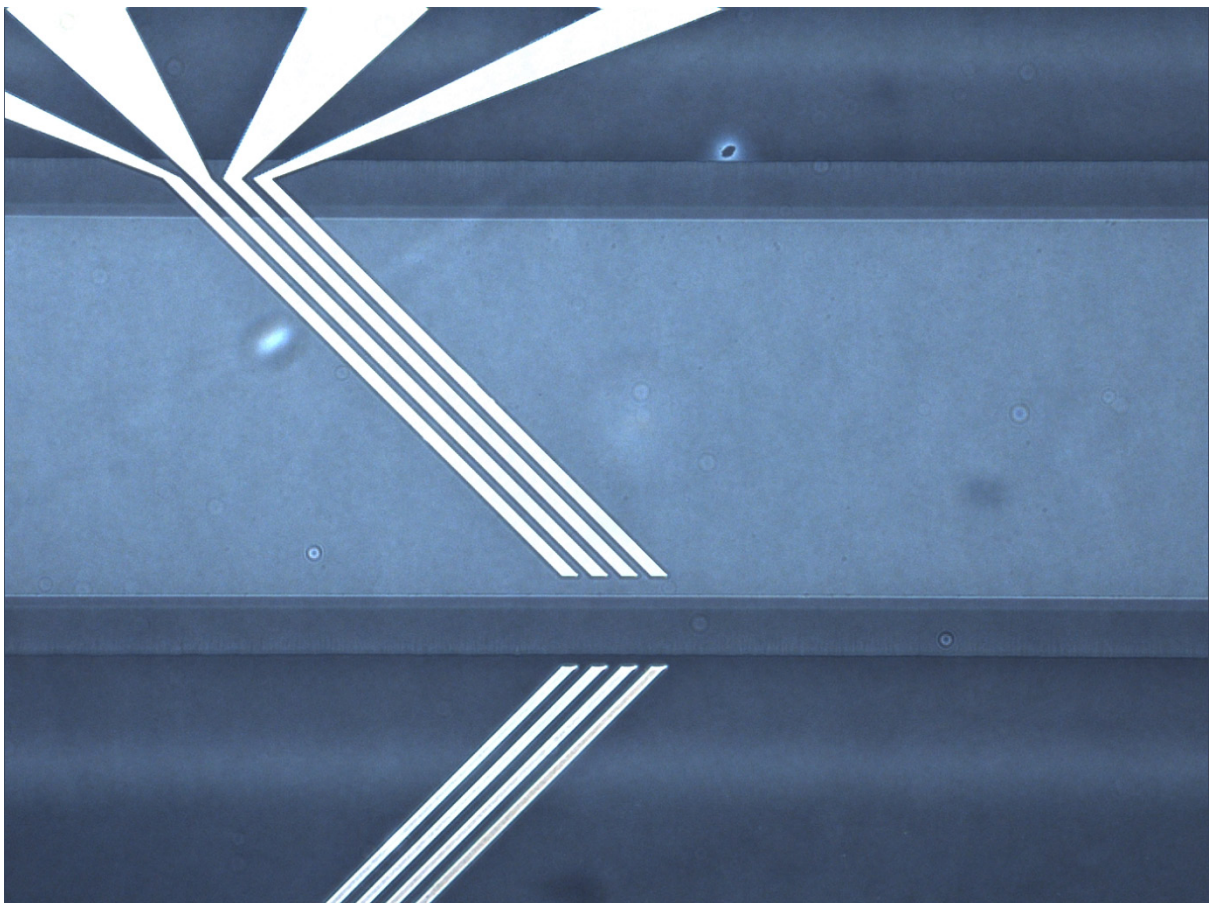


Figure 61 Lower part of the focusing electrodes is not in contact with the medium (chip 5.3).

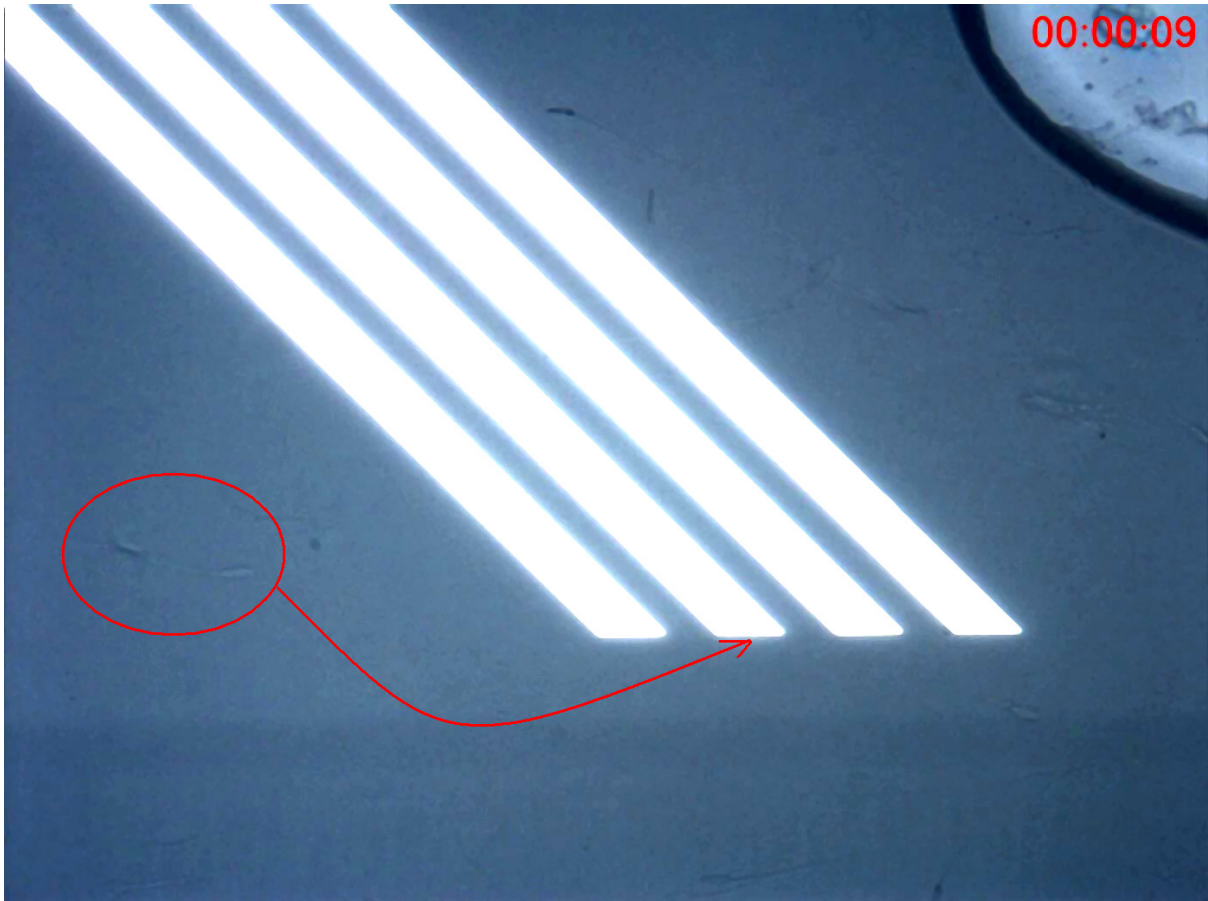


Figure 62 Spermatozoa are first pushed downward and are then pulled onto the electrodes. The electrode fingers on the outer left and the second from right are connected to the signal output of the function generator. The other two electrode fingers are connected to ground.

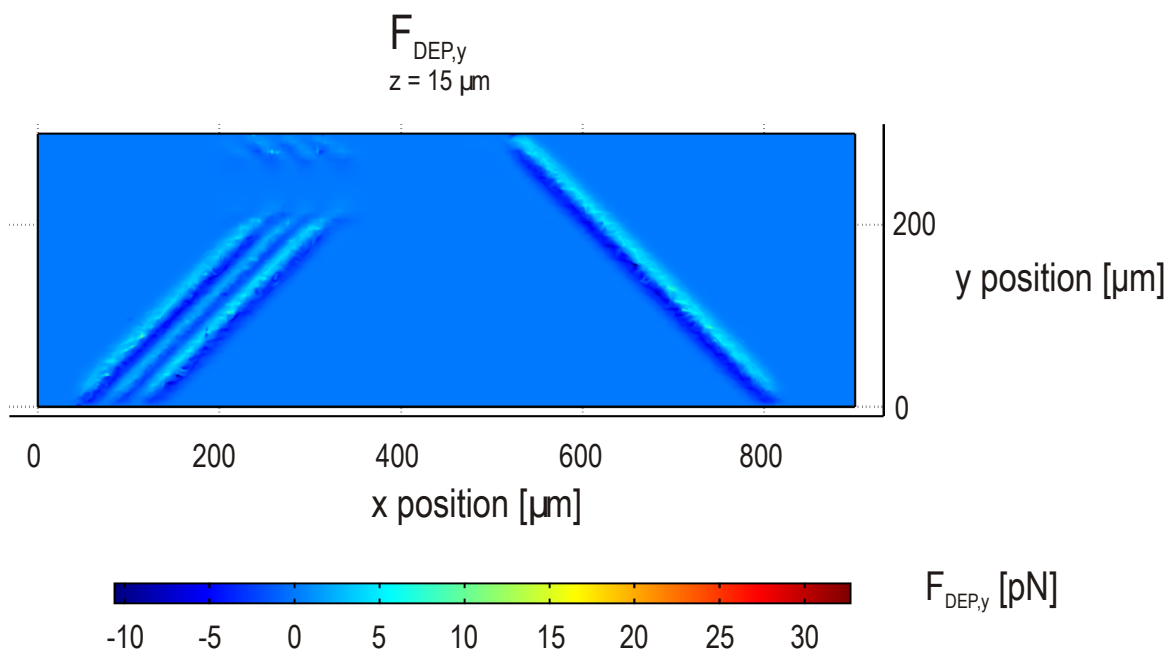


Figure 63 Simulated DEP force in the y direction.

Table 15 Focusing electrode results.

<i>Chip</i>	<i>Electrode configuration</i>	<i>Voltage [V_{pp}]</i>	<i>Voltage [V_{rms}]</i>	<i>Frequency [MHz]</i>	<i>behavior</i>	<i>Movie file</i>
5.3	45° focusing	15	4.99	1	Deflected and attracted	110621-08_5.3_45focu_01MHz-15Vpp_Off-8sOn-60sOff.avi

6.3.3 Encountered experimental problems

During the experiments problems with air bubbles inside the fluidic channels were encountered. Air bubbles inside the medium used, tend to stick inside the channels. So when air bubbles flowed into the channels it was very often not possible to push them out of the channel. Therefore the whole experiment must be stopped. These bubbles could arise from the degassing of the medium. But very often air in the fluidic in- or outlet was pushed inside the channel when the flow rate was decreased. Due to the limited time available for this project unfortunately these problems could not be sufficiently solved.

7 Conclusions and recommendations

Only a limited time is available for a master thesis research, for Electrical Engineering this is 28 weeks. Due to unexpected exceptional problems with a mask machine, the production of the chips was delayed by several weeks. Bonding issues caused additional time delay. The wafers to be bonded were aligned by eye and bonded by hand, which resulted in only three chips without any obvious bonding issues. Expected standard experimental problems with air bubbles and leakage caused additional delay. Although a realistic planning had been made at the start and carefully monitored during the thesis work, the unprecedented extent of problems encountered was more than reasonable could be expected. As a result only limited time remained available to obtain experimental results.

In the next section conclusions based on the obtained experimental results are presented. Recommendations for future research are formulated in the last section.

7.1 Conclusions

Theoretical values for the electrical parameters of interest, the complex permittivity of the medium and a spermatozoon, are obtained from literature. These two parameters are used to calculate the Clausius-Mossotti factor, which is needed to calculate the DEP force. This factor is dependent on the frequency of the applied electrical field. A theoretical plot how the Clausius-Mossotti factor changes with frequency is made. These calculations showed that it is not possible to separate dead and living spermatozoa based on their physical properties, with the medium used. The calculated Clausius-Mossotti factor is verified with measurements. Only three measurements were performed. Due to this limited number no definite conclusions can be drawn, although the measurements do confirm the theoretical values.

A chip design based on the idea to deflect non-motile spermatozoa by means of a negative DEP force has been simulated. These simulations showed that it was possible to create a DEP force strong enough to deflect these spermatozoa. The simulated design has been realized in a glass-glass chip and tested. From experiments it appeared indeed possible to stop and deflect spermatozoa inside a flowing medium. However, due to experimental problems and limited time it was not possible to find the optimal parameters to separate motile and non-motile spermatozoa.

A second chip design was used a DEP force to focus spermatozoa inside a laminar flow with a DEP force. The geometry of the electrodes used in this design did not show the expected behavior. Spermatozoa were initially focused, but at some point were also attracted by these focusing electrodes, which in turn disturbed the focusing effect.

7.2 Recommendations

More experiments are necessary to make any definite conclusions about the verification of the Clausius-Mossotti factor and to tune the applied voltage and its frequency to demonstrate the sorting function of motile and non-motile spermatozoa. Not only the electrical parameters should be investigated, also the behavior of the spermatozoa is of particular interest. The spermatozoa do not swim in straight lines and can even swim against the flow. So the behavior of the spermatozoa at the electrodes should also be investigated

A redesign of the focusing electrodes based on the performed simulations is necessary to test the sorting function of the laminar flow chip. A possible new design is shown in Figure 64. The laminar flow chip has an advantage over the DEP sorting chips. The DEP forces used in

the focusing chip do not need to discriminate between motile and non-motile spermatozoa. Therefore the used voltage and frequency are less strict.

Sorting of dead and living spermatozoa should be possible with a medium with a higher conductivity than the medium used in this research.

Until now all experiments are performed with boar semen. The chip is intended to be used with human semen, which should be verified with additional experiments.

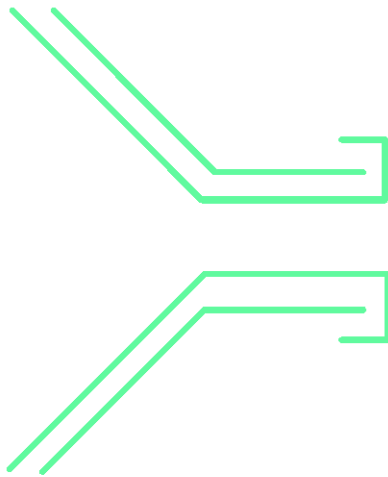


Figure 64 New design of the focusing electrodes. Cells coming for the left are focused between the two electrode pairs. Cells cannot reach places at which they will be attracted to the electrodes.

Literature

1. World Health Organization, *WHO laboratory manual for the examination and processing of human semen, Fifth Edition*, ed. T.G. Cooper. 2010: World Health Organization.
2. Segerink, L.I., et al., *On-chip determination of spermatozoa concentration using electrical impedance measurements*. *Lab on a Chip*, 2010. **10**(8): p. 1018-1024.
3. Raterink, R.-J., *Detecting human spermatozoa using electrical conductivity measurements*. 2008, University of Twente: Enschede.
4. Seo, D.-b., et al., *Development of sorting, aligning, and orienting motile sperm using microfluidic device operated by hydrostatic pressure*. *Microfluidics and Nanofluidics*, 2007. **3**(5): p. 561-570.
5. Ohta, A.T., et al., *Motile and non-motile sperm diagnostic manipulation using optoelectronic tweezers*. *Lab on a Chip*, 2010. **10**(23): p. 3213-3217.
6. Wikipedia. *Sperm - Wikipedia, the free encyclopedia*. 2011 [21-02-2011]; Available from: <http://en.wikipedia.org/wiki/Sperm>.
7. Coppola, M.A., et al., *SpermCheck® Fertility, an immunodiagnostic home test that detects normozoospermia and severe oligozoospermia*. *Human Reproduction*, 2010. **25**(4): p. 853-861.
8. Herr, J.C., et al., *Progress in developing an immunochromatographic device for sperm detection*. *Clinical Immunology Newsletter*, 1999. **19**(4-5): p. 52-58.
9. ContraVac. *ContraVac - Products for Male Fertility*. 2011 [20-04-2011]; Available from: <http://www.contravac.com/products/spermcheck/fertility.php>.
10. Cho, B.S., et al., *Passively Driven Integrated Microfluidic System for Separation of Motile Sperm*. *Analytical Chemistry*, 2003. **75**(7): p. 1671-1675.
11. Pethig, R., *Dielectric and Electronic Properties of Biological Materials*. 1979: John Wiley & Sons.
12. Gascoyne, P.R.C. and J. Vykoukal, *Particle separation by dielectrophoresis*. *ELECTROPHORESIS*, 2002. **23**(13): p. 1973-1983.
13. Stratton, J.A., *Electromagnetic theory*. 1941, New York [u.a.]: McGraw-Hill.
14. Gascoyne, P.R.C. and J.V. Vykoukal, *Dielectrophoresis-based sample handling in general-purpose programmable diagnostic instruments*. *Proceedings of the IEEE*, 2004. **92**(1): p. 22-42.
15. Hughes, M.P., *Strategies for dielectrophoretic separation in laboratory-on-a-chip systems*. *ELECTROPHORESIS*, 2002. **23**(16): p. 2569-2582.
16. Hu, X., et al., *Marker-specific sorting of rare cells using dielectrophoresis*. *Proceedings of the National Academy of Sciences of the United States of America*, 2005. **102**(44): p. 15757-15761.

17. Nascimento, J.M., et al., *The use of optical tweezers to study sperm competition and motility in primates*. Journal of The Royal Society Interface, 2008. **5**(20): p. 297-302.
18. Wikipedia. *Thermal conductivity - Wikipedia, the free encyclopedia*. 2011 10-05-2011 17-05-2011]; Available from: http://en.wikipedia.org/wiki/Thermal_conductivity.
19. Wikipedia. *Heat capacity - Wikipedia, the free encyclopedia*. 2011 12-05-2011 17-05-2011]; Available from: http://en.wikipedia.org/wiki/Heat_capacity.
20. Heida, T., *Dielectrophoresis of neuronal cells - Trapping forces and viability*. 2002, Enschede.
21. Doh, I. and Y.-H. Cho, *A continuous cell separation chip using hydrodynamic dielectrophoresis (DEP) process*. Sensors and Actuators A: Physical, 2005. **121**(1): p. 59-65.
22. Díaz, R. and S. Payen, *Biological cell separation using dielectrophoresis in a microfluidic device*, University of California: Berkeley.
23. Fuhr, G., et al., *High-frequency electric field trapping of individual human spermatozoa*. Human Reproduction, 1998. **13**(1): p. 136-141.
24. Asami, K., *Characterization of biological cells by dielectric spectroscopy*. Journal of Non-Crystalline Solids, 2002. **305**(1-3): p. 268-277.
25. Burgarella, S., M. Bianchessi, and M. De Fazio. *Numerical Modelling of Dielectrophoretic Forces Acting upon Biological Cells in Silicon Lab-On-Chip Devices*. in *COMSOL Users Conference 2007*. 2007. Grenoble.
26. Dürr, M., et al., *Microdevices for manipulation and accumulation of micro- and nanoparticles by dielectrophoresis*. ELECTROPHORESIS, 2003. **24**(4): p. 722-731.
27. Olthuis, W., W. Streekstra, and P. Bergveld, *Theoretical and experimental determination of cell constants of planar-interdigitated electrolyte conductivity sensors*. Sensors and Actuators B: Chemical, 1995. **24**(1-3): p. 252-256.
28. Langereis, G.R., *An integrated sensor system for monitoring washing processes*. 1999.
29. Hoogma, E., *Separation of beads using dielectrophoresis on a chip*. 2009, University of Twente: Enschede.
30. Verkerk, G., et al., *Binas*. 4 ed. 1998, Groningen: Wolters-Noordhoff.

Appendix A Maple code

A.1 Maple – singleshell_3formulas.mw

Maple 13 worksheet used to calculate the three single shell models

```
epsilon[pBurgarella] := proc (f) options operator, arrow; epsilon[m](f)*(r^3/(r-
d)^3+(2*epsilon[i](f)-2*epsilon[m](f))/(epsilon[i](f)+2*epsilon[m](f)))/(r^3/(r-d)^3-
(epsilon[i](f)-epsilon[m](f))/(epsilon[i](f)+2*epsilon[m](f))) end proc;
epsilon[pAsami] := proc (f) options operator, arrow;
epsilon[m](f)*(2*epsilon[m](f)+epsilon[i](f)-2*v*(epsilon[m](f)-
epsilon[i](f)))/(2*epsilon[m](f)+epsilon[i](f)+v*(epsilon[m](f)-epsilon[i](f))) end proc;
epsilon[pOhta] := proc (f) options operator, arrow;
r*C[m]*epsilon[i](f)/(epsilon[i](f)+r*C[m]) end proc;
v := (1-d/r)^3;
epsilon[m] := proc (f) options operator, arrow; epsilon[mr]-((1/2)*I)*sigma[m]/(Pi*f) end
proc;
epsilon[i] := proc (f) options operator, arrow; epsilon[ir]-((1/2)*I)*sigma[i]/(Pi*f) end
proc;
epsilon[med] := proc (f) options operator, arrow; epsilon[medr]-((1/2)*I)*sigma[med]/(Pi*f)
end proc;
d := 0.8e-8;
r := 0.8e-5;
epsilon[mr] := 3*0.885e-11;
sigma[m] := 0.3e-5;
epsilon[ir] := 50*0.885e-11;
sigma[i] := .45;
epsilon[medr] := 78*0.885e-11;
sigma[med] := 1.4;
C[m] := epsilon[mr]/d;
evalf(epsilon[pAsami](0.5e7));
evalf(epsilon[pBurgarella](0.5e7));
evalf(epsilon[pOhta](0.5e7));
```

A.2 Maple – CellConstant.wms

Maple 13 classic worksheet used to calculate the cell constant (κ), the double layer capacitance (C_{dl}), the parasitic cell capacitance (C_{cell}) and the fluid resistance (R_{el}).

```
> K:=ki->int(1/sqrt((1-t^2)*(1-ki^2*t^2)),t=0..1);
> k:=s/(s+2*w);
> kappa:=(2/L)*(K(k)/K(sqrt(1-k^2)));
> Rel:=kappa/sigma;
> Ccell:=epsilon/kappa;
> Cdl:=L*w*Cdlsq;
> Cdlsq:=0.15;
> s:=10.6e-6;
> w:=14.1e-6;
> L:=424e-6;
> sigma:=0.7;
> epsilon:=78*8.85e-12;
> evalf(0.15*w*L);
> evalf(kappa);
> evalf(Rel);
> evalf(Ccell);
> evalf(Cdl);
```

A.3 Maple – ElectrochemicalCellImpedance.mw

Maple 13 worksheet used to calculate and plot the electrochemical cell impedance.

```
Zcell := proc (f) options operator, arrow; 2*Rl+X(f)/((2*I)*Pi*f*Ccell*X(f)+1) end proc;
X := proc (f) options operator, arrow; Rel-I/(Pi*f*Cdl) end proc;
Rl := 44;
Cdl := 0.897e-9;
Ccell := 0.248e-12;
Rel := 0.397e4;
with(plots);
loglogplot(abs(Zcell(f)), f = 1. .. 0.1e13, color = RGB(.2031, .6953, .1992), thickness = 3,
  axis[1] = [gridlines = [6, colour = blue, subticks = 1]], axis[2] = [gridlines = [8, colour
    = blue, subticks = 9]], labels = ["frequency [Hz]", "|Z(f)|"]);
```

A.4 Maple – SingleShell_Ohta.wm

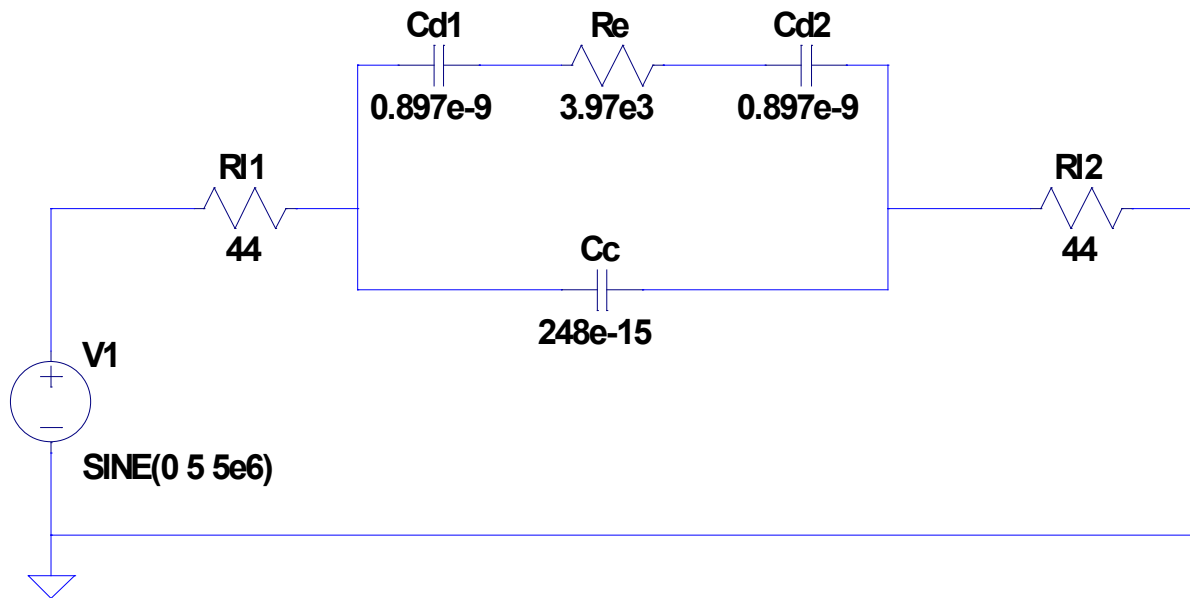
Maple 13 worksheet used to calculate the permittivity of a spermatozoon with the equations and parameters used by Ohta et al. (2010) [5]. The Clausius-Mossotti factor is calculated and plotted.

```
with(plots);
epsilon[pliving] := proc (f) options operator, arrow;
  r*C[s]*epsilon[int](f)/(epsilon[int](f)+r*C[s]) end proc;
epsilon[pdead] := proc (f) options operator, arrow;
  r*C[s]*epsilon[med](f)/(epsilon[med](f)+r*C[s]) end proc;
CM[living] := proc (f) options operator, arrow; (epsilon[pliving](f)-
  epsilon[med](f))/(epsilon[pliving](f)+2*epsilon[med](f)) end proc;
CM[dead] := proc (f) options operator, arrow; (epsilon[pdead](f)-
  epsilon[med](f))/(epsilon[pdead](f)+2*epsilon[med](f)) end proc;
epsilon[int] := proc (f) options operator, arrow; epsilon[intr]-((1/2)*I)*sigma[int]/(Pi*f)
  end proc;
epsilon[med] := proc (f) options operator, arrow; epsilon[medr]-((1/2)*I)*sigma[med]/(Pi*f)
  end proc;
r := 0.329e-5;
epsilon[intr] := 154*0.885e-11;
sigma[int] := .73;
epsilon[medr] := 78*0.885e-11;
sigma[med] := .7;
C[s] := 0.126e-1;
evalf(epsilon[pliving](0.5e7));
evalf(epsilon[pdead](0.5e7));
evalf(CM[living](0.5e7));
evalf(CM[dead](0.5e7));

plotcmliving := semilogplot(Re(CM[living](f)), f = 0.1e4 .. 0.1e10, color = RGB(.2031, .6953,
  .1992), thickness = 3);
plotcmdead := semilogplot(Re(CM[dead](f)), f = 0.1e4 .. 0.1e10, color = RGB(.8086, 0, 0.4453e-
  1), thickness = 3);
display(plotcmliving, plotcmdead, axis[1] = [location = low, gridlines = [6, colour = blue,
  subticks = 1]], axis[2] = [gridlines = [8, colour = blue, subticks = 1]], labels =
  ["frequency", "Re{Fcm}"]);
```

Appendix B LTspice IV model

The model used to calculate the voltage used to create the electric field for the DEP force is shown in Figure 65.



.tran 0 400e-9 0

Figure 65 LTspice electrochemical cell model

Appendix C Matlab scripts

C.1 Matlab - ImpedanceMeasurements.m

Matlab script used to take the mean of the impedance measurements and to plot the results.

```
%% karakterisatie figuur UFLOW
% Original from L.I. Segerink
% Modified by C.E. van Eijkeren
% 08 June 2011

clear all; close all;
Pathname1='S:\s0027634\afstud\Metingen\Impedance-20110607\c3-1_fl\ISplot_';
for i=1:25
    tM(i,1)=importdata([Pathname1, num2str(i+1), '.txt'], '\t', 8 );
    % Always discart measurement 1 therefore: num2str(i+1)
    tM_imp(i,:)=tM(i,1).data(:,2)';
    tM_phase(i,:)=tM(i,1).data(:,3)';
end
freqM=tM(1,1).data(:,1)';

h=figure();
subplot(2,1,1);
hold on, set(gca,'XScale','log','YScale','log');

for j=1:20;
    hM=plot(freqM,tM_imp(j,:), 'Color', [202/256 255/256 112/256]);
end

hM_m=plot(freqM,mean(tM_imp), 'Color', [105/256 139/256 34/256]);
xlabel('frequency/Hz'); ylabel('|Z|/\Omega');

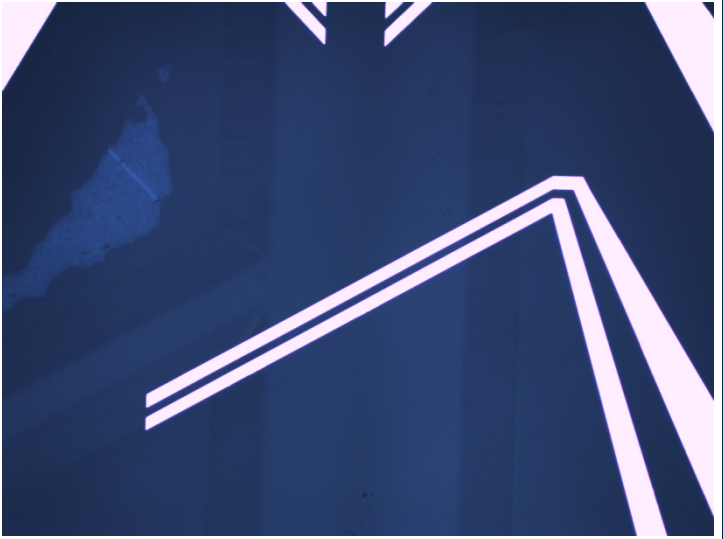
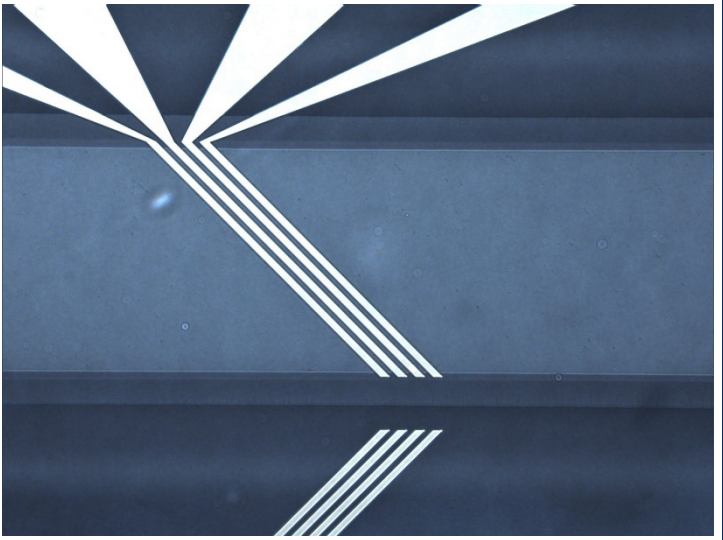
subplot(2,1,2); hold on, set(gca,'XScale','log','YScale','linear');
for j=1:20;
    hM=plot(freqM,tM_phase(j,:), 'Color', [202/256 255/256 112/256]);
end

hM_m=plot(freqM,mean(tM_phase), 'Color', [105/256 139/256 34/256]);
xlabel('frequency/Hz'); ylabel('phase/degree');
```

Appendix D Chip results, numbering and wafer layout

In Table 16 the chip names and the corresponding chip numbers are given. A picture of the electrodes of the chips is also shown.

Table 16 Chip numbers and pictures of the electrodes

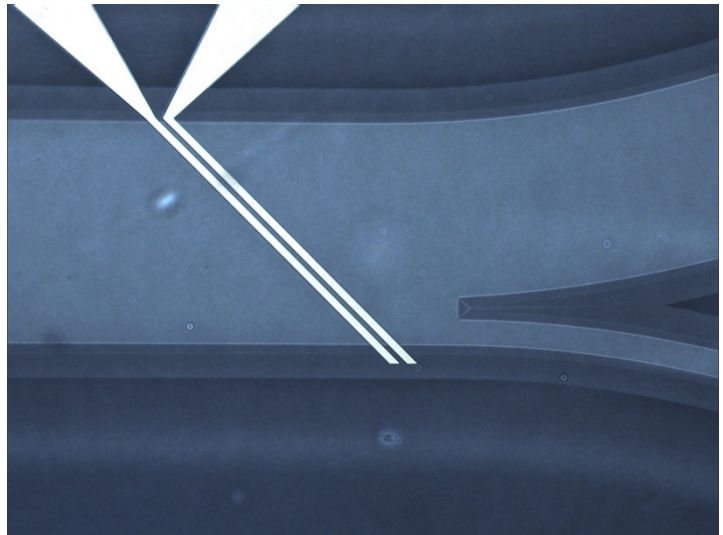
<i>Chip number</i>	<i>Chip type</i>	
1.1	60° far	
Bonding problems		
Focusing electrodes too far to the left		
Sorting electrodes are OK		
1.2	Laminar 45°	
Bonding problems		
Focusing electrodes too low (outside the channel)		

1.2

Laminar 45°

Bonding problems

Focusing electrodes too low (outside the channel)



1.3

45° far

Bonding problems

Focusing electrodes too far to the left

Sorting electrodes too high



2.1

60° mid

Bonding problems

Focusing electrodes too far to the left

Sorting electrodes are OK



2.2

45° far

Bonding OK

Focusing electrodes a bit too far to the left

Sorting electrodes a bit too high

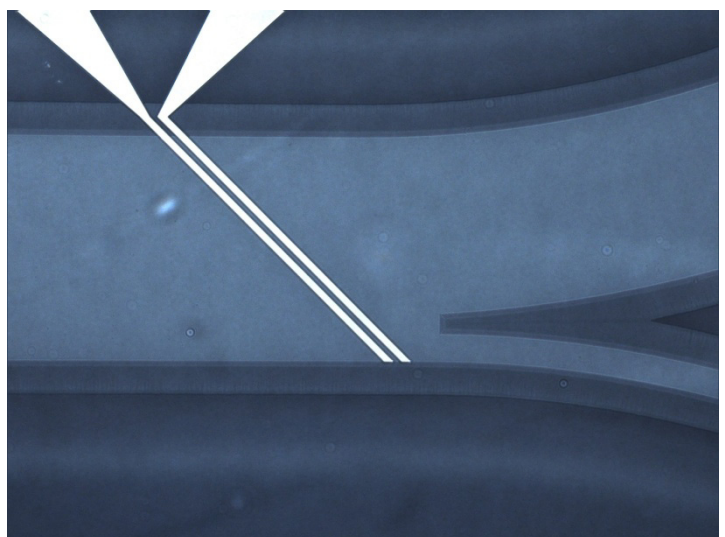
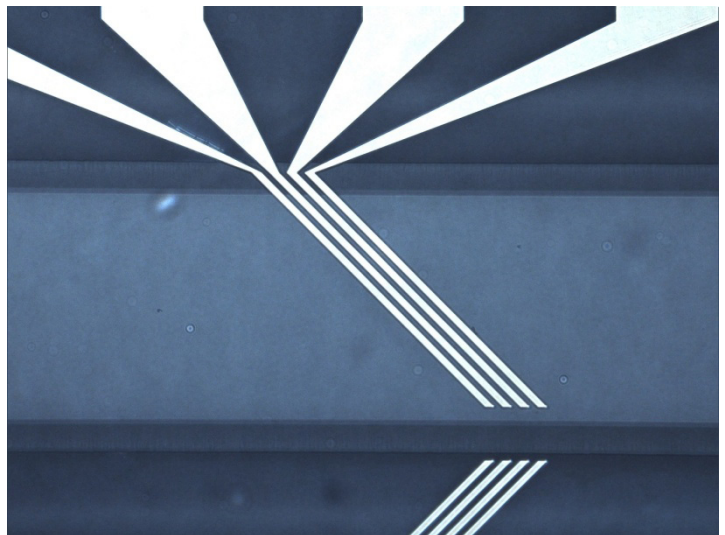


2.3

Laminar 45°

Bonding problems

Focusing electrodes too low



3.1

Laminar 60°

Bonding problems

Focusing electrodes too low (outside the channel)



3.2

45° mid

Bonding problems

Focusing electrodes too far to the left

Sorting electrodes are OK



3.3

60° far

Bonding problems

Focusing electrodes a bit too far to the left

Sorting electrodes are OK



4.1

45° far

Bonding problems

Focusing electrodes OK

Sorting electrodes OK



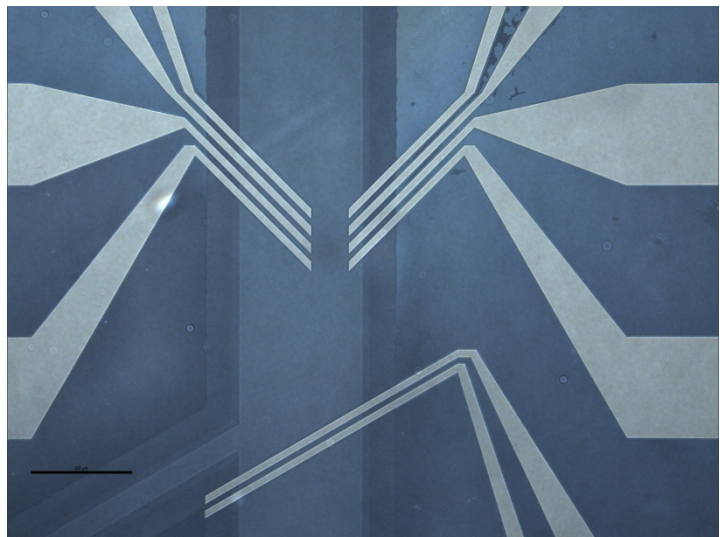
4.2

60° far

Bonding problems

Focusing electrodes OK

Sorting electrodes OK



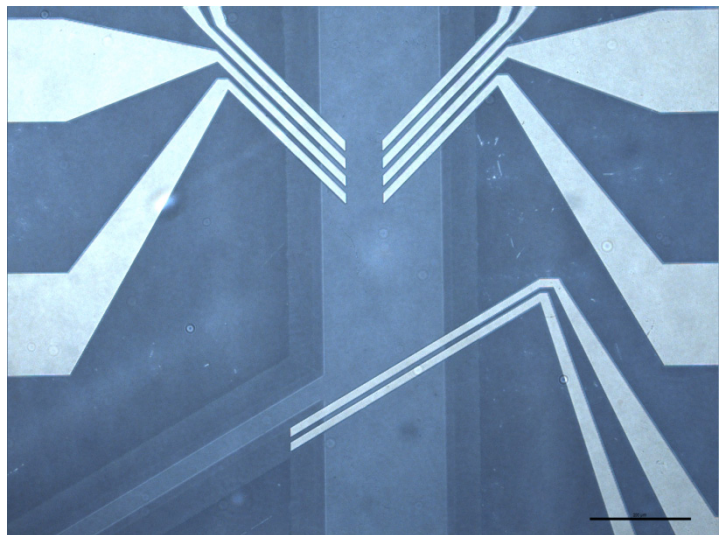
4.3

60° mid

Bonding problems

Focusing electrodes a bit too far to the left

Sorting electrodes are OK



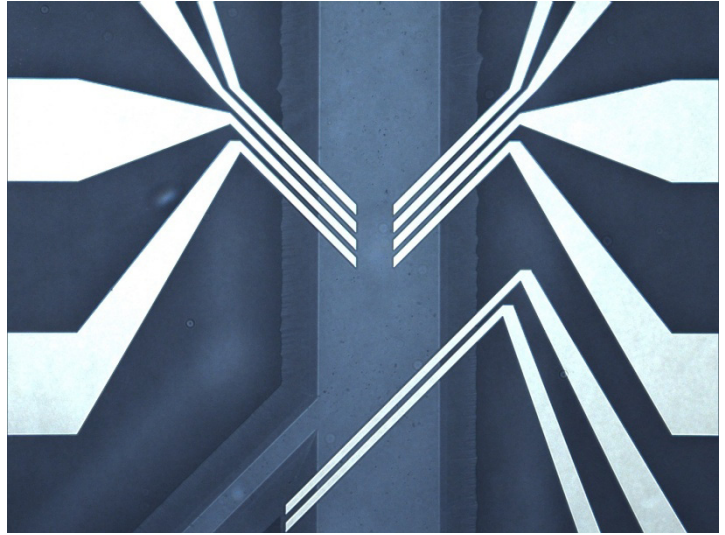
5.1

45° mid

Bonding
problems

Focusing
electrodes OK

Sorting
electrodes OK



5.2

60° far

Bonding OK

Focusing
electrodes OK

Sorting
electrodes OK

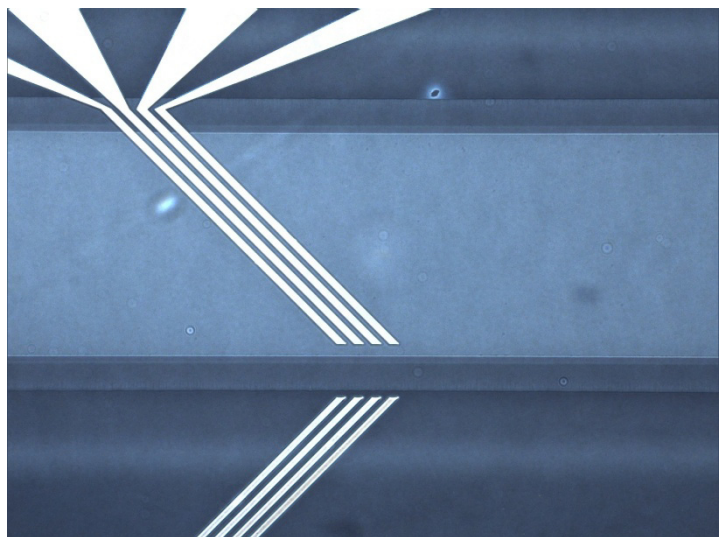


5.3

Laminar 60°

Bonding OK

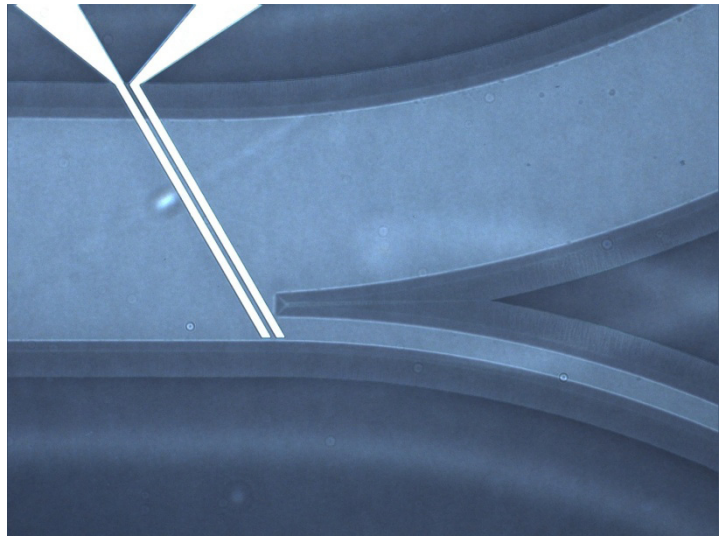
Focusing
electrodes a bit
too low



5.3
Bonding OK

Laminar 60°

Focusing
electrodes a bit
too low



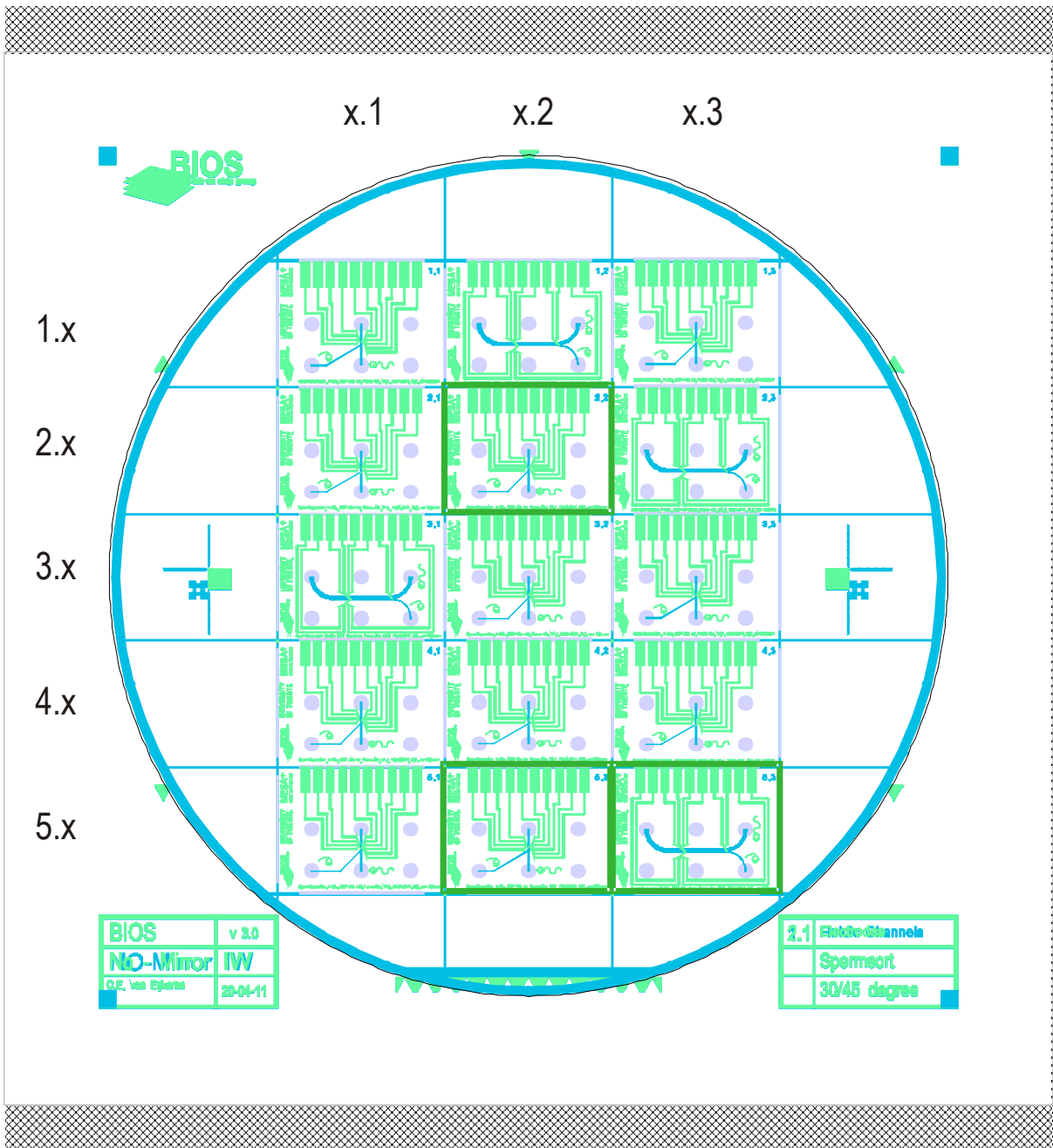


Figure 66 Overview of the wafer. The chip numbers correspond to the row and column numbers. The chips indicated with a green border are the chips with the best bonding result.

